METHODS FOR THE IMPROVED DETECTION OF TUBERCULOSIS BIOMARKERS WITH AN EMPHASIS TOWARDS POINT-OF-NEED DIAGNOSTICS

by

Nicholas Andrew Owens

A dissertation submitted to the faculty of
The University of Utah
in partial fulfillment of the requirements for the degree of

Doctor of Philosophy

Department of Chemistry

The University of Utah

December 2017

The University of Utah Graduate School

STATEMENT OF DISSERTATION APPROVAL

The dissertation of **Nicholas Andrew Owens**

has been approved by the following supervisory committee members:

Marc Porter	, Chair	**08/01/2017** Date Approved
Joel Harris	, Member	**08/01/2017** Date Approved
Shelley Minteer	, Member	**08/01/2017** Date Approved
Ilya Zharov	, Member	**08/01/2017** Date Approved
Bruce Gale	, Member	**08/01/2017** Date Approved

and by **Cynthia Burrows** , Chair/Dean of

the Department/College/School of **Chemistry**

and by David B. Kieda, Dean of The Graduate School.

ABSTRACT

The effective diagnosis of infectious diseases, like tuberculosis (TB), through the detection of biomarkers indicative of active infection, continues to challenge the scientific community. Due to the consistently high burden of disease in low-income economies, there has been a renewed interest to transition the capabilities of the diagnostic tests from the research laboratory to point-of-need (PON) applications. To identify the characteristics of these PON tests, the World Health Organization has established the *ASSURED* (affordable, sensitive, specific, user-friendly, rapid, equipment-free, and delivered to those in need) guidelines.

Using the detection of mannose-capped lipoarabinomannan (ManLAM), a TB biomarker, as a model system, the research presented herein focuses on approaches to meet the challenges faced by modern infectious disease diagnostics with an emphasis on transitioning state-of-the-art surface-enhanced Raman scattering (SERS) immunoassays toward PON applications within the framework of the *ASSURED* guidelines. First, we build on previous work investigating the underpinnings of an acid treatment method to improve the detection of ManLAM in the serum of infected individuals. This work demonstrates that while acid treatment improves the detection of ManLAM, assay performance is hindered because of the acid-induced degradation of ManLAM and the incomplete decomplexation of endogenous serum proteins. Through the application of an

enzymatic sample treatment process, this work also shows that improved ManLAM recoveries lead to improved clinical accuracies.

To increase assay performance, we developed, charactered, and validated a novel surface-enhanced resonance Raman scattering (SERRS) immunoassay. This improves the limit of detection (~10x) and analytical sensitivity (~39x) for ManLAM measurements compared to an analogous SERS immunoassay. The remainder of the work validates the use of a handheld Raman spectrometer for the detection of phospho-*myo*-inositol-capped LAM (PILAM), a ManLAM simulant. This work demonstrates the ability to achieve low limits of detection (~0.2 ng/mL) for PILAM in human serum and document the impact of excitation wavelength and the plasmonic coupling between the labels and planar gold substrates as a basis for further improvements in SERS immunoassays. Taken together, this work begins to establish approaches for improved methodologies to combat the burden of infectious diseases, and to demonstrate the applicability of SERS detection beyond the research laboratory.

TABLE OF CONTENTS

LIST OF SCHEMES

LIST OF TABLES

LIST OF FIGURES

ABBREVIATIONS

σ_{Blank} .....standard deviation of blank sample
σ_x.....standard deviation of first measurement distinguishable from the blank
A_{Blank} .....absorbance for blank sample
I_{Blank}.....intensity of blank sample
λ_{ex} .....excitation wavelength
λ_{sc} .....wavelength of the scattered radiation
Ab.....antibody
ACN.....acetonitrile
AET.....2-aminoethanethiol
Ag.....antigen
AIDS .....acquired immune deficiency syndrome
AU.....absorbance units
AuNP.....gold nanoparticle
BB .....borate buffer
BBT.....2.0 mM borate buffer with 0.1% Tween 20
BSA.....bovine serum albumin
Cy5.....Cyanine 5
Cy5-SH .....thiolated Cyanine 5
CCD .....charge coupled device
CV.....coefficient of variance
DSNB.....5,5'-dithiobis (succinimidyl-2-nitrobenzoate)
DSP .....dithiobis (succinimidyl propionate)
EF.....enhancement factor
EIC.....extracted ion chromatography
ELISA .....enzyme-linked immunosorbent assay
ERL.....extrinsic Raman label
FIND .....Foundation for Innovative and New Diagnostics
FN .....false negative
FP .....false positive
GC.....glassy carbon
GC-MS.....gas chromatography-mass spectrometry
HIV .....human immunodeficiency virus
HRP.....horseradish peroxidase
IR-ERS.....infrared external reflection spectroscopy
IRS .....infrared spectroscopy

LAM.....lipoarabinomannan
LMICs.....low- to middle-income countries
LOB.....limit of blank
LOD.....limit of detection
ManLAM.....mannose-capped lipoarabinomannan
MCT.....mercury cadmium telluride
Msm.....*Mycobacterium smegmatis*
Mtb.....*Mycobacterium tuberculosis*
MWCO.....molecular weight cut off
NAAT.....nucleic acid amplification test
NHS.....n-hydroxysuccinimide
NP.....nanoparticle
ODT.....octadecanethiol
PABL.....polyclonal rabbit antibody for Mtb
PBS.....phosphate-buffered saline
PBST.....10 mM phosphate-buffered saline with 1% Tween 20
PCA.....perchloric acid
PCR.....polymerase chain reaction
PDMS.....poly (dimethyl siloxane)
PILAM.....phospho-myo-inositol-capped lipoarabinomannan
PIM.....phosphatidylinositol mannoside anchor
PK.....proteinase K
PON.....point of need
R.....reflectance of sample
R_o.....reflectance of reference
RIA.....radioimmunoassay
RRM.....Raman reporter molecule
RRS.....resonance Raman spectroscopy
SB.....StartingBlock™
SBR.....signal-to-blank ratio
SEM.....scanning electron microscopy
SERS.....surface-enhanced Raman scattering
SERRS.....surface-enhanced resonance Raman scattering
SPI.....solid-phase immunoassay
SPR.....surface plasmon resonance
SSM.....sputum smear microscopy
T20.....Tween 20
TB.....tuberculosis
TFA.....trifluoroacetic acid
TIC.....total ion chromatography
TMB.....3,3’,5,5’-tetramethylbenzidine
TN.....true negative
TP.....true positive
TSG.....template-stripped gold
UV-Vis.....ultraviolet-visible
WHO.....World Health Organization

ACKNOWLEDGEMENTS

I would like to express my appreciation to all of the people who have made my graduate career such a unique learning experience. I will be forever grateful to my family and friends for their support in my endeavors. Furthermore, I am grateful to my colleagues who have taught me so much and constantly pushed me to be a better scientist. I would like to give special thanks to my advisor, Marc Porter, for mentoring me and providing the resources and freedom to do research that I strongly believe in.

CHAPTER 1

INTRODUCTION

1.1 Overview

The early and effective diagnosis of infectious diseases through the detection of biomarkers indicative of pathogenic agents continues to challenge the scientific and medical community. Efforts to improve existing diagnostic methods as well as to develop novel detection strategies for disease biomarkers have seen renewed interest in recent years due to the emergence of new disease strains and the consistently high burden of disease. As an example, The World Health Organization (WHO) reports that tuberculosis (TB) has surpassed human immunodeficiency virus infection and acquired immune deficiency syndrome (HIV/AIDS) as the world's deadliest infectious disease, with an estimated 1.37 million deaths worldwide in 2015.[1-2] This report also indicates that the greatest impact of infectious diseases is experienced by low-income economies, where infectious diseases accounted for 5 of the top 10 leading causes of death in 2015 (table 1.1).[1-2] The work in this Dissertation focuses on improving existing infectious disease diagnostic modalities and on developing novel detection strategies designed to transition today's laboratory bound tests to a point-of-need (PON) platform. TB will be used as a proving ground for all of this work.

Table 1.1. Leading causes of death in low-income economies worldwide in 2015.[2]

Rank	Description	Estimated number of deaths per 100,000 population
1	Lower respiratory infections	84.9
2	Diarrheal disease	57.2
3	Stroke	49.6
4	Ischemic heart disease	48.6
5	HIV/AIDS	47.7
6	Tuberculosis	34.5
7	Malaria	34.4
8	Preterm birth complications	32.1
9	Birth asphyxia and birth trauma	30.5
10	Road injuries	28.5

HIV/AIDS: human immunodeficiency virus and acquired immune deficiency syndrome

The sensitive detection of disease-related biomolecules can have a strong positive impact on patient outcomes by enabling diagnosis and subsequent treatment earlier in the disease's progression.[3-4] Additionally, these approaches may have merit in use as part of disease surveillance systems, limiting the spread of infectious diseases and reducing the disease burden.[5] However, the effectiveness of a diagnostic test depends on a number of factors such as sensitivity, cost, analysis time, and reliability. Other issues include the accessibility to a patient population, availability of local infrastructure and technical expertise, and societal attitudes towards health care.[1, 5-6]

Building on previous work in our laboratory on the development of a novel immunoassay for TB diagnostics, this Dissertation is focused on further improvements in the platform. This Dissertation is organized into five chapters. The first chapter, the Introduction, provides context for this work by describing the ideal characteristics of a diagnostic test and the important techniques used throughout. The second chapter investigates the underpinnings of sample treatment as a means to liberate a marker indicative of TB infection from a human serum matrix and how sample treatment markedly improves clinical accuracy. The third chapter describes the development of a novel sensing strategy that is based on surface-enhanced resonance Raman scattering (SERRS) and reports on a measurement of its performance with respect to TB biomarker detection. The fourth chapter investigates the utility of a handheld Raman spectrometer for TB marker measurements with emphasis on the challenges associated with transitioning a new measurement technology from the laboratory benchtop to the field. The fifth and final chapter concludes with a discussion regarding the broader implications of this work and its future directions.

1.2 Infectious Disease Diagnostics (Tuberculosis as a Model System)

A brief definition for a diagnostic test in the medical field is one that detects the presence of disease. For applications in infectious disease diagnostics, most tests are designed to detect a biomolecule specific to a given pathogen or the pathogen itself. These tests can be qualitative or quantitative, their primary function being to provide health care providers the necessary information to make an informed decision on diagnosis and treatment. The effectiveness of a diagnostic test is framed by its clinical accuracy.[7-10] Clinical accuracy is comprised of two components: (1) clinical sensitivity, which is the ability of the test to correctly identify an infected patient as a true positive (TP) relative to missing infected patients, as false negatives (FN); and (2) clinical specificity, which is the ability of the test to correctly identify noninfected patients as a true negative (TN), relative to misdiagnosing noninfected patients as false positives (FP). Clinical sensitivity and clinical specificity, expressed as percent, are summarized in equations 1.1 and 1.2, respectively.[8]

$$Clinical\ Sensitivity = \frac{TP}{TP + FN} \times 100 \tag{1.1}$$

$$Clinical\ Specificity = \frac{TN}{TN + FP} \times 100 \tag{1.2}$$

While an effective diagnostic test must be clinically accurate, the real-world effectiveness of a test is strongly dependent on a large number of extrinsic factors. These include a balance between clinical accuracy and the cost per test, turnaround time, technical complexity, and accessibility.[5, 11-15] Patients in high-income economies often have less to fear from these extrinsic factors as there are typically testing redundancies in place to ensure rapid and accurate diagnosis.[16] In fact, infectious diseases like TB are not found

among the leading causes of death in upper-middle and upper-income economies.[2] However, the effect on lower-middle and lower-income economies can be devastating.[1-2] Often, low-income and resource-limited areas where many infectious diseases like TB are endemic, such as equatorial Africa and Asia, have compounding factors that further hinder the effectiveness of a given diagnostic method.[1-2, 5, 17]

In many resource-limited economies, the effectiveness of a diagnostic test can also be affected by the lack of adequate medical facilities and skilled personnel, and poor infrastructure in terms of electrical power and clean water.[5] The consistently high economic and societal burden caused by infectious diseases has fueled research efforts aimed specifically at effective PON testing methods to circumvent these challenges.[5] As guidance, the WHO has set forth the *ASSURED* (affordable, sensitive, specific, user-friendly, rapid, equipment-free, and delivered to those in need) criteria to describe the characteristics of an ideal PON test.[17-18] It is important to note that recent iterations have amended the equipment requirement to include inexpensive and robust portable equipment.[5, 19] The development of an effective PON test for TB begins to address the elements of the *ASSURED* criteria, and research aimed at overcoming challenges in meeting these criteria serves as the underlying context for this Dissertation.

TB is caused by a bacterial infection of *Mycobacterium tuberculosis*, (Mtb). In addition, while treatment options (*i.e.*, antibiotics) are available, effective diagnostic methods suitable for PON applications are lacking.[1, 5, 15] The gold standard for TB testing rests on a well-established bacterial culture method.[1, 20] Because Mtb is a slow growing bacterium, this test can take several weeks and requires sophisticated medical facilities and highly trained personnel.[1, 20-22] Serological tests for TB are available, but the poor

diagnostic performance of these tests caused the WHO to call for a ban of such tests in resource-limited regions.[23-24] This leaves clinical suspicion and a relatively quick sputum smear microscopy (SSM) test as the most common approaches for TB diagnosis in PON settings.[25] However, both SSM and bacterial culture are only reliable at advanced stages of infection, limiting the potential benefits of early detection.[25] Furthermore, SSM and bacterial culture are ineffective for diagnosing extrapulmonary TB, which accounts for ~10% of infections worldwide.[1] As a consequence of the testing limitations, it is estimated that 1 in 3 infected individuals go undiagnosed/unreported.[1] Previous work in our laboratory focused on the development of a simple immunoassay-based test for a TB biomarker, specifically lipoarabinomannan (LAM), figure 1.1, as a means to address many of the challenges faced with diagnosing TB.[26-27]

Using TB as a proving ground, this Dissertation builds on this past work in an effort to fill in the void left by today's diagnostic tools. It is important to note there are two forms of LAM used throughout this work: (1) phospho-*myo*-inositol-capped LAM (PILAM), which is derived from *Mycobacterium smegmatis* (Msm) and serves as a nonpathogenic simulant suitable for TB diagnostic assay development, and (2) mannose-capped LAM (ManLAM), which is indicative of pathogenic Mtb.[28-35] Both are carbohydrate molecules found in the bacterial cell wall and have similar molecular weights, 17.3±5.0 kDa.[28-30, 36-39] While the exact degree of branching and extent of capping agents may vary somewhat, the representative structures of PILAM and ManLAM are depicted in figure 1.1.[28-30, 36-40]

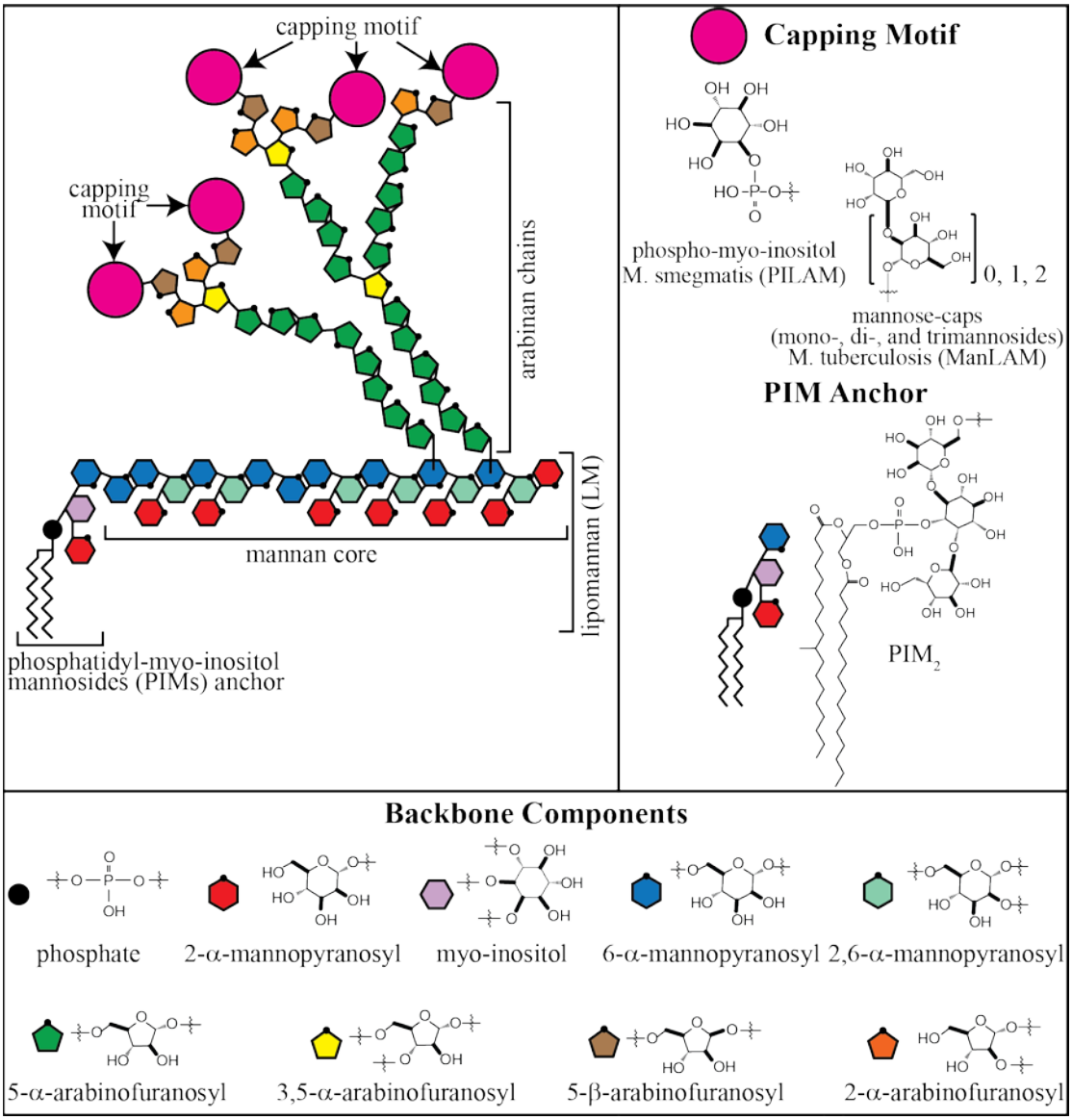

Figure 1.1. Representative structure of lipoarabinomannan (LAM): (1) phosphatidylinositol mannoside (PIM_2) anchor, (2) mannan core, (3) arabinan side chains, and (4) capping motifs. The branching, capping motifs, and overall molecular weight vary somewhat across different mycobacteria. Both phospho-*myo*-inositol-capped LAM (PILAM) from nonpathogenic *M. smegmatis* and mannose-capped (ManLAM) from *M. tuberculosis* are used throughout this work.[40]

1.3 Immunoassays as Diagnostic Tools

Immunoassays as a modern diagnostic tool can be traced to work by Landsteiner *et al*. on the detection of haptens in 1945.[41] An immunoassay relies on antibodies as molecular recognition elements to improve the sensitivity and selectivity of a diagnostic platform.[42] Continued research in this area led to the development of a solid-phase immunoassay (SPI), which had improved sensitivity relative to the typical radioimmunoassays available at the time; and, due to its ease of use, the basic format is still in use today.[43] Figure 1.2 summarizes the principal components of a typical SPI, including (1) the solid support, which is modified with an antibody to selectively capture the target analyte, and (2) a labeling method using a tracer antibody, which selectively labels the captured analyte. Due to the heterogeneous nature of SPIs, excess solution and interfering molecules can be easily rinsed away before the labeling step, leading to a significant improvement compared to the previously used cleanup methods (*e.g.*, ion exchange, electrophoresis, gel filtration, and precipitation techniques).[43] SPIs are incredibly flexible platforms and are compatible with a wide range of detection strategies based on spectroscopic techniques (*e.g.*, absorption, fluorescence, and chemiluminescence), electrochemical techniques, and scintillation counting, depending on the chemical label affixed to the tracer antibodies.[44-48] To further expand the utility of SPIs, recent work has focused on the development of nanoparticle-based detection strategies, including quantum dots and noble metal nanoparticles for spectroscopic detection, and magnetic nanoparticles for detection by giant magnetoresistance.[49-59] A more detailed overview of enzyme-linked immunosorbent assays (ELISAs) and immunoassays based on surface-enhanced Raman scattering (SERS) detection, the two primary assay techniques used throughout the research described herein,

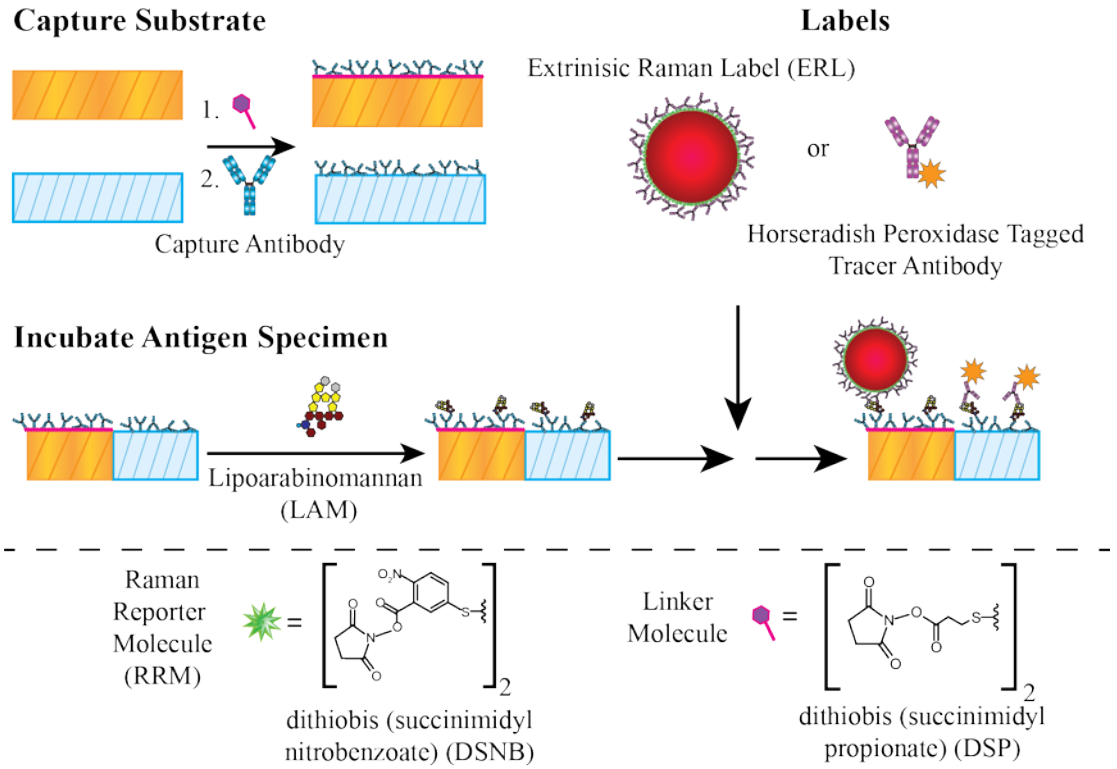

Figure 1.2. Example formats for solid-phase immunoassays with emphasis on the labels used in enzyme-linked immunosorbent assays (ELISA) and surface-enhanced Raman scattering (SERS) immunoassays for the detection of tuberculosis biomarkers. The two assays are operationally similar, but the SERS immunoassay used a gold nanoparticle based label, which is designed to intrinsically amplify the response with respect to antigen capture as opposed to the enzymatic amplification of ELISA. Figure 1.3 overviews the format for ELISA.

is presented in the following section.

1.4 The Enzyme-linked Immunosorbent Assay (ELISA) and Surface-enhanced Raman Scattering (SERS) Immunoassay

ELISA emerged in the early 1970s and, as described by Van Weemen *et al.*, uses an enzyme as the basis for a detection strategy.[60] These assays rely on the extrinsic signal amplification from an enzyme-tagged antibody binding to a captured antigen on the surface, caused by the high turnover rate of the enzyme for its substrate that produces a highly colored or fluorescent product; this type of assay has been extensively reviewed elsewhere.[44, 61-63] Much of the work described in Chapter 2 utilizes a tracer antibody that we functionalize with horseradish peroxidase that, during the color development step, facilitates the oxidation of 3,3',5,5'-tetramethylbenzidine to 3,3',5,5'-tetramethylbenzidine diimine, which absorbs strongly at 450 nm, for spectroscopic detection (figure 1.3).[64] Despite widespread use, ELISAs have some key limitations, particularly when attempting to transition a detection strategy from the highly controlled environment of the research laboratory to a PON setting. Changes in the reaction environment of the enzyme (*e.g.*, temperature, pH, and ionic strength) can change the enzymatic activity altering the performance of the assay.[62, 65] Enzymatic activity can also be degraded by denaturation due to the conjugation chemistries used to link the enzyme to the tracer antibody.[66] Finally, while ELISAs are extensible (*i.e.*, they have been employed to detect different analytes by changing the capture and tracer antibodies), their application for multiplexed detection (*i.e.*, the detection of multiple analytes simultaneously) is limited by the overlap of the large widths of the optical transitions involved in the spectroscopic detection.[67-68]

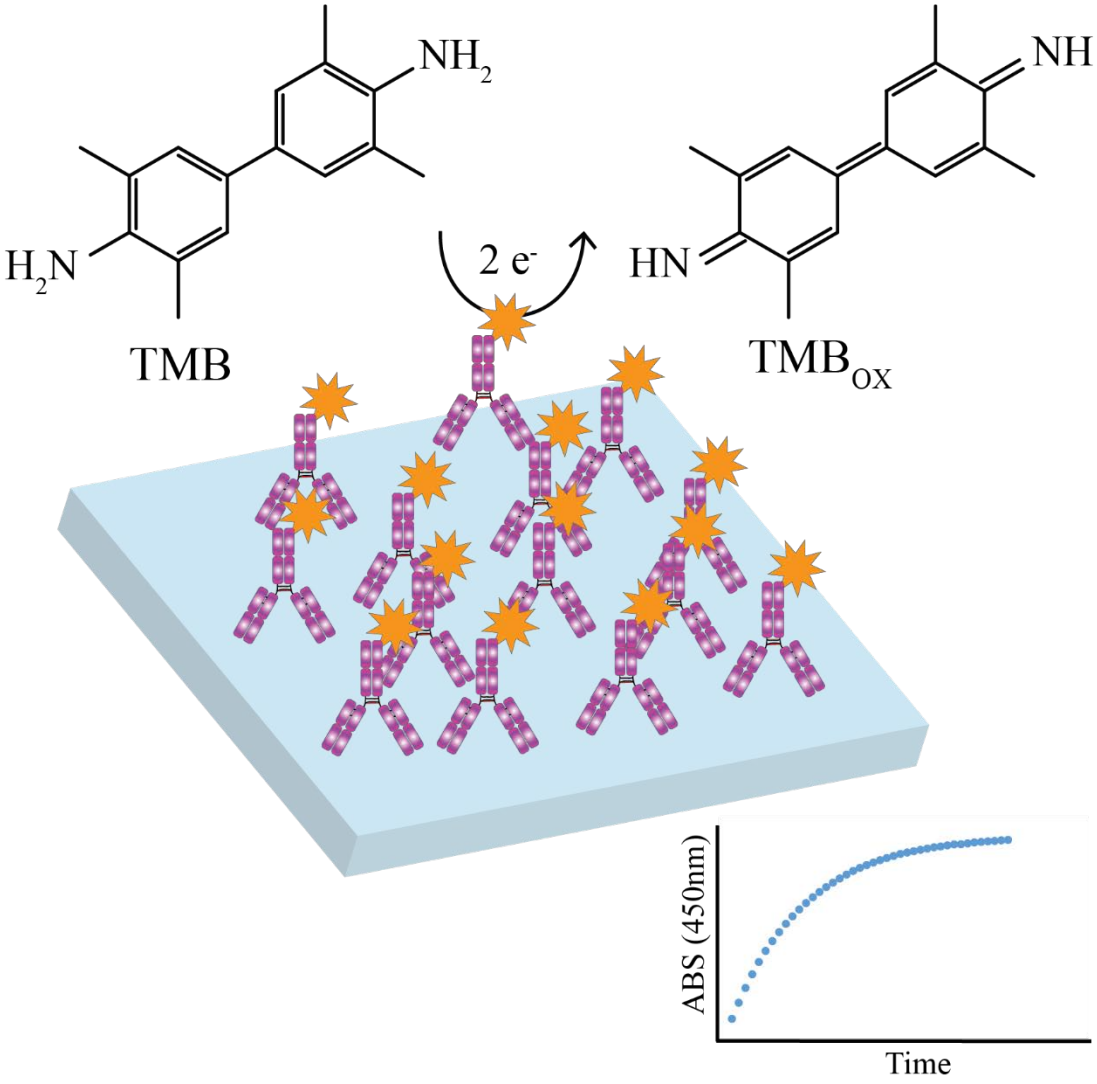

Figure 1.3. Depiction of the oxidation of colorless 3,3',5,5'-tetramethylbenzidine to the highly colored 3,3',5,5'-tetramethylbenzidine diimine.

To overcome the limitations of ELISA and many other detection strategies, our laboratory was among the first to develop a SERS immunoassay for disease marker detection.[55-56] Unlike ELISA, the SERS immunoassay for the detection of TB biomarkers, PILAM and ManLAM, uses the intrinsic signal enhancement arising from functionalized gold nanoparticles, or extrinsic Raman labels (ERLs), that plasmonically couple with the underlying gold support (figure 1.4), for highly sensitive detection.[26-27, 69] While some aspects of the enhancement mechanism are still under investigation, it is now widely accepted that the signal enhancement of the traditionally weak Raman phenomena derives primarily from an electromagnetic enhancement mechanism.[70-74] The electromagnetic enhancement derives from the amplification of an electric field by localized surface plasmon resonance.[55-56, 70-79] When using a smooth gold substrate to support the capture antibody, the plasmonic interactions between the gold nanoparticle and gold substrate further amplify the response.[55-56, 70-79] Enhancement factors of 10^5-10^6 are typical, but can be up to 10^{14} in a few isolated instances.[72, 74, 80-82] The theory and mechanism of the SERS enhancement mechanism have been refined since the discovery of SERS in the early 70s.[71-72, 80] Research has also investigated the impact of size, shape, and composition of the nanoparticle, and the influence of the dielectric properties of the surrounding medium.[73, 76, 83-88]

SERS immunoassays have several advantages compared to ELISAs. The electromagnetic enhancement mechanism results in a signal intensity comparable to or greater than those from fluorescence-based detection.[59, 89-90] Raman bands are ~40x narrower than typical fluorescence or absorption bands, reducing the potential spectral overlap, and therefore improving the level of multiplexing achievable with SERS

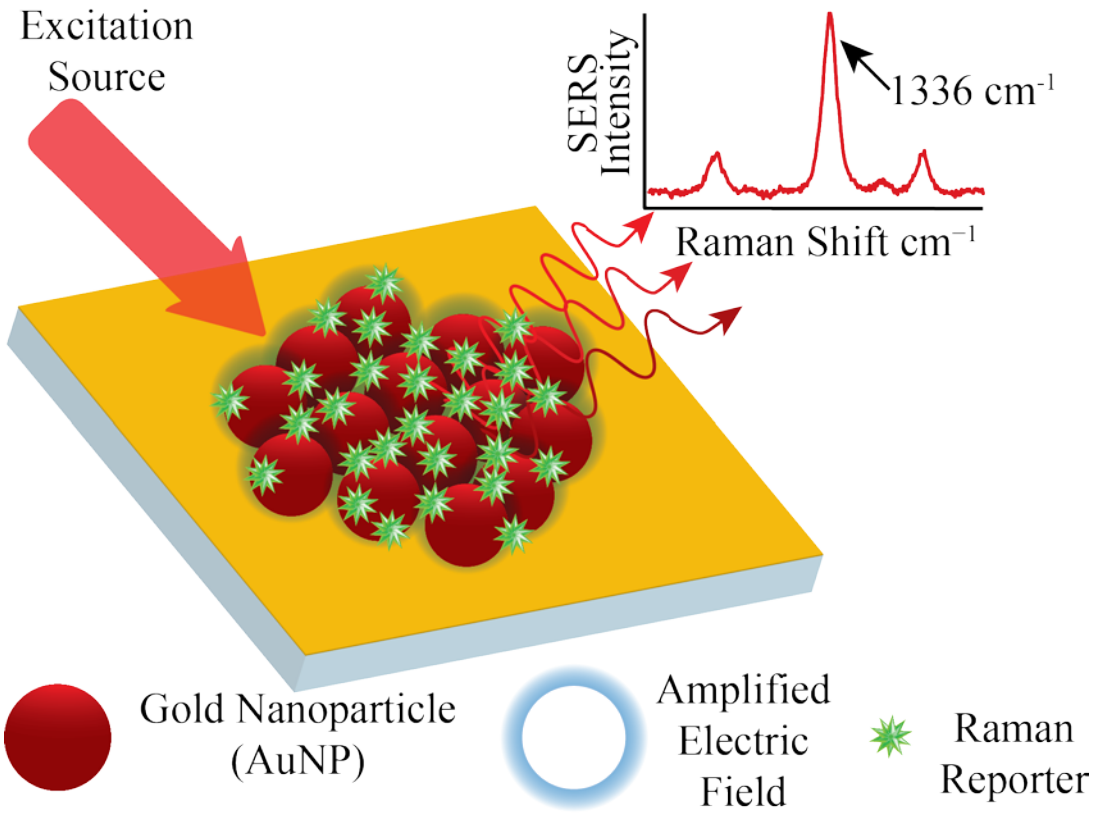

Figure 1.4. Depiction of the surface-enhanced Raman scattering immunoassay readout and the Raman spectra of the Raman reporter molecule, 5,5‘-dithiobis (succinimidyl-2-nitrobenzoate) (DSNB), on the nanoparticle surface. The height of the symmetric nitro stretch, $\nu_s(NO_2)$, of DSNB at 1336 cm^{-1} is used to indirectly quantify the labeled antigen on the surface after its capture by immobilized surface antibodies and subsequently labelling with the nanoparticle-based label.

immunoassays.[72, 91-92] Because the plasmonics of the system is tunable, background fluorescence is reduced by the use of longer wavelength excitation sources, such as HeNe lasers at 633 nm.[93] Alternatively, as discussed in Chapter 3, exploiting the intrinsic electronic transitions of a RRM can be used to further improve the detection strength in SERRS-based immunoassays. In addition, SERS detection is attractive as a method to facilitate PON applications, because it is less affected by environmental factors, such as pH, ionic strength, and natural quenchers like oxygen.[93] Given these advantages, Chapter 4 explores the transition of SERS towards a PON platform using inexpensive and reliable handheld spectrometers.[94-96] Chapter 5 included a summary of the conclusions from this work as well as briefly discusses the future direction of these projects.

1.5 Surface-enhanced Resonance Raman Scattering (SERRS)

SERRS is a special case of SERS in which the excitation wavelength induces an electronic transition in the Raman reporter molecule.[97-100] This can result in an increase in signal by as much as a 10^6.[79] In the late 1990s, Nie *et al*. reported single molecule detection for a fluorescent dye on colloidal silver aggregates.[98] They found that while the majority of the signal enhancement derives from the SERS mechanism, the electronic excitation of the dye molecule with the 514 nm source also contributed to the overall signal enhancement.[98] Since then, SERRS has been used to study conformational changes in proteins, for multiplexed measurements of DNA oligonucleotides, intracellular imaging and detection, and the detection of waterborne pathogens.[101-104] Despite the sensitive detection achievable with SERRS measurements, it has seen relatively few applications compared to SERS, in part due to the difficulty in maintaining stable colloidal labels once

they have been modified with a resonance-enhancing dye.[79] While there are reports of researchers attempting to circumvent this issue by functionalizing a planar substrate with the RRM to allow for subsequent detection by SERRS, this area of study is somewhat limited with respect to the detection of disease biomarkers for infectious disease diagnostics.[79, 103, 105-106] Chapter 3 describes the development and application of a novel chemically modified SERRS immunoassay for the detection of ManLAM from whole serum.

1.6 Sample Preparation in Diagnostics

"Matrix effects" is a term broadly applied in diagnostics, and is ascribed to the deleterious effects that ancillary components in a sample matrix can have on analyte detection.[107] Matrix effects can limit assay sensitivity and reproducibility, and as such, the reduction or management of matrix effects can be a critical component in the development of an analytical measurement.[107-108] Much of the work described herein revolves around the detection of PILAM and ManLAM in human serum, the part of blood remaining after separation from whole cells and clotting factors.[109] Human serum is a complex biological sample matrix containing proteins, polysaccharides, fatty acids, electrolytes, and numerous other small molecules that may interfere with analyte detection. [107, 110-111] The Human Metabolome Database, a multiagency initiative, currently contains 74,461 unique metabolomic entries, and it is linked to several other databases that add to this number.[112-114] Because of the complexity of human serum and the negative effects endogenous serum components can have on analyte detection in immunoassays, a large number of methods have been developed to limit matrix effects.[62, 107-108]

As found in our laboratory, and well documented in the literature, matrix effects often manifest in two ways when developing immunoassay methodologies for use in human serum.[26-27, 107-108, 115] First, surface passivation, in which specific or secondary interactions occur between the antibody-modified capture surface and serum proteins, can block the surface from binding a target analyte.[47, 62, 108] Second, the formation of protein-analyte complexes can inhibit the capture or labeling of the analyte.[62, 108] Formation of complexes is a known issue in TB diagnostics. It has been shown that TB markers like ManLAM shed from Mtb during the course of infection can form complexes with proteins in human serum.[26-27, 31, 116-127]

Methods to disrupt protein complexes vary from single-step treatments that require no further processing to multistep separations that remove the treatment agent and renormalize the sample matrix before performing an assay. As an example of a single-step treatment method, diluting the serum sample with a suitable buffer matrix is often effective at limiting matrix effects, by simply decreasing the concentration of the offending species until its effect is lowered to an acceptable level.[107, 128] However, when attempting to detect an analyte like ManLAM at extremely low concentrations, this method dilutes the analyte, adding to the detection challenge. More complex multistep procedures have been developed to more selectively denature proteins. Multistep methods can include the use of organic solvents, salts, detergents, heat, and acids. [92, 113-117] These methods denature proteins by affecting the electrostatic and hydrophobic interactions within the protein, ultimately leading to noncovalent aggregation.[108, 129-133] Finally, a popular treatment method employed in DNA tests and proteomics uses serine proteases like trypsin and proteinase K (PK) to denature serum proteins.[134-136] For example, PK is a broad spectrum

protease and, given the proper conditions, can effectively reduce proteins to small fragments that can be removed during a subsequent heating step. PK is often used to isolate DNA segments from serum samples for polymerase chain reaction analysis.[135, 137]

One of the treatment procedures used in this Dissertation builds on our previous work that describes the initial development and application of a perchloric acid (PCA) treatment method to facilitate the low level detection of PILAM and ManLAM from human serum.[26-27] This approach is overviewed in figure 1.5. The PCA treatment method seems ideal, at first glance, as it is rapid, inexpensive, and easy to use. The change in pH protonates the carboxylate groups of proteins which, when combined with the ability of the acid to hydrolyze proteins, drives the noncovalent aggregation of these serum proteins.[133, 138-146] As described in some of the original work using trifluoracetic acid for protein removal, the effect of acid treatment is dependent on protein size. [139, 144, 146] Larger proteins precipitate from solution more readily than smaller proteins, meaning the method can be tailored to target specific size ranges of proteins by varying the amount of acid added.[139, 144, 146] However, treatment methods that denature proteins can change subsequent activity, indicating the proteins may have been permanently degraded in the process.[144, 147] As such, a major focus of this Dissertation details an investigation into the challenges associated with use of a PCA treatment method to improve the detection of ManLAM in human serum and enhance clinical accuracy of our diagnostic platform.

1.7 Dissertation Overview

The majority of the work in this Dissertation builds on the above subject areas with the goal of investigating and developing methods to advance a diagnostic test for TB.

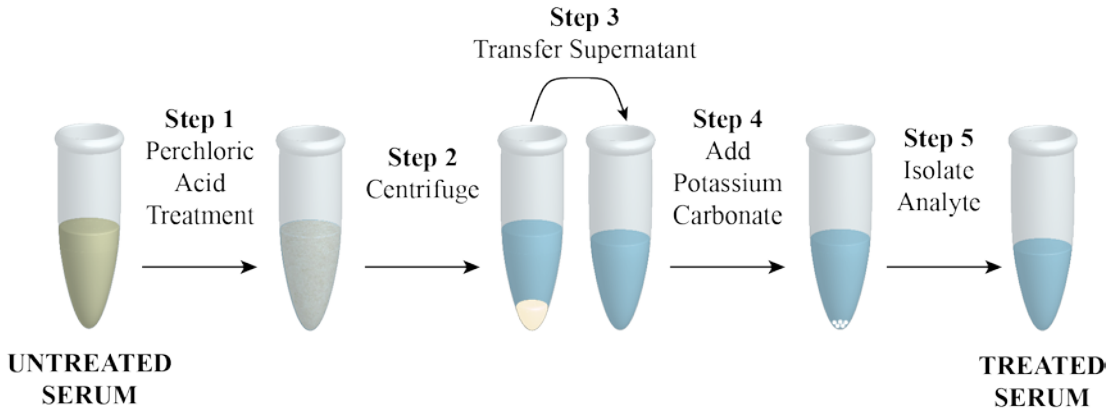

Figure 1.5. Step-by-step depiction of the perchloric acid-based sample treatment method used to improve the detectability of PILAM spiked in serum samples. The majority of the protein is removed due to the noncovalent aggregation induced with the addition of acid (Step 1). This is followed by a separation and transfer step to separate the PILAM-containing supernatant from the denatured protein (Steps 2-3). Finally, the solution is neutralized and the PILAM-containing supernatant is transferred once again (Steps 4-5).[26]

Moreover, the platform described herein is extensible to addressing challenges faced by many new and existing disease diagnostic tests. Chapter 2 describes the investigation of methodologies to recover ManLAM from human serum, while maintaining its detectability. This chapter concludes with a study detailing how the recovery of ManLAM affects the clinical accuracy of an ELISA test designed for TB diagnostics when assaying patient samples. Chapter 3 describes a novel chemical-based, resonance-enhancing substrate for SERRS detection that has the potential to improve assay sensitivity while also beginning to circumvent the requirement for sophisticated research-grade instrumentation. Chapter 4 builds on the theme of transitioning sophisticated laboratory-based diagnostics towards a PON platform through the validation of a handheld Raman spectrometer and its applicability in detecting and quantifying PILAM from a complex sample matrix. Finally, Chapter 5 includes a summation of the work described herein, as well as a brief discussion regarding future directions of this work and its context in the realm of infectious disease diagnostics, particularly with respect to improving the tools available for TB diagnostics.

1.8 References

1. World Health Organization, *Global Tuberculosis Report 2015*; **2015**.

2. World Health Organization, *Global Health Observatory (GHO) Data: Top 10 Causes of Death*; **2017**.

3. Harris, R. C.; Grandjean, L.; Martin, L. J.; Miller, A. J.; Nkang, J.-E. N.; Allen, V.; Khan, M. S.; Fielding, K.; Moore, D. A., The Effect of Early Versus Late Treatment Initiation After Diagnosis on the Outcomes of Patients Treated for Multidrug-resistant Tuberculosis: a Systematic Review. *BMC Infect. Dis.* **2016,** *16* (1), 193.

4. Schumacher, S. G.; Sohn, H.; Qin, Z. Z.; Gore, G.; Davis, J. L.; Denkinger, C. M.; Pai, M., Impact of Molecular Diagnostics for Tuberculosis on Patient-important Outcomes: a Systematic Review of Study Methodologies. *PLoS One* **2016,** *11* (3), e0151073.

5. Pai, N. P.; Vadnais, C.; Denkinger, C.; Engel, N.; Pai, M., Point-of-Care Testing for Infectious Diseases: Diversity, Complexity, and Barriers in Low-and Middle-Income Countries. *PLoS Med.* **2012,** *9* (9), e1001306.

6. Pai, M.; Minion, J.; Steingart, K.; Ramsay, A., New and Improved Tuberculosis Diagnostics: Evidence, Policy, Practice, and Impact. *Curr. Opin. Pulm. Med.* **2010,** *16* (3), 271-284.

7. Armbruster, D. A.; Pry, T., Limit of Blank, Limit of Detection and Limit of Quantitation. *Clin. Biochem. Rev.* **2008,** *29* (Suppl 1), S49-S52.

8. Lalkhen, A. G.; McCluskey, A., Clinical Tests: Sensitivity and Specificity. *Cont. Educ. Anaesth. Crit. Care Pain.* **2008,** *8* (6), 221-223.

9. EP17-A, N., Protocols for the Determination of Limits of Detection and Limits of Quantitation. *CLISI.* **2004,** *5*.

10. Moretti, M.; Sisti, D.; Rocchi, M. B.; Delprete, E., CLSI EP17-A Protocol: A Useful Tool for Better Understanding the Low End Performance of Total Prostate-Specific Antigen Assays. *Clin. Chim. Acta* **2011,** *412* (11), 1143-1145.

11. Theron, G.; Pooran, A.; Peter, J.; van Zyl-Smit, R.; Mishra, H. K.; Meldau, R.; Calligaro, G.; Allwood, B.; Sharma, S. K.; Dawson, R., Do Adjunct Tuberculosis Tests, When combined with Xpert MTB/RIF, Improve Accuracy and the Cost of Diagnosis in a Resource-Poor Setting? *Eur. Respir. J.* **2012,** *40* (1), 161-168.

12. Liong, M.; Hoang, A. N.; Chung, J.; Gural, N.; Ford, C. B.; Min, C.; Shah, R. R.; Ahmad, R.; Fernandez-Suarez, M.; Fortune, S. M., Magnetic Barcode Assay for Genetic Detection of Pathogens. *Nat. Commun.* **2013,** *4*, 1752.

13. Wang, S.; Lifson, M. A.; Inci, F.; Liang, L.-G.; Sheng, Y.-F.; Demirci, U., Advances in Addressing Technical Challenges of Point-of-Care Diagnostics in Resource-Limited Settings. *Expert Rev. Mol. Diagn.* **2016,** *16* (4), 449-459.

14. McNerney, R.; Daley, P., Towards a Point-of-Care Test for Active Tuberculosis: Obstacles and Opportunities. *Nat. Rev. Microbiol.* **2011,** *9* (3), 204-213.

15. Srivastava, S. K.; van Rijn, C. J. M.; Jongsma, M. A., Biosensor-Based Detection of Tuberculosis. *RSC Adv.* **2016,** *6* (22), 17759-17771.

16. Horton, J. B.; Hollier, L. H., The Current State of Health Care Reform: The Physicians' Burden. *Aesthetic Surg. J.* **2012,** *32* (2), 230-235.

17. Mabey, D.; Peeling, R. W.; Ustianowski, A.; Perkins, M. D., Tropical Infectious Diseases: Diagnostics for the Developing World. *Nat. Rev. Microbiol.* **2004,** *2* (3), 231-240.

18. Peeling, R. W.; Holmes, K. K.; Mabey, D.; Ronald, A., Rapid Tests for Sexually Transmitted Infections (STIs): The Way Forward. *Sex Transm. Infect.* **2006,** *82* (suppl 5), v1-v6.

19. Wu, G.; Zaman, M. H., Low-cost Tools for Diagnosing and Monitoring HIV Infection in Low-resource Settings. *Bull. W. H. O.* **2012,** *90* (12), 914-920.

20. Pai, M.; O'brien, R., New Diagnostics for Latent and Active Tuberculosis: State of the Art and Future Prospects. *Semin. Respir. Crit. Care Med.* **2008,** *29* (05), 560-568.

21. Araj, G. F., Comparative Performance of PCR-based Assay Versus Microscopy and Culture for the Direct Detection of *Mycobacterium tuberculosis* in Clinical Respiratory Specimens in Lebanon. *Int. J. Tubercul. Lung Dis.* **2000,** *4* (9), 877-881.

22. Levy, H., A Reevaluation of Sputum Microscopy and Culture in the Diagnosis of Pulmonary Tuberculosis. *Chest* **1989,** *95* (6), 1193-1197.

23. Organization, W. H., WHO Warns Against the Use of Inaccurate Blood Tests for Active Tuberculosis. *Saudi Med. J.* **2011,** *32* (10), 1095-1096.

24. World Health Organization, Commercial Serodiagnostic Tests for Diagnosis of Tuberculosis: *Policy Statement*. **2011**.

25. Steingart, K. R.; Ng, V.; Henry, M.; Hopewell, P. C.; Ramsay, A.; Cunningham, J.; Urbanczik, R.; Perkins, M. D.; Aziz, M. A.; Pai, M., Sputum Processing Methods to Improve the Sensitivity of Smear Microscopy for Tuberculosis: A Systematic Review. *Lancet Infect. Dis.* **2006,** *6* (10), 664-674.

26. Crawford, A. C.; Laurentius, L. B.; Mulvihill, T. S.; Granger, J. H.; Spencer, J. S.; Chatterjee, D.; Hanson, K. E.; Porter, M. D., Detection of the Tuberculosis Antigenic Marker Mannose-Capped Lipoarabinomannan in Pretreated Serum by Surface-enhanced Raman Scattering. *Analyst* **2017,** *142*, 186-196.

27. Laurentius, L. B.; Crawford, A. C.; Mulvihill, T. S.; Granger, J. H.; Robinson, R.; Spencer, J. S.; Chatterjee, D.; Hanson, K. E.; Porter, M. D., Importance of Specimen Pretreatment for the Low-level Detection of Mycobacterial Lipoarabinomannan in Human Serum. *Analyst* **2017,** *142* (1), 177-185.

28. Chatterjee, D.; Khoo, K.-H., Mycobacterial Lipoarabinomannan: An Extraordinary Lipoheteroglycan with Profound Physiological Effects. *Glycobiology* **1998,** *8* (2), 113-120.

29. Petzold, C. J.; Stanton, L. H.; Leary, J. A., Structural Characterization of Lipoarabinomannans from Mycobacterium tuberculosis and Mycobacterium smegmatis by ESI Mass Spectrometry. *J. Am. Soc. Mass Spectrom.* **2005,** *16* (7), 1109-1116.

30. Venisse, A.; Berjeaud, J. M.; Chaurand, P.; Gilleron, M.; Puzo, G., Structural Features of Lipoarabinomannan from Mycobacterium Bovis BCG. Determination of Molecular Mass by Laser Desorption Mass Spectrometry. *J. Biol. Chem.* **1993,** *268* (17), 12401-12411.

31. Khoo, K.-H.; Douglas, E.; Azadi, P.; Inamine, J. M.; Besra, G. S.; Mikušová, K.; Brennan, P. J.; Chatterjee, D., Truncated Structural Variants of Lipoarabinomannan in Ethambutol Drug-Resistant Strains of Mycobacterium smegmatis: Inhibition of Arabinan Biosynthesis by Ethambutol. *J. Biol. Chem.* **1996,** *271* (45), 28682-28690.

32. Singh, A. K.; Reyrat, J. M., Laboratory Maintenance of Mycobacterium smegmatis. *Curr. Prot. Microbio.* **2009**, 10C. 1.1-10C. 1.12.

33. Maura, R. B.; Férnandez, S.; Reyes, G.; Perez, J. L.; Reyes, F.; de los Angeles García, M.; Fariñas, M.; Infante, J. F.; Tirado, Y.; Puig, A., Evaluation of the Potential of Mycobacterium Smegmatis as Vaccine Candidate Against Tuberculosis by in Silico and in Vivo Studies. *VacciMonitor* **2010,** *19* (1), 20-26.

34. Mohan, A.; Padiadpu, J.; Baloni, P.; Chandra, N., Complete Genome Sequences of a Mycobacterium smegmatis Laboratory Strain (MC2 155) and Isoniazid-Resistant (4XR1/R2) Mutant Strains. *Genome Announcements* **2015,** *3* (1).

35. Waagmeester, A.; Thompson, J.; Reyrat, J.-M., Identifying Sigma Factors in Mycobacterium Smegmatis by Comparative Genomic Analysis. *Trends Microbiol.* **2005,** *13* (11), 505-509.

36. Lawn, S. D., Point-of-Care Detection of Lipoarabinomannan (LAM) in Urine for Diagnosis of HIV-associated Tuberculosis: A State of the Art Review. *BMC Infect. Dis.* **2012,** *12* (1), 103.

37. Arias-Bouda, L. M. P.; Nguyen, L. N.; Ho, L. M.; Kuijper, S.; Jansen, H. M.; Kolk, A. H., Development of Antigen Detection Assay for Diagnosis of Tuberculosis Using Sputum Samples. *J. Clin. Microbiol.* **2000,** *38* (6), 2278-2283.

38. Al-Sayyed, B.; Piperdi, S.; Yuan, X.; Li, A.; Besra, G. S.; Jacobs, W. R.; Casadevall, A.; Glatman-Freedman, A., Monoclonal Antibodies to Mycobacterium Tuberculosis CDC 1551 Reveal Subcellular Localization of MPT51. *Tuberculosis* **2007,** *87* (6), 489-497.

39. Chatterjee, D.; Bozic, C. M.; McNeil, M.; Brennan, P. J., Structural Features of the Arabinan Component of the Lipoarabinomannan of Mycobacterium Tuberculosis. *J. Biol. Chem.* **1991,** *266* (15), 9652-9660.

40. Crawford, A. C. Surface-enhanced Raman Scattering for the Reliable and Reproducible Detection of Disease Antigens in Biologically Relevant Media. Dissertation, The University of Utah, **2016**.

41. Holborow, E., The Specificity of Serological Reactions (Revised Edition). *Immunology* **1964,** *7* (2), 195.

42. Mix, E.; Goertsches, R.; Zett, U. K., Immunoglobulins—Basic Considerations. *J. Neurol.* **2006,** *253* (5), v9-v17.

43. Catt, K.; Niall, H.; Tregear, G., Solid Phase Radioimmunoassay. *Nature* **1967,** *213* (5078), 825-827.

44. Diamandis, E. P.; Christopoulos, T. K., *Immunoassay*. Academic Press: **1996**.

45. Hemmilä, I., Fluoroimmunoassays and Immunofluorometric Assays. *Clin. Chem.* **1985,** *31* (3), 359-370.

46. Collins, W., *Alternative Immunoassays*. John Wiley and Sons Inc.: **1985**.

47. Price, C. P.; Newman, D. J., *Principles and Practice of Immunoassay*. Springer: **1991**.

48. Nargessi, R.; Landon, J., Indirect Quenching Fluoroimmunoassay. *Methods Enzymol.* **1981,** *74*, 60-79.

49. Lyon, L. A.; Musick, M. D.; Natan, M. J., Colloidal Au-enhanced Surface Plasmon Resonance Immunosensing. *Anal. Chem.* **1998,** *70* (24), 5177-5183.

50. Sun, B.; Xie, W.; Yi, G.; Chen, D.; Zhou, Y.; Cheng, J., Microminiaturized Immunoassays Using Quantum Dots as Fluorescent Label by Laser Confocal Scanning Fluorescence Detection. *J. Immunol. Methods* **2001,** *249* (1), 85-89.

51. Goldman, E.; Balighian, E.; Kuno, M.; Labrenz, S.; Anderson, G.; Mauro, J.; Mattoussi, H., Luminescent Quantum Dot-Adaptor Protein-Antibody Conjugates for Use in Fluoroimmunoassays. *Phys. Status Solidi B* **2002,** *229* (1), 407-414.

52. Hahn, M. A.; Tabb, J. S.; Krauss, T. D., Detection of Single Bacterial Pathogens with Semiconductor Quantum Dots. *Anal. Chem.* **2005,** *77* (15), 4861-4869.

53. Millen, R. L.; Kawaguchi, T.; Granger, M. C.; Porter, M. D.; Tondra, M., Giant Magnetoresistive Sensors and Superparamagnetic Nanoparticles: A Chip-scale Detection Strategy for Immunosorbent Assays. *Anal. Chem.* **2005,** *77* (20), 6581-6587.

54. Wang, S. X.; Li, G., Advances in Giant Magnetoresistance Biosensors with Magnetic Nanoparticle Tags: Review and Outlook. *IEEE Trans. Magn.* **2008,** *44* (7), 1687-1702.

55. Driskell, J. D.; Kwarta, K. M.; Lipert, R. J.; Porter, M. D.; Neill, J. D.; Ridpath, J. F., Low-level Detection of Viral Pathogens by a Surface-enhanced Raman Scattering Based Immunoassay. *Anal. Chem.* **2005,** *77* (19), 6147-6154.

56. Grubisha, D. S.; Lipert, R. J.; Park, H.-Y.; Driskell, J. D.; Porter, M. D., Femtomolar Detection of Prostate-specific Antigen: An Immunoassay Based on Surface-enhanced Raman Scattering and Immunogold Labels. *Anal. Chem.* **2003,** *75* (21), 5936-5943.

57. Rohr, T. E.; Cotton, T.; Fan, N.; Tarcha, P. J., Immunoassay Employing Surface-enhanced Raman Spectroscopy. *Anal. Biochem.* **1989,** *182* (2), 388-398.

58. Zhang, X.; Young, M. A.; Lyandres, O.; Van Duyne, R. P., Rapid Detection of an Anthrax Biomarker by Surface-enhanced Raman Spectroscopy. *J. Am. Chem. Soc.* **2005,** *127* (12), 4484-4489.

59. Granger, J.; Granger, M.; Firpo, M.; Mulvihill, S.; Porter, M., Toward Development of a Surface-enhanced Raman Scattering (SERS)-based Cancer Diagnostic Immunoassay Panel. *Analyst* **2013,** *138* (2), 410-416.

60. Van Weemen, B.; Schuurs, A., Immunoassay Using Antigen—enzyme Conjugates. *FEBS Lett.* **1971,** *15* (3), 232-236.

61. Lequin, R. M., Enzyme Immunoassay (EIA)/Enzyme-linked Immunosorbent Assay (ELISA). *Clin. Chem.* **2005,** *51* (12), 2415-8.

62. Wild, D., *The Immunoassay Handbook: Theory and Applications of Ligand Binding, ELISA and Related Techniques*. Newnes: **2013**.

63. Voller, A.; Bidwell, D., *The Enzyme Linked Immunosorbent Assay (ELISA). Vol. 2. A Review of Recent Developments with Abstracts of Microplate Applications*. MicroSystems Ltd, Summerfield House: Vale, Guernsey, Channel Islands, **1980**.

64. Josephy, P. D.; Eling, T.; Mason, R. P., The Horseradish Peroxidase-catalyzed Oxidation of 3, 5, 3', 5'-tetramethylbenzidine. Free Radical and Charge-transfer Complex Intermediates. *J. Biol. Chem.* **1982,** *257* (7), 3669-3675.

65. Crowther, J. R., *The ELISA Guidebook*. Human Press: **2001**; Vol. 149.

66. Wardley, R.; Crowther, J. R., *The ELISA: Enzyme-linked Immunosorbent Assay in Veterinary Research and Diagnosis*. Springer Science & Business Media: **1982**; Vol. 22.

67. Jenkins, S. H., Homogeneous Enzyme Immunoassay. *J. Immunol. Methods* **1992,** *150* (1-2), 91-97.

68. Tighe, P. J.; Ryder, R. R.; Todd, I.; Fairclough, L. C., ELISA in the Multiplex Era: Potentials and Pitfalls. *Proteomics: Clin. Appl.* **2015,** *9* (3-4), 406-422.

69. Granger, J. H.; Schlotter, N. E.; Crawford, A. C.; Porter, M. D., Prospects for Point-of-Care Pathogen Diagnostics Using Surface-enhanced Raman Scattering (SERS). *Chem. Soc. Rev.* **2016,** *45* (14), 3865-3882.

70. Moskovits, M., Surface-Enhanced Spectroscopy. *Rev. Mod. Phys.* **1985,** *57* (3), 783-826.

71. Kneipp, K.; Moskovits, M.; Kneipp, H., *Surface-enhanced Raman Scattering: Physics and Applications*. Springer: **2006**; Vol. 103.

72. Stiles, P.; Dieringer, J.; Shah, N.; Van Duyne, R., Surface-Enhanced Raman Spectroscopy. *Annual Review of Analytical Chemistry* **2008,** *1* (1), 601-626.

73. Okamoto, T.; Yamaguchi, I., Optical Absorption Study of the Surface Plasmon Resonance in Gold Nanoparticles Immobilized onto a Gold Substrate by Self-assembly Yechnique. *J. Phys. Chem. B* **2003,** *107* (38), 10321-10324.

74. Schatz, G. C.; Van Duyne, R. P., Electromagnetic Mechanism of Surface-Enhanced Spectroscopy. *Handb. Vib. Spectrosc.* **2002**.

75. Moskovits, M., Surface Roughness and the Enhanced Intensity of Raman Scattering by Molecules Adsorbed on Metals. *J. Chem. Phys.* **1978,** *69* (9), 4159-4161.

76. Kelly, K. L.; Coronado, E.; Zhao, L. L.; Schatz, G. C., The Optical Properties of Metal Nanoparticles: The Influence of Size, Shape, and Dielectric Environment. *J. Phys. Chem. B* **2003,** *107* (3), 668-677.

77. Park, H.-Y.; Driskell, J.; Kwarta, K.; Lipert, R.; Porter, M.; Schoen, C.; Neill, J.; Ridpath, J.; Kneipp, K.; Moskovits, M.; Kneipp, H., *Surface-enhanced Raman Scattering: Physics and Applications*. Springer: **2006**; Vol. 103, p 427-446.

78. Park, H.-Y.; Driskell, J. D.; Kwarta, K. M.; Lipert, R. J.; Porter, M. D.; Schoen, C.; Neill, J. D.; Ridpath, J. F., Ultrasensitive Imunoassays Based on Surface-Enhanecd Raman Scattering by Immunogold Labels. In *Surface-Enhanced Raman Scattering - Physics and Applications*, Kneipp, K.; Moskovits, M.; Kneipp, H., Eds. Springer: **2006**; pp 427-446.

79. McNay, G.; Eustace, D.; Smith, W. E.; Faulds, K.; Graham, D., Surface-enhanced Raman Scattering (SERS) and Surface-enhanced Resonance Raman Scattering (SERRS): A Review of Applications. *Appl. Spectrosc.* **2011,** *65* (8), 825-837.

80. Schatz, G. C., Theoretical Studies of Surface Enhanced Raman Scattering. *Acc. Chem. Res.* **1984,** *17* (10), 370-376.

81. Zeman, E. J.; Schatz, G. C., An Accurate Electromagnetic Theory Study of Surface Enhancement Factors for Silver, Gold, Copper, Lithium, Sodium, Aluminum, Gallium, Indium, Zinc, and Cadmium. *J. Phys. Chem.* **1987,** *91* (3), 634-643.

82. Sharma, B.; Frontiera, R.; Henry, A.-I.; Ringe, E.; Van Duyne, R., SERS: Materials, Applications, and the Future. *Mater. Today* **2012,** *15* (1-2), 16-25.

83. Driskell, J. D.; Lipert, R. J.; Porter, M. D., Labeled Gold Nanoparticles Immobilized at Smooth Metallic Substrates: Systematic Investigation of Surface Plasmon Resonance and Surface-enhanced Raman Scattering. *J. Phys. Chem. B* **2006,** *110* (35), 17444-17451.

84. Yoon, J. K.; Kim, K.; Shin, K. S., Raman Scattering of 4-aminobenzenethiol Sandwiched Between Au Nanoparticles and a Macroscopically Smooth Au Substrate: Effect of Size of Au Nanoparticles. *J. Phys. Chem. C* **2009,** *113* (5), 1769-1774.

85. Knight, M. W.; Wu, Y.; Lassiter, J. B.; Nordlander, P.; Halas, N. J., Substrates Matter: Influence of an Adjacent Dielectric on an Individual Plasmonic Nanoparticle. *Nano Lett.* **2009,** *9* (5), 2188-2192.

86. Kim, K.; Lee, H. B.; Yoon, J. K.; Shin, D.; Shin, K. S., Ag Nanoparticle-mediated Raman Scattering of 4-aminobenzenethiol on a Pt Substrate. *J. Phys. Chem. C* **2010,** *114* (32), 13589-13595.

87. Li, L.; Hutter, T.; Finnemore, A. S.; Huang, F. M.; Baumberg, J. J.; Elliott, S. R.; Steiner, U.; Mahajan, S., Metal Oxide Nanoparticle Mediated Enhanced Raman Scattering and its Use in Direct Monitoring of Interfacial Chemical Reactions. *Nano Lett.* **2012,** *12* (8), 4242-4246.

88. Mubeen, S.; Zhang, S.; Kim, N.; Lee, S.; Krämer, S.; Xu, H.; Moskovits, M., Plasmonic Properties of Gold Nanoparticles Separated from a Gold Mirror by an Ultrathin Oxide. *Nano Lett.* **2012,** *12* (4), 2088-2094.

89. Bantz, K.; Meyer, A.; Wittenberg, N.; Im, H.; Kurtuluş, Ö.; Lee, S.; Lindquist, N.; Oh, S.-H.; Haynes, C., Recent Progress in SERS Biosensing. *Phys. Chem. Chem. Phys.* **2011,** *13* (24), 11551-11567.

90. Porter, M. D.; Lipert, R.; Siperko, L.; Wang, G.; Narayanan, R., SERS as a Bioassay Platform: Fundamentals, Design, and Applications. *Chem. Soc. Rev.* **2008,** *37* (5), 1001-1011.

91. Wang, G.; Park, H.-Y.; Lipert, R. J.; Porter, M. D., Mixed Monolayers on Gold Nanoparticle Labels for Multiplexed Surface-Enhanced Raman Scattering Based Immunoassays. *Anal. Chem.* **2009,** *81* (23), 9643-9650.

92. Laing, S.; Gracie, K.; Faulds, K., Multiplex in Vitro Detection Using SERS. *Chem. Soc. Rev.* **2016,** *45* (7), 1901-1918.

93. Ni, J.; Lipert, R. J.; Dawson, G. B.; Porter, M. D., Immunoassay Readout Method Using Extrinsic Raman Labels Adsorbed on Immunogold Colloids. *Anal. Chem.* **1999,** *71* (21), 4903-4908.

94. Jentzsch, P. V.; Ramos, L. A.; Ciobotă, V., Handheld Raman Spectroscopy for the Distinction of Essential Oils Used in the Cosmetics Industry. *Cosmetics* **2015,** *2* (2), 162-176.

95. Roy, E. G.; Dentinger, C.; Robotham, C. In *Detection of Homemade Explosives Using Raman Excitation at 1064 nm*, Proc. SPIE 9454, Detection and Sensing of Mines, Explosive Objects, and Obscured Targets: **2015**, pp 94540U-94540U-5.

96. Zheng, J.; Pang, S.; Labuza, T. P.; He, L., Semi-Quantification of Surface-enhanced Raman Scattering Using a Handheld Raman Spectrometer: A Feasibility Study. *Analyst* **2013,** *138* (23), 7075-7078.

97. Tolaieb, B.; Constantino, C. J.; Aroca, R. F., Surface-enhanced Resonance Raman Scattering as an Analytical Tool for Single Molecule Detection. *Analyst* **2004,** *129* (4), 337-341.

98. Nie, S.; Emory, S. R., Probing Single Molecules and Single Nanoparticles by Surface-enhanced Raman Scattering. *Science* **1997,** *275* (5303), 1102-1106.

99. McCreery, R. L., *Raman Spectroscopy for Chemical Analysis*. John Wiley & Sons, Inc.: New York, 2000.

100. Stacy, A.; Van Duyne, R., Surface Enhanced Raman and Resonance Raman spectroscopy in a Non-aqueous Electrochemical Environment: Tris (2, 2′-

bipyridine) Ruthenium (II) Adsorbed on Silver from Acetonitrile. *Chem. Phys. Lett.* **1983,** *102* (4), 365-370.

101. Murgida, D. H.; Hildebrandt, P., Heterogeneous Electron Transfer of Cytochrome C on Coated Silver Electrodes. Electric Field Effects on Structure and Redox Potential. *J. Phys. Chem. B* **2001,** *105* (8), 1578-1586.

102. Faulds, K.; Jarvis, R.; Smith, W. E.; Graham, D.; Goodacre, R., Multiplexed Detection of Six Labelled Oligonucleotides Using Surface Enhanced Resonance Raman Scattering (SERRS). *Analyst* **2008,** *133* (11), 1505-1512.

103. Qian, X.; Peng, X.-H.; Ansari, D. O.; Yin-Goen, Q.; Chen, G. Z.; Shin, D. M.; Yang, L.; Young, A. N.; Wang, M. D.; Nie, S., In Vivo Tumor Targeting and Spectroscopic Detection with Surface-enhanced Raman Nanoparticle Tags. *Nat. Biotechnol.* **2008,** *26* (1), 83-90.

104. Rule, K. L.; Vikesland, P. J., Surface-enhanced Resonance Raman Spectroscopy for the Rapid Detection of Cryptosporidium Parvum and Giardia Lamblia. *Environ. Sci. Technol.* **2009,** *43* (4), 1147-1152.

105. Limaj, O.; Etezadi, D.; Wittenberg, N. J.; Rodrigo, D.; Yoo, D.; Oh, S.-H.; Altug, H., Infrared Plasmonic Biosensor for Real-time and Label-free Monitoring of Lipid Membranes. *Nano Lett.* **2016,** *16* (2), 1502-1508.

106. Braun, G.; Lee, S. J.; Dante, M.; Nguyen, T.-Q.; Moskovits, M.; Reich, N., Surface-enhanced Raman Spectroscopy for DNA Detection by Nanoparticle Assembly onto Smooth Metal Films. *J. Am. Chem. Soc.* **2007,** *129* (20), 6378-6379.

107. Chiu, M. L.; Lawi, W.; Snyder, S. T.; Wong, P. K.; Liao, J. C.; Gau, V., Matrix Effects—A Challenge Toward Automation of Molecular Analysis. *JALA.* **2010,** *15* (3), 233-242.

108. Tate, J.; Ward, G., Interferences in Immunoassay. *Clin. Biochem. Rev.* **2004,** *25* (2), 105-120.

109. Martin, E., *Concise Medical Dictionary*. Oxford University Press: USA, **2015**.

110. Issaq, H. J.; Xiao, Z.; Veenstra, T. D., Serum and Plasma Proteomics. *Chem. Rev.* **2007,** *107* (8), 3601-3620.

111. Psychogios, N.; Hau, D. D.; Peng, J.; Guo, A. C.; Mandal, R.; Bouatra, S.; Sinelnikov, I.; Krishnamurthy, R.; Eisner, R.; Gautam, B., The Human Serum Metabolome. *PLoS One* **2011,** *6* (2), e16957.

112. Wishart, D. S.; Tzur, D.; Knox, C.; Eisner, R.; Guo, A. C.; Young, N.; Cheng, D.; Jewell, K.; Arndt, D.; Sawhney, S., HMDB: the Human Metabolome Database. *Nucleic Acids Res.* **2007,** *35* (suppl 1), D521-D526.

113. Wishart, D. S.; Knox, C.; Guo, A. C.; Eisner, R.; Young, N.; Gautam, B.; Hau, D. D.; Psychogios, N.; Dong, E.; Bouatra, S., HMDB: a Knowledgebase for the Human Metabolome. *Nucleic Acids Res.* **2008,** *37* (suppl_1), D603-D610.

114. Wishart, D. S.; Jewison, T.; Guo, A. C.; Wilson, M.; Knox, C.; Liu, Y.; Djoumbou, Y.; Mandal, R.; Aziat, F.; Dong, E., HMDB 3.0—The Human Metabolome Database in 2013. *Nucleic Acids Res.* **2012**, gks1065.

115. Wild, D., *The Immunoassay Handbook*. Gulf Professional Publishing: **2005**.

116. Sarkar, P.; Biswas, D.; Sindhwani, G.; Rawat, J.; Kotwal, A.; Kakati, B., Application of Lipoarabinomannan Antigen in Tuberculosis Diagnostics: Current Evidence. *Postgrad. Med. J.* **2014**.

117. Dorman, S., Advances in the Diagnosis of Tuberculosis: Current Status and Future Prospects. *Int. J. Tubercul. Lung. Dis.* **2015,** (19(5)), 504-516.

118. Tessema, T. A.; Hamasur, B.; Bjune, G.; Svenson, S.; Bjorvatn, B., Diagnostic Evaluation of Urinary Lipoarabinomannan at an Ethiopian Tuberculosis Centre. *Scand. J. Infect. Dis.* **2001,** *33* (4), 279-284.

119. Vergne, I.; Gilleron, M.; Nigou, J., Manipulation of the Endocytic Pathway and Phagocyte Functions by Mycobacterium Tuberculosis Lipoarabinomannan. *Front. Cell. Infect. Microbiol.* **2014,** *4*.

120. Wood, R.; Racow, K.; Bekker, L.-G.; Middelkoop, K.; Vogt, M.; Kreiswirth, B.; Lawn, S., Lipoarabinomannan in Urine During Tuberculosis Treatment: Association with Host and Pathogen Factors and Mycobacteriuria. *BMC Infect. Dis.* **2012,** *12* (1), 47.

121. Lawn, S. D.; Gupta-Wright, A., Detection of Lipoarabinomannan (LAM) in Urine is Indicative of Disseminated TB with Renal Involvement in Patients Living with HIV and Advanced Immunodeficiency: Evidence and Implications. *Trans. R. Soc. Trop. Med. Hyg.* **2016,** *110* (3), 180-185.

122. Cox, J. A.; Lukande, R. L.; Kalungi, S.; Van Marck, E.; Van de Vijver, K.; Kambugu, A.; Nelson, A. M.; Colebunders, R.; Manabe, Y. C., Is Urinary Lipoarabinomannan the Result of Renal Tuberculosis? Assessment of the Renal Histology in an Autopsy Cohort of Ugandan HIV-Infected Adults. *PLoS One* **2015,** *10* (4), e0123323.

123. Sakamuri, R.; Price, D.; Lee, M.; Cho, S.; Barry, C.; Via, L.; Swanson, B.; Mukundan, H., Association of Lipoarabinomannan with High Density Lipoprotein in Blood: Implications for Diagnostics. *Tuberculosis* **2013,** *93* (3), 301-307.

124. Bhattacharya, A.; Ranadive, S. N.; Kale, M.; Bhattacharya, S., Antibody-Based Enzyme-Linked Immunosorbent Assay for Determination of Immune Complexes in Clinical Tuberculosis 1, 2. *Am. Rev. Respir. Dis.* **1986,** *134* (2), 205-209.

125. Simonney, N.; Molina, J.; Molimard, M.; Oksenhendler, E.; Lagrange, P., Circulating Immune Complexes in Human Tuberculosis Sera: Demonstration of Specific Antibodies Against Mycobacterium tuberculosis Glycolipid (DAT, PGLTb1, LOS) Antigens in Isolated Circulating Immune Complexes. *Eur. J. Clin. Invest.* **1997,** *27* (2), 128-134.

126. Samuel, A.; Ashtekar, M.; Ganatra, R., Significance of Circulating Immune Complexes in Pulmonary Tuberculosis. *Clin. Exp. Immunol.* **1984,** *58* (2), 317.

127. Mehta, P.; Khuller, G., Comparative Evaluation of the Diagnostic Significance of Circulating Immune Complexes and Antibodies to Phosphatidylinositomannosides in Pulmonary Tuberculosis by Enzyme-linked Immunosorbent Assay. *Med. Microbiol. Immunol.* **1989,** *178* (4), 229-233.

128. Harris, D. C., *Quantitative Chemical Analysis*. Macmillan: **2010**.

129. Burgess, R. R., Protein Precipitation Techniques. *Methods Enzymol.* **2009,** *463*, 331-342.

130. Pinto, M.; Morange, M.; Bensaude, O., Denaturation of Proteins During Heat Shock. In Vivo Recovery of Solubility and Activity of Reporter Enzymes. *J. Biol. Chem.* **1991,** *266* (21), 13941-13946.

131. Sawyer, W. H.; Puckridge, J., The Dissociation of Proteins by Chaotropic Salts. *J. Biol. Chem.* **1973,** *248* (24), 8429-8433.

132. Stoscheck, C.; Deutscher, M. P., Quantitation of Protein: Guide to Protein Purification. *Methods in Enzymilogy* **1990,** *182*, 50-68.

133. Scopes, R. K., *Protein Purification: Principles and Practice*. Springer: **1994**.

134. Bajorath, J.; Saenger, W.; Pada Pal, G., Autolysis and Inhibition of Proteinase K, a Subtilisin-Related Serine Proteinase Isolated From the Fungus Tritirachium Album Limber. *Biochim. Biophys. Acta. Protein. Struct. Mol. Enzymol.* **1988,** *954* (1988), 176-182.

135. Hansen, J. N., Isolation of Higher Molecular Weight DNA from Bacillus Cereus T Using Proteinase K. *Prep. Biochem.* **1974,** *4* (6), 473-488.

136. Yang, H.; Amft, M.; GrundwÜrmer, J. M.; Li, X.; Grotemeyer, J., Primary Structures of Proteins Characterized by Proteinase K Digestion and Matrix-Assisted Laser Desorption/Ionization Mass Spectrometry. *J. Pept. Sci.* **1997,** *50* (5), 402-406.

137. Honore-Bouakline, S.; Vincensini, J.; Giacuzzo, V.; Lagrange, P.; Herrmann, J., Rapid Diagnosis of Extrapulmonary Tuberculosis by PCR: Impact of Sample Preparation and DNA Extraction. *J. Clin. Microbiol.* **2003,** *41* (6), 2323-2329.

138. Anderson, A., Factors Affecting the Amount and Composition of the Serum Seromucoid Fraction. *Nature* **1965,** *208* (5009), 491-492.

139. Sivaraman, T.; Kumar, T.; Jayaraman, G.; Yu, C., The Mechanism of 2, 2, 2-trichloroacetic Acid-induced Protein Precipitation. *J. Protein Chem.* **1997,** *16* (4), 291-297.

140. Thurlkill, R. L.; Grimsley, G. R.; Scholtz, J. M.; Pace, C. N., pK Values of the Ionizable Groups of Proteins. *Protein Sci.* **2006,** *15* (5), 1214-1218.

141. Pace, C. N.; Grimsley, G. R.; Scholtz, J. M., Protein Ionizable Groups: pK Values and Their Contribution to Protein Stability and Solubility. *J. Biol. Chem.* **2009,** *284* (20), 13285-13289.

142. Kauzmann, W., Some Factors in the Interpretation of Protein Denaturation. *Adv. Prot. Chem.* **1959,** *14*, 1-63.

143. Zhang, Y.; Cremer, P. S., Interactions Between Macromolecules and Ions: The Hofmeister Series. *Curr. Opin. Chem. Biol.* **2006,** *10* (6), 658-663.

144. Rajalingam, D.; Loftis, C.; Xu, J. J.; Kumar, T. K. S., Trichloroacetic Acid-induced Protein Precipitation Involves the Reversible Association of a Stable Partially Structured Intermediate. *Protein Sci.* **2009,** *18* (5), 980-993.

145. Goto, Y.; Takahashi, N.; Fink, A. L., Mechanism of Acid-induced Folding of Proteins. *Biochemistry* **1990,** *29* (14), 3480-3488.

146. Burston, D.; Tombs, M.; Apsey, M.; Maclagan, N., The Perchloric Acid Soluble Basic and Acidic Proteins of the Cytoplasm: Variation in Cancer. *Br. J. Cancer* **1963,** *17* (1), 162.

147. Fic, E.; Kedracka-Krok, S.; Jankowska, U.; Pirog, A.; Dziedzicka-Wasylewska, M., Comparison of Protein Precipitation Methods for Various Rat Brain Structures Prior to Proteomic Analysis. *Electrophoresis* **2010,** *31* (21), 3573-3579.

CHAPTER 2

INVESTIGATING METHODS TO IMPROVE THE DETECTION OF MANNOSE-CAPPED LIPOARABINOMANNAN FOR TUBERCULOSIS DIAGNOSTICS

2.1 Introduction

A recent report by the World Health Organization (WHO) estimates there were 1.37 million deaths associated with tuberculosis (TB) infections in 2015.[1] While timely treatment often results in positive patient outcomes (83% success rate for nondrug-resistant TB)[1], the early and accurate diagnosis of TB remains a significant technical barrier to reducing mortality. The impact of TB is especially burdensome in low- to middle-income countries (LMICs), where limited access to healthcare, economic barriers, and social stigma results in 1 in every 3 infected individuals remaining undiagnosed or unreported.[1-4] This unfortunate set of circumstances places the development of a rapid, accurate, and low-cost TB test as a vital step in ultimately reducing the consequences associated with TB infection.[5-6] This Chapter investigates the impact of sample treatment on an antigenic marker for the clinical diagnosis of TB patient samples, as a potential means to reduce the burden of disease associated with TB.

The most common point-of-need (PON) diagnostic test for TB screening used in LMICs today is sputum smear microscopy (SSM), a reflection of its relatively rapid turn-

around time, low cost, and ease of use.[7] This methodology, however, requires an advanced stage of infection in order to be effective, which severely limits its utility for early stage diagnosis.[7] The gold standard for TB diagnosis is bacterial culture of sputum samples.[1, 8] While having a high clinical accuracy, this method has a turnaround time of a few weeks, requires a sophisticated laboratory infrastructure for effective implementation, and cannot diagnose extrapulmonary TB, which accounts for ~10% of all TB cases.[9-11] New nucleic acid amplification tests (NAATs) also have a high level of diagnostic accuracy and have shown promise in detecting patients with extrapulmonary TB, but their high cost and limited ease of use continue to hinder their widespread usage in PON applications.[12-15]

In light of these challenges, a number of recent studies have focused on the development of tests for the direct detection of primary antigenic markers of *Mycobacterium tuberculosis* (Mtb), the causative agent of TB, in serum, urine, and other body fluids.[16-18] One marker in particular, mannose-capped lipoarabinomannan (ManLAM), has been the subject of several investigations regarding its utility as a clinical marker for TB infection.[19-26] ManLAM is a highly branched lipoglycan (17.3±5.0 kDa) that makes up roughly 40% of the mycobacterium cell wall. [27-31] While the exact structure (*e.g.,* degree of branching and extent of capping motifs) can vary somewhat, a representative structure of ManLAM is shown in scheme 2.1.[27-29, 32] The potential value of ManLAM as a marker arises from the fact that it is unique to mycobacteria and it is a major virulence factor in the infectious pathology of Mtb.[33-34] Moreover, ManLAM is readily shed from Mtb into the circulatory system, meaning the presence and quantity of ManLAM is strongly linked to active TB infection.[20, 30, 35-36]

Studies of the clinical accuracy of TB diagnosis for ManLAM have shown high

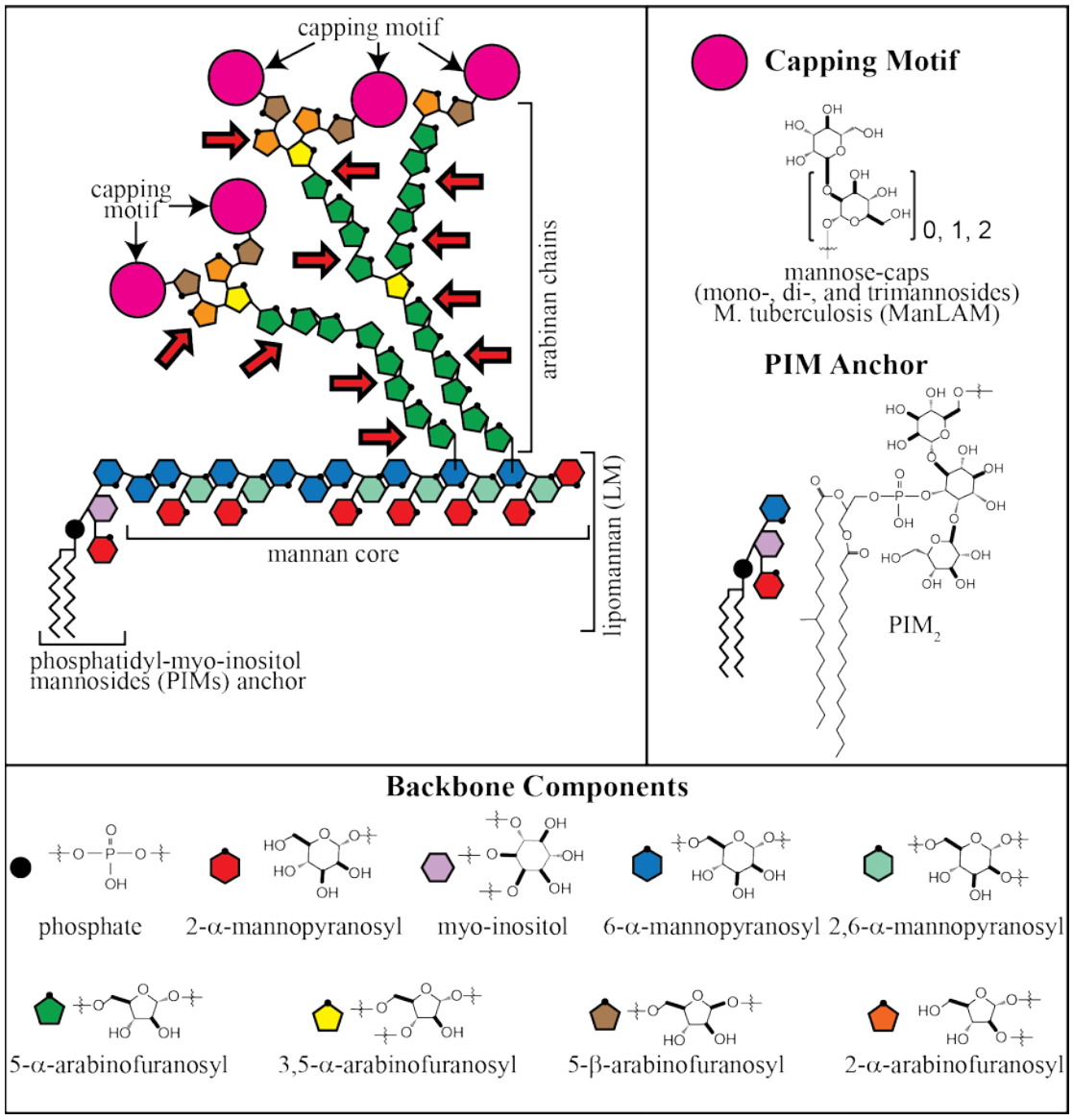

Scheme 2.1. Representative structure of lipoarabinomannan (LAM): (1) phosphatidylinositol mannoside (PIM_2) anchor, (2) mannan core, (3) arabinan side chains, and (4) capping motifs. The branching, capping motifs, and overall molecular weight vary somewhat across different mycobacteria. Mannose-capped LAM (ManLAM) is from *M. tuberculosis* and is used in this work. The red arrows indicate the 5-α-arabinofuranosyl and 2-α-arabinofuranosyl components, the groups most susceptible to acid hydrolysis (see discussion).

clinical specificities (*i.e.*, the reliability of a test to correctly identify a healthy patient as healthy), but widely varied clinical sensitivities (*i.e.*, the reliability of a test to correctly identify a sick patient as sick).[37-38] As we recently demonstrated, one important contributor to the poor clinical sensitivity of these measurements is the complexation of ManLAM with endogenous proteins and other constituents in serum, which hinders detection (capture and/or labeling) in a sandwich immunoassay.[20, 39-42]

Along these lines, we reported that the treatment of phospho-myo-inositol-capped lipoarabinomannan LAM (PILAM) that had been spiked into human serum with a perchloric acid (PCA) treatment process significantly improved the detection of PILAM in a sandwich immunoassay.[43] PILAM is a cell wall analog to ManLAM, but originates from *M. smegmatis*, which is frequently used as a nonpathogenic model organism for Mtb.[44-45] Our work demonstrated that denaturing the proteins in PILAM-spiked serum samples through acidification with PCA improves detection limits for this simulant by ~1500x.[43] We subsequently found that treatment of serum spiked with ManLAM and then processed with PCA enabled the detection of ManLAM at levels ~250x lower than that for the same samples in the absence of PCA treatment.[46] We also showed that when applying PCA treatment to a pilot set of TB patient specimens [24 TB-positive specimens (culture-confirmed), and 10 healthy controls], ManLAM was measurable in 21 of the 24 TB-positive specimens, but was not detectable in any of the healthy controls.[46] While recognizing that this study used a very small specimen set, these results provided important evidence for the potential utility of ManLAM as a TB marker and demonstrated the need for the further development of a sample treatment method to disrupt complexation and further enhance the detection of ManLAM in human serum.

This Chapter reports on ongoing efforts to delineate the impact of PCA treatment on the detection of ManLAM in serum using an enzyme-linked immunosorbent assay (ELISA)[47-50] (scheme 2.2). The goal of this work is to gain further insights into the possible pathways by which sample treatment improves ManLAM detection. The initial results from this effort indicate that while PCA treatment improved ManLAM detection, the amount of ManLAM actually measured was ~75% lower than spike in levels. We therefore hypothesized that there were three possible origins for this low recovery: (1) passivation of the capture surface by materials in the pretreated serum; (2) degradation of ManLAM due to its susceptibility to acid hydrolysis as investigated through filtration of degraded and intact ManLAM; [26-28, 51] and (3) the inability of PCA acidification to fully release ManLAM from complexation. The impact of each of these processes are investigated herein. The final aspect of this work explores the impact of ManLAM recovery from patient samples on the clinical accuracy of our test for active TB infection.

2.2 Experimental

2.2.1 Materials

Dulbecco's PBS buffer packs (10 mM PBS and 150 mM NaCl), StartingBlock (SB), 3,3′,5,5′-tetramethylbenzidine (TMB), and proteinase K (PK, 28.9 kDa) were purchased from Thermo Scientific. All buffers were prepared with 18.2 MΩ H_2O, purified by a Barnstead ultrapure water system. Dithiothreitol [(DTT) ≥ 99%] was purchased from Acros Organics and fresh 250 mM solutions were prepared in PBS buffer immediately before each experiment. Chloroform, Tween 20 (T20), 70% PCA, and potassium carbonate were acquired from Fisher Scientific. Trifluoroacetic acid, sodium borohydride, pyridine,

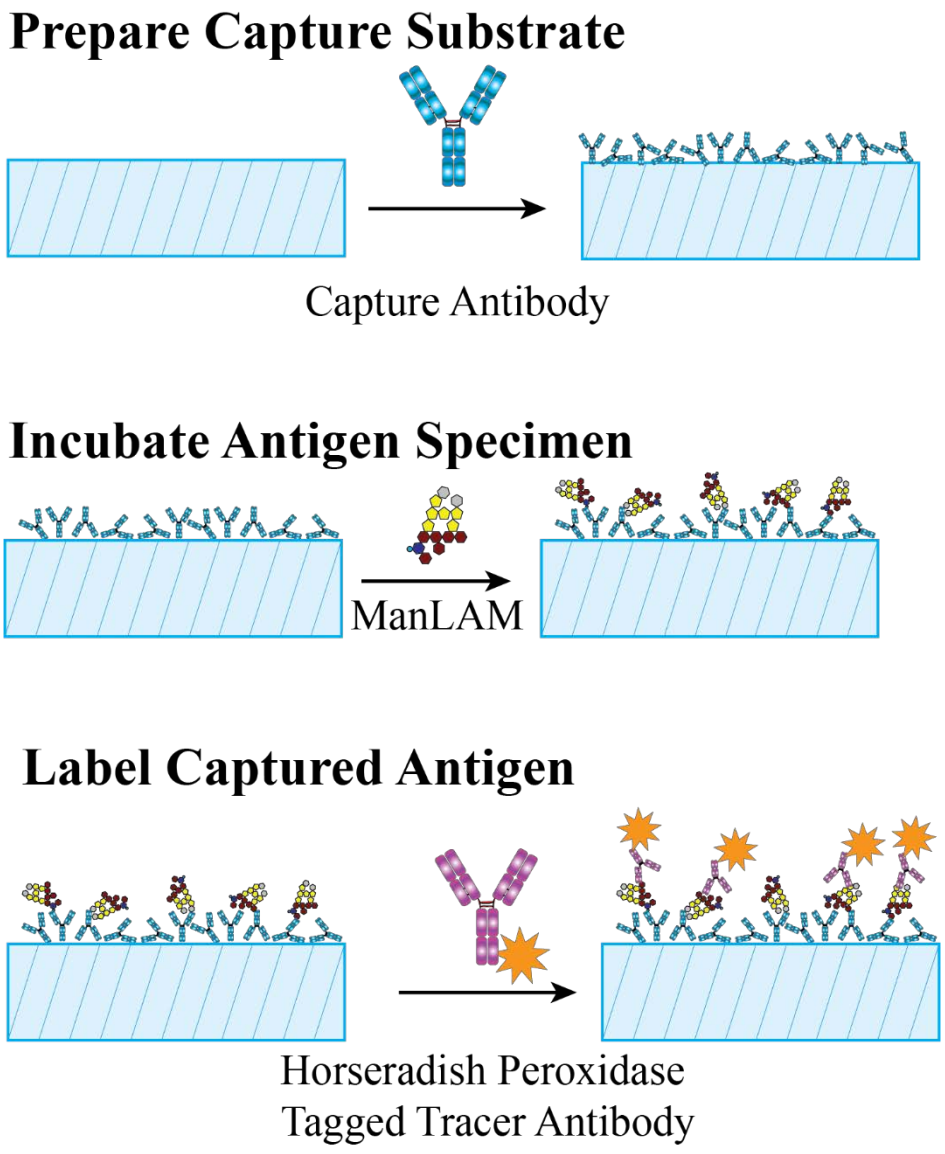

Scheme 2.2. Depiction of the enzyme-linked immunosorbent assay format including: (1) the antibody functionalized solid support; (2) the exposure to antigen-containing specimen; and (3) the subsequent labeling with a tracer antibody.

acetic anhydride, 3-OMe glucose, bovine serum albumin (BSA), and concentrated sulfuric acid were obtained from Sigma Aldrich. Sulfuric acid (2N) was prepared by dilution with purified water. High affinity polystyrene 96-well microplates (Costar 3590) were purchased from Corning International. Pooled AB human male serum, hereafter referred to simply as human serum, was acquired from Innovative Diagnostics Inc. Streptavidin-modified horseradish peroxidase (HRP) and microplate sealers were obtained from R&D Systems.

A VF-5ms (5% phenyl methylpolysiloxane) chromatography column was obtained from Agilent. $^{13}C_5$-D-arabinose was purchased from Cambridge Isotope Laboratories. A polyclonal rabbit antibody for Mtb (PABL), which served as the capture antibody, was acquired and used as received from Virostat (Cat. No. 4601). The ELISA tracer antibody, a monoclonal antibody (A194-01) for Mtb, was provided by Dr. Abraham Pinter at Rutgers University. ManLAM was isolated and purified by Dr. Delphi Chatterjee's laboratory at Colorado State University.[29, 52] Sulfo-NHS Biotin and Zeba Spin desalting columns, 0.5 mL sample volume with a molecular weight cut off (MWCO) filter of 7 kDa, were obtained from Thermo Scientific. Additional Amicon 3 kDa MWCO filters were acquired from EMD Millipore. A biotin quantification kit was purchased from Pierce Biotechnology and used following the package insert. TB-suspect patient samples were supplied by the Foundation for Innovative and New Diagnostics (FIND).

2.2.2 Enzyme-linked Immunosorbent Assay (ELISA)

ELISA experiments were performed using high affinity 96-well microplates. To prepare a functionalized capture surface, PABL was diluted to 10 µg/mL in PBS, and 100

µL of the diluted solution was added to each well. The plates were sealed and incubated at 2-8° C for ~16 h to coat the wells with physisorbed antibody. The plate was then placed in a VorTemp™ incubator and rocker platform at a temperature of 30 °C and rotated at 250 RPM for 30 min. The capture antibody solution was removed by aspiration and the microwells rinsed. The aspiration and rinse steps were performed between each of the following assay steps (*i.e.*, blocking, antigen incubation, labeling, and HRP incubation) using a BioTek MultiFlo™ FX automated plate washer. Each rinse cycle was repeated three times using 300 µL of PBS with 0.05% Tween 20 (PBST) (v/v) at a flow rate of 422 µL/s (~1.49 m/s). Next, 200 µL of SB was added to each well and incubated for 1 h in the VorTemp™ incubator and rocker platform (30 °C and 250 RPM) in order to passivate uncoated portions of the polystyrene surface. All subsequent steps (*i.e.*, antigen incubation, labeling, and HRP incubation) used the same conditions. ManLAM solutions for these experiments were prepared in PBS, PBS containing 1% BSA, and human serum with and without PCA treatment. After preparation, 100 µL of the ManLAM-containing samples were added to the plate and incubated for 2 h.

Biotinylation of the A194-01 monoclonal antibodies followed the EZ-Link Sulfo-NHS-Biotin standard protocol provided by Thermo Scientific.[53] In brief, a 10 mM sulfo-NHS biotin solution was added at 50 times molar excess to a 1 mg/mL (6.7×10^{-6} M) solution of antibody and kept on ice for 3 h. Excess biotin was removed using a Zeba Spin desalting column by centrifuging at 1358 *g* for 1 min. The concentration of antibody and extent of biotinylation was determined to be 1.01±0.01 mg/mL with a biotin-to-antibody ratio of 3.65:1, as measured using the Pierce biotin quantification kit. The modified A194-01 antibody was diluted to 200 ng/mL in PBS for the labeling step of the assay.

Captured ManLAM was labeled by adding 100 µL of the diluted tracer antibody to each well for 2 h. After the stock Streptavidin-HRP solution was diluted 1:200 in PBS, 100 µL of the solution was added to each well and incubated for 25 min. Color development was performed by adding 100 µL of TMB per well and incubating for an additional 25 min before the addition of 50 µL of a 2 N H_2SO_4 stop solution. The absorbance of the solution in the wells was immediately measured at 450 and 570 nm using a BioTek ELx800™ plate reader. The reported absorbances equal the absorbance at 450 nm minus that at 570 nm.

2.2.3 Acid Treatment Procedure

The PCA treatment of ManLAM-spiked serum samples has been described in our previous work.[43, 46] In brief, the samples are acidified to pH ~1 in order to denature serum proteins through the addition of 4 µL of PCA per 100 µL of sample. The samples are then vortexed for 10 s and immediately centrifuged at ~12,000 g for 5 min to pellet denatured proteins and other aggregated materials. A portion of the resulting clear supernatant containing the ManLAM is transferred to a new microcentrifuge tube that contains 9 µL of 2.0 M K_2CO_3 per 100 µL of starting sample volume to neutralize the samples to pH ~7.5. These samples are then stored at 2-8 ºC for 60 min to accelerate precipitation of $KClO_4$, after which the samples are centrifuged for 5 min at 270 g to ensure the precipitate has settled. The ManLAM-containing supernatant is transferred to a new microcentrifuge tube and brought to ambient laboratory temperature prior to running the assay.

2.2.4 Proteinase K (PK) Treatment Method

In brief, stock solutions of 250 mM DTT and 20 mg/mL PK were prepared in PBS ~30 min before use. PK and DTT were added to the samples to final concentrations of 200 µg/mL and 5.0 mM, respectively. The overall change in sample volume was ~1%. The samples were incubated for 60 min using the VorTemp™ at 50° C and 250 RPM. PK was then inactivated by heating the solution to 95-100° C for 10 min, which also promotes the noncovalent aggregation of denatured serum proteins.[54-56] Finally, the samples were centrifuged at 12,000 g for 10 min, after which the clear, ManLAM-containing supernatant was transferred to a new microcentrifuge tube. The solution was equilibrated to ambient laboratory conditions before running the assay for ManLAM.

2.2.5 Carbohydrate Analysis Using Gas Chromatography-Mass Spectrometry (GC-MS)

To examine the potential degradation of ManLAM by PCA treatment, experiments were designed to test for the most likely ManLAM hydrolysis products [*i.e.*, fragments from the arabinan side chain (scheme 2.1)].[26-28, 51, 57-59] For these measurements, ManLAM samples were prepared in PBS and divided into two 500 µL fractions; one fraction was subjected to PCA treatment and the other to the same processing steps, but PBS was used in place of the PCA treatment reagents. The samples were then passed through a 3 kDa MWCO filter to separate intact ManLAM from any degradation products. This approach separates the degradation products below the 3 kDa cutoff of the filter from those above the cutoff and intact ManLAM. In other words, the membrane retains intact ManLAM and larger fragments, while the smaller, degraded fractions pass through the membrane. The

filtration step was carried out a total of 4 times through a 3 kDa MWCO filter at 1398 *g* for 10 min. After the first filtration, the next three filtrations replenished the fluid phase by the addition of 200 µL of H_2O. The filtrate and the retentate after the final filtration were collected separately and lyophilized. $^{13}C_5$-D-arabinose (1.0 µg) and 3-OMe glucose (1.0 µg) were added to each sample as internal standards for arabinose and mannose, respectively.

The alditol acetate derivatization process used for the GC-MS analysis of arabinose and mannose, and the method for using the internal standards have been detailed elsewhere.[26, 57] Briefly, the samples undergo alditol acetate derivatization per the following steps: (1) trifluoroacetic acid [(TFA) 2 M] hydrolysis; (2) reduction with $NaBH_4$; and (3) acetylation with pyridine and acetic anhydride. The samples were then partitioned between water and chloroform, and the organic layer, which contains the derivatized materials, was collected. Finally, the samples were dried under high purity N_2 and reconstituted in 100 µL chloroform (HPLC grade) for analysis by GC-MS.

GC-MS analyses were carried out using a Varian CP 3800 gas chromatograph coupled to a MS320 mass spectrometer fitted with a J&W VF5ms (5% phenyl methylpolysiloxane) capillary column (30 m x 0.25 mm x 0.25 µm) column. The oven temperature upon injection was held at 100 °C for 1 min, and then ramped at 20 °C/min to 150 °C, 5 °C/min to 240 °C, and, finally, at 30 °C/min to 300 °C. The arabinose and the $^{13}C_5$-arabinose internal standards have characteristic ions at *m/z* 217 and 220, respectively. The quantity of these two compounds was determined from the extracted ion chromatogram (EIC). The quantity of the mannose and 3-OMe glucose was determined using the total ion chromatogram (TIC). The amounts of arabinose and mannose, both of

which are indicative of the amount of ManLAM in a sample, were determined from the intensity ratio of the *m/z* peaks for arabinose and mannose relative to those of $^{13}C_5$-arabinose and 3-OMe glucose, respectively. Next, the peak ratios were multiplied by the mass of added $^{13}C_5$-arabinose and 3-OMe glucose, which was 1000 ng for each. To account for the higher ion abundance of mannose relative to 3-OMe glucose, the resultant peak ratio was divided by a response factor of 1.44. Because ManLAM is composed of ~60% arabinose and ~40% mannose, the measured quantities of these two species can be used to calculate the original amount of ManLAM in the PCA-treated and untreated sample factions.[26, 60-61]

2.2.6 Patient Sample Cohort

Anonymized archived patient serum samples were provided by FIND. These samples were collected from adult male and female patients with TB-suspect symptoms from clinics in South Africa, Vietnam, and Peru. The samples were separated into serum and subsequently frozen (-80° C) shortly after collection. Each sample was analyzed to determine HIV and TB status; TB status was based on SSM, bacterial culture and chest x-ray (if available). For the analysis described herein, 106 total patient samples were analyzed with 54 TB-positive and 52 TB-negative based on the results from the bacterial culture tests.

The assay results were analyzed using the methods described in our previous works.[46, 62] In brief, the patient samples were analyzed in duplicate, due to the small volumes available. A patient sample was designated TB-positive if the signal response for each duplicate was greater than the limit of detection (LOD) and TB-negative if the

response for each duplicate was below the LOD. In the few instances where there was disagreement between the replicates for a given patient sample, the sample was marked as indeterminate and removed from subsequent analysis. The LOD is the calculated ManLAM concentration which produces an absorbance distinguishable from samples devoid of ManLAM (blanks) ; LOD is described by equation 2.1.

$$LOD = A_{Blank} + 3 * \sigma_{Blank} \quad (2.1)$$

where A_{Blank} is the average absorbance for the blank samples and σ_{Blank} denotes the standard deviation from replicate measurements.

The performance of the assay as a diagnostic tool is described by its clinical accuracy.[63] Clinical accuracy is defined by two metrics, clinical sensitivity and clinical specificity. Clinical sensitivity is a measure of how accurately a diagnostic test correctly determines infected patients as being infected, and is defined as the number of true positives (TPs) (*i.e.,* correctly identifying an infected patient) divided by the sum of TPs plus false negatives (FNs). An FN occurs when a sick patient is determined to be healthy. Clinical specificity is a measure of the how accurately a diagnostic test correctly determines a healthy patient as being healthy. In this case, the number of true negatives (TNs) (*i.e.*, correctly identifying a healthy patient) is divided by the sum of the TNs plus false positives (FPs). A false positive is a result that determines a healthy patient as being sick. These metrics are expressed as percent in equations 2.2 and 2.3.[63]

$$Sensitivity = \frac{TP}{TP + FN} \times 100 \quad (2.2)$$

$$Specificity = \frac{TN}{TN + FP} \times 100 \quad (2.3)$$

2.2.7 Ethical Statement

The anonymized TB-suspect patient samples used herein were provided by FIND and collected with informed consent in accordance with the protocols of the Declaration of Helsinki. The designated sample numbers used to index the samples are arbitrary and cannot be traced back to the patients. The Institutional Review Board at Colorado State University approved the study; and, as a pre-existing collection, the Institutional Review Board at the University of Utah considered the study described herein exempt from further review. None of the authors have access to any identifying patient information.

2.3 Results and Discussion

2.3.1 Measured ManLAM Recoveries from PCA-Treated and Untreated Samples

ManLAM was spiked into human serum or into PBS with 1% BSA and then diluted with the appropriate diluent to 1000, 500, 100, and 50 pg/mL. Sample blanks consisted of stock human serum or PBS with 1% BSA. The serum samples spiked with ManLAM were split in half. One half of these samples was PCA treated; the other half of samples used serum instead of PCA reagents. The remaining steps were identical for both subsets. The samples prepared in PBS with 1% BSA were processed the same way as the PCA-treated samples, except PBS with 1% BSA was used in place of the PCA treatment reagents. Due to dilution from PCA treatment, the final ManLAM concentrations in the spiked samples after the treatment process were 850, 425, 85, and 42.5 pg/mL.

Figure 2.1 shows the ELISA responses as a function of ManLAM concentration for the three different sample sets. As expected, the response increases as a function of

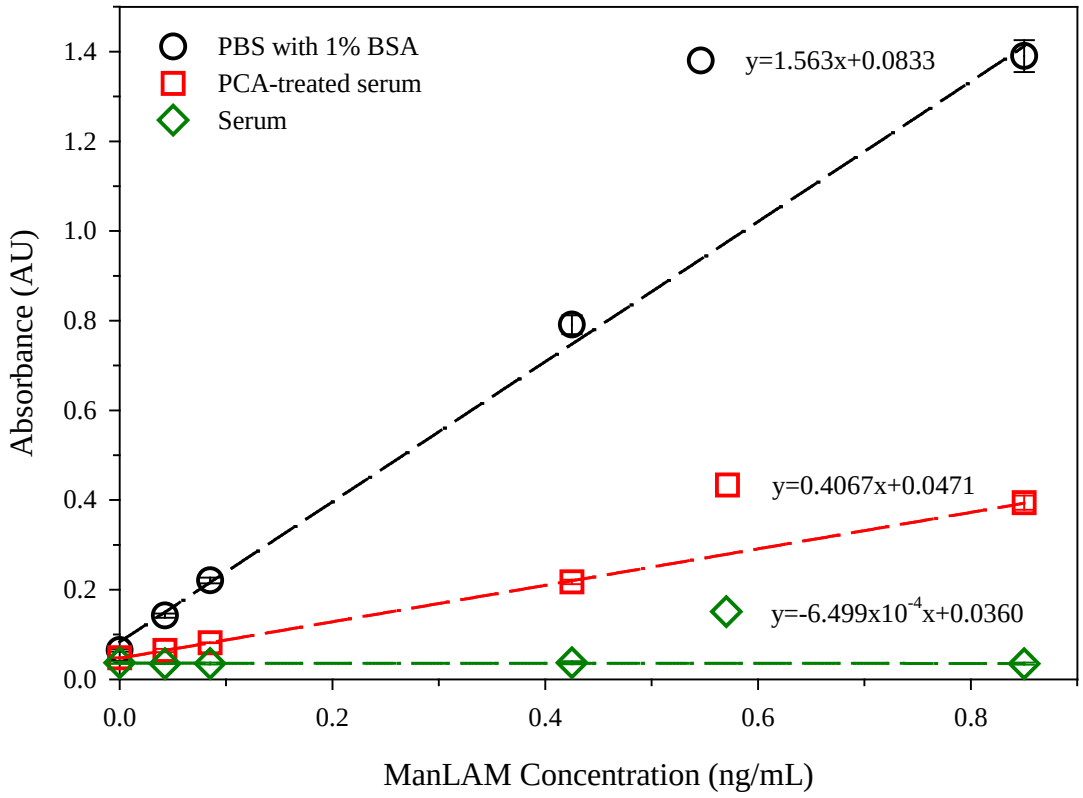

Figure 2.1. ELISA dose-response plots for ManLAM spiked into PBS containing 1% BSA (black), PCA-treated human serum (red), and whole serum (green).

ManLAM concentration for the samples in PBS with 1% BSA and in PCA-treated serum. However, the samples analyzed directly from untreated serum show no detectable concentration dependence (*i.e.*, all of the responses were statistically indistinguishable from that of blank serum the Student's t-test is applied). The untreated serum responses indicate that ManLAM is unable to bind to the capture surface and/or be effectively labeled after capture by the tracer antibody. After PCA treatment, however, there is a measurable dependence of the response by ELISA to ManLAM concentration. The difference between untreated whole serum and treated serum indicates that PCA treatment removes proteins that passivate the capture surface, which prevents ManLAM capture, and/or frees ManLAM from protein complexation, which enables its capture and labeling.

While there is a readily measurable response in the PCA-treated samples, the signal strengths are significantly lower than those for the ManLAM samples prepared in PBS with 1% BSA. In this example, the absorbance after PCA treatment for ManLAM spiked into serum at 850 pg/mL is only 28% of that for the sample prepared in PBS with 1% BSA at the same spike-in level, indicating suboptimal ManLAM recovery. Furthermore, replicate assays (n=5) with each sample concentration performed in triplicate have shown recoveries as low as ~10%, which resulted in an average recovery of 22±11% for initial ManLAM concentrations between 85 pg/mL and 1.0 ng/mL. The difference in assay performance is also evident from the fact that the analytical sensitivity (*i.e.*, slope of the linear least squares fitted calibration line) is a factor of ~4 lower in the treated serum samples relative to the PBS with 1% BSA samples. Taken together, these results indicate that PCA sample treatment significantly improves ManLAM detection over that of untreated serum, but that the overall recovery is low, only 22±11%, and highly varied.

As noted earlier, the lower response for the PCA-treated samples may be due to capture surface passivation and/or the ineffective decomplexation of ManLAM. It is also possible that the susceptibility of glycofuranosyl groups to acid hydrolysis[26-28, 51] alters the structure of ManLAM in a way that degrades the epitope sites used for antibody recognition. The next sections investigate the possible contributions of each pathway.

2.3.2 Capture Surface Passivation

There are a large number of components in human serum (*e.g.*, proteins, carbohydrates, and electrolytes) that can potentially passivate the immobilized capture antibodies and, therefore, limit ManLAM capture.[64-66] Our previous work showed that the total protein content remaining in a serum sample after PCA treatment was 4% (2 mg/mL) of that in as-received human serum (55 mg/mL). In other words, there is still a significantly higher amount (2 mg/mL) of protein relative to the ManLAM spike-in levels (≤1.0 ng/mL). To determine if surface passivation plays a role in the measurement, capture substrates were first blocked with PCA-treated serum or with whole serum. A set of substrates was also prepared using SB as a comparative reference. The three sets of wells were then exposed to ManLAM solutions prepared in PBS containing 1% BSA at concentrations of 0, 500, and 1000 pg/mL, and the remaining steps of the assay were conducted as described previously.

Figure 2.2 presents the dose-response curves obtained for three sets of samples. The plot for the capture surface treated with SB is nearly indistinguishable from that in figure 2.1, which demonstrates the level of assay-to-assay reproducibility. In contrast, the responses when blocking with whole serum are lower than those of the assay using SB as

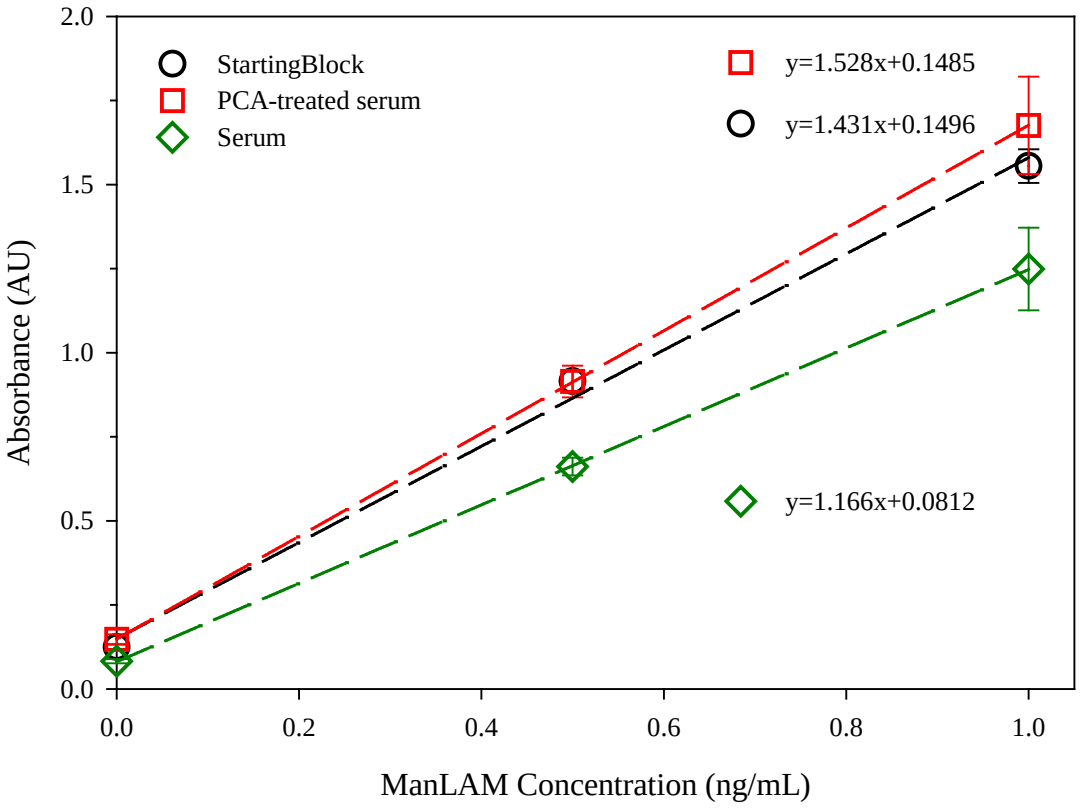

Figure 2.2. ELISA dose-response plots for capture substrates blocked with SB (black), PCA pretreated human serum (red), and untreated human serum (green). ManLAM solutions were prepared in PBS containing 1% BSA.

a blocker; an average decrease of 24±6% was observed for the 500 and 1000 pg/mL samples. Furthermore, the slope of the linear fit line when blocking with whole serum is 14% lower than that with SB blocking. This difference suggests that one or more components present in whole serum interfere with the ability of the capture surface to effectively bind ManLAM. These interactions appear to be relatively robust as the effects persist through the washing steps performed between the end of blocking and the step to capture ManLAM.

The PCA-treated serum samples, however, follow a response that is almost identical to that for ManLAM in PBS with 1% BSA. The analytical sensitivities for the two dose-response plots are statistically indistinguishable using a Student's t-test at a 95% confidence interval. This result indicates that, unlike the surface blocked with whole serum, the residual materials in the PCA-treated samples do not measurably passivate the surface or otherwise interfere with ManLAM capture. We can conclude that surface passivation is not a likely contributor to the diminished recovery of ManLAM from the PCA-treated serum samples (figure 2.1), and that the reduced signal observed is caused by other factors.

2.3.3 Acid Degradation of ManLAM

As noted, ManLAM has been found to be susceptible to acid hydrolysis, but the extent of the possible cleavage of its arabinose side chains due to PCA treatment has not yet been examined in detail.[28, 67-68] Preliminary data using a glycan microarray suggest that the capture antibody is selective to the arabinan side chains and mannose capping motifs (private communication with Todd Lowary, Dept. of Chemistry, University of Alberta, June 13, 2017).[69] As such, it is possible that any structural degradation of ManLAM could

lead to decreased ManLAM-antibody affinity, resulting in a lower ELISA signal, as observed in figure 2.1.[70]

To determine if the PCA treatment process alters the structure of ManLAM, carbohydrate analysis by GC-MS was performed on as-prepared and PCA-treated samples of ManLAM spiked into PBS. These samples were prepared in PBS devoid of BSA to eliminate protein content as a variable and to avoid the endogenous arabinose found in human serum (private communication with Prithwiraj De, Colorado State University, July 9, 2017). Our discussion of the analysis will assume that intact ManLAM remains in the retentate during the filtration step and that degradation products from acid hydrolysis pass through the filter (see section 2.2.5). By measuring the total arabinose and mannose content in all four sets of samples and by recognizing that ManLAM is composed of ~60% arabinose and ~40% mannose by weight, it is therefore possible to determine the total amount of ManLAM originally present in the sample and to qualitatively determine if PCA treatment degrades ManLAM. The typical sample recovery and LOD (absolute mass) for this method is ~95% and 500 pg, respectively.

The results from the GC-MS analysis are summarized in table 2.1, which includes the measured amounts of arabinose and mannose in the filtrate and retentate for the PCA-treated and untreated samples. The quantities of arabinose and mannose were used to calculate the initial amount of ManLAM in the samples. For the untreated samples, there was no detectable amount of arabinose or mannose in the filtrate, indicating that, in the absence of PCA-treatment, the structure of ManLAM is unaltered by the other solution processing steps.

The results for the PCA treated samples are markedly different. Arabinose is

Table 2.1. GC-MS results for samples of ManLAM prepared in PBS buffer with and without subsequent PCA treatment.

	Untreated Samples		PCA-treated Samples	
	Retentate (ng)	Filtrate (ng)	Retentate (ng)	Filtrate (ng)
Arabinose	12.6±3.9[†]	ND*	5.2±0.2	8.6±2.1
Calculated ManLAM from Arabinose	21.0±6.5	ND	8.7±0.3	14.1±2.1
Mannose	9.2±4.5	ND	9.0±0.3	ND
Calculated ManLAM from Mannose	23.0±11.2	ND	22.5±0.8	ND

[*]ND: Not detectable (*i.e.*, sample contains <500 pg).
[†]Errors represent the standard deviation of three replicate samples (n=3).

detectable in both the filtrate and retentate, whereas mannose is only measurable in the retentate. A little more than 60% (8.6±2.1 ng) of the total measured arabinose in the PCA-treated samples is found in the filtrate; the remaining 40% (5.2±0.2 ng) is in the retentate. This indicates that a significant portion of the arabinose groups in the side chains are cleaved during the PCA treatment process. The cleaved arabinose groups are most likely initially a mixture of monosaccharides and short (n=2 or 3) polysaccharides from the terminal ends of the side chains, which are further degraded to monosaccharides by TFA during the alditol acetate derivatization process.[27-28, 57-59] Unlike arabinose, mannose is only detected in the retentate of both the PCA treated and untreated samples, 9.0±0.3 and 9.2±4.5 ng, respectively. This indicates that the core mannan structure of ManLAM remains intact during the PCA treatment process and that the only detectable structural degradation occurs in the arabinan side chains.

Based on the measured arabinose and mannose content, the calculated amounts of intact ManLAM in the retentate of the untreated samples were 21.0±6.5 ng and 23.0±11.2 ng, respectively. The calculated intact ManLAM content in the retentate and filtrate of the PCA samples was 8.7±0.3 ng and 14.4±2.1 ng, respectively, based on the measured arabinose content. The ManLAM content determined from the total arabinose detected in both the filtrate and retentate was 23.1±1.9 ng. This is in good agreement with the calculated total ManLAM content, 22.5±0.8 ng, based on the measured mannose found in the retentate. The agreement of the mass of mannose and arabinose in the treated and untreated samples confirms the reliability of the GC-MS analysis.

To determine the effect of degradation on the ELISA measurements, a set of ManLAM dilutions were prepared in PBS and split into two equal volume fractions. Like

the GC-MS experiments, one set of fractions underwent PCA treatment and the other used PBS in place of the PCA treatment reagents. All remaining solution handling steps were the same for both fractions. These samples were prepared without BSA to remain consistent with the samples used for the GC-MS experiments. The ELISA dose-response plots from these measurements are presented in figure 2.3. The responses from the samples subjected to PCA treatment are significantly less than those from the untreated samples. In this case, PCA- treated ManLAM in PBS, samples have ~23% reduction in signal sensitivity compared to the untreated samples. However, replicate assays (n=5) have shown a loss of as much as 40% at ManLAM concentrations ≥ 42.5 pg/mL with an average of 26±10%, highlighting how the extent of ManLAM degradation may impact immunorecognition with the antibodies on the underlying capture surface.

Interestingly, the difference in the ELISA sample sets differs from the analogous results for the GC-MS analysis. The GC-MS data indicated that ~60% of the ManLAM was degraded by PCA treatment to a level sufficient to pass through a 3 kDa MWCO filter. While the implications are not yet clear, these results suggest that the assay detects a portion of the degraded ManLAM, most likely part of the degraded fraction remaining in the retentate. The ELISA results also support the conclusion that the degradation of ManLAM occurs primarily at the arabinose side chains because the capture antibody in particular recognizes structural elements on the side chain, rather than at the mannan core. Therefore, changes to the side chain structure would result in a reduction of the antibody binding affinity. The next section examines the contribution of decomplexation efficiency to the differences shown in figure 2.1.

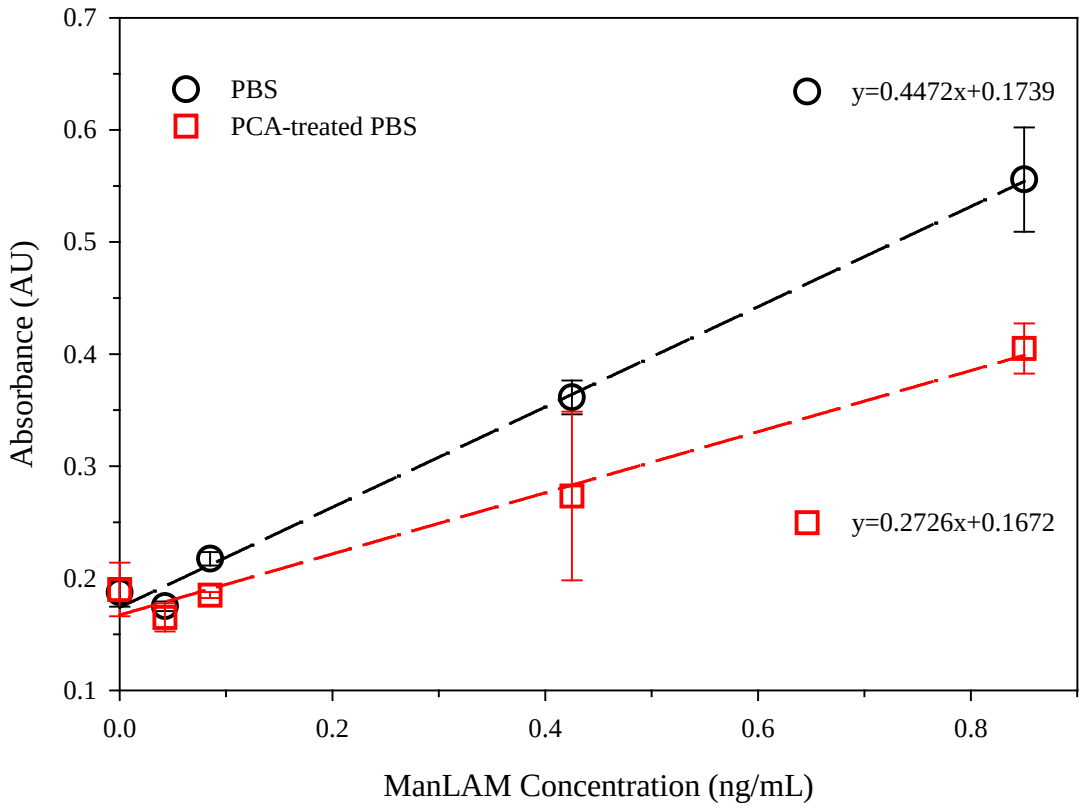

Figure 2.3. ELISA response for ManLAM spiked into PBS and for ManLAM spiked into PBS and then subjected to PCA treatment.

2.3.4 Extent of Decomplexation

In an effort to identify other possible cause(s) for reduced ManLAM recovery, we investigated another possible approach to disrupt ManLAM complexation without inducing ManLAM degradation. Serine proteases such as trypsin and PK are workhorses used for purifying a target from proteinaceous material and the isolation of DNA and RNA.[15, 71-73] PK is a nonspecific, broad spectrum, serine protease that targets only proteins and can effectively degrade proteins to short chain polypeptides ($n \geq 4$).[71-73] Following an established PK treatment, this section investigates the use of PK to break up ManLAM-protein complexation without inducing the ManLAM degradation observed in the PCA treatment procedure.[74] For this, ManLAM was spiked into whole serum and 10 mM PBS with 1% BSA from 42.5 pg/mL to 1.0 ng/mL plus a blank (0 pg/mL), and analyzed by ELISA. Portions of the samples prepared in whole serum were also PCA or PK treated before running ELISA. The as-is PBS with 1% BSA samples were used as the comparator for calculating ManLAM recovery factors.

As shown in figure 2.4, the ManLAM recovery is significantly larger when treated with PK compared to PCA. The recovery using PK treatment is 47±7% compared to 22±11% using PCA treatment. In figure 2.1, there is a ~65% loss of signal in the PCA pretreated samples; however, the loss is highly varied, indicating the importance of further characterizing the extent of ManLAM degradation as it relates to detection by immunorecognition. Taken together, the ELISA (figure 2.3) and the GC-MS results indicate the degradation of ManLAM accounts for 40-60% of the lost signal in figure 2.1. We therefore believe that the remaining ~10-25% of reduced signal is the result of incomplete decomplexation. Preliminary results from work aimed at fine tuning the PK

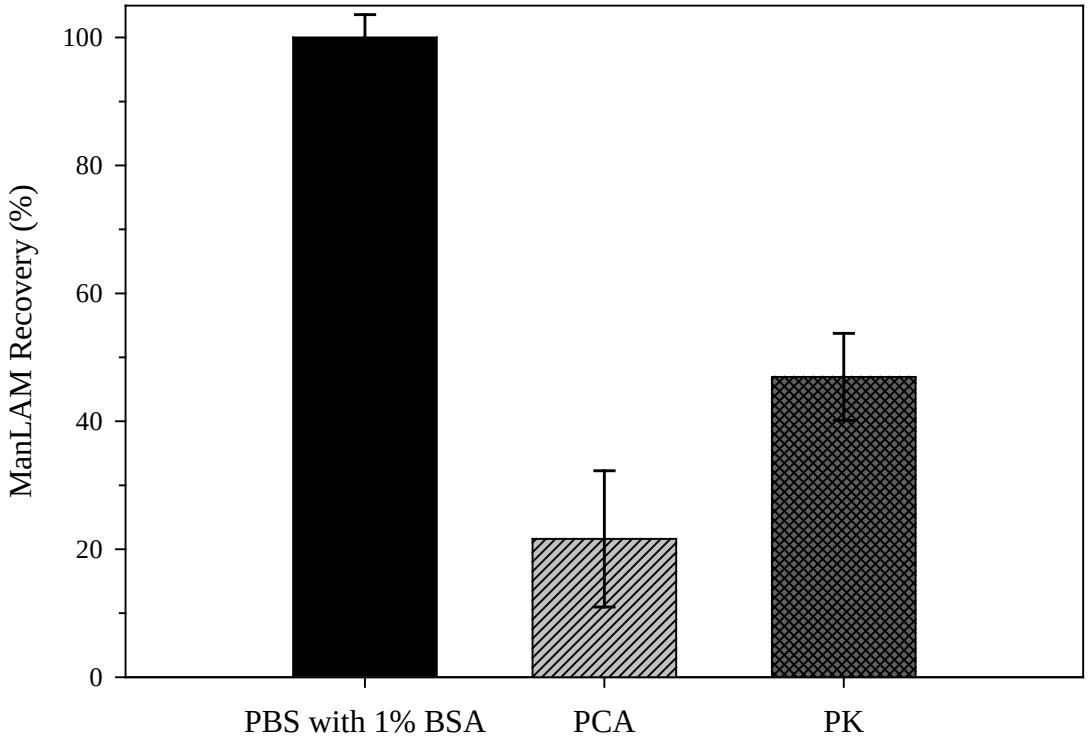

Figure 2.4. ManLAM recovery as a function of treatment type, normalized to response of ManLAM in PBS containing 1% BSA. On average, the samples treated with the proteinase K treatment method show a ~2x improvement (47±7% compared to 22±11%) in ManLAM recovery relative to PCA treatment. The average and standard deviations arise from averaging the calculated recovery for ManLAM spiked into serum and buffer samples from 85 pg/mL to 1.0 ng/mL for 5 PCA treatment assays and 3 proteinase K treatment assays, each run as triplicates.

digestion, which are beginning to show higher levels of ManLAM recovery, are consistent with this viewpoint. These results show that the search for an ideal treatment method has begun to bear fruit, but there appears to be room for improvement. To assess how these findings affect the clinical accuracy of a TB diagnostic test, the next section describes the analysis of a small set of patient samples that were TB-positive or TB-suspect, but ultimately negative by SSM and bacterial culture.

2.3.5 Impact of ManLAM Recovery on Clinical Accuracy

To test the impact of the higher level of ManLAM recovery found with PK treatment, comparative ELISA measurements were run on 106 TB-positive and TB-negative patient serum samples that were provided by FIND. Of the 106 patient samples, 57 were PCA treated and 49 were PK treated. Figure 2.5 summarizes the clinical accuracy results, as determined by our ELISA procedure, from the PCA-and PK-treated patient samples. The small volumes of each sample precluded side-by-side analysis using both PCA and PK treatment methods.

The results in figure 2.5 show that the clinical sensitivity of samples treated with PK are significantly greater by ~20% than that of the PCA treated samples, 77% of PK compared with 57% for PCA. This result supports the viewpoint that the improved signal recovery shown in figure 2.4 for the PK treatment method results in a notable improvement in clinical sensitivity. If ManLAM is liberated to a greater extent and without apparent degradation, TB-positive patients can be diagnosed using ManLAM as a marker with a higher degree of accuracy.

Clinical specificity also improves slightly with PK treatment relative to PCA-

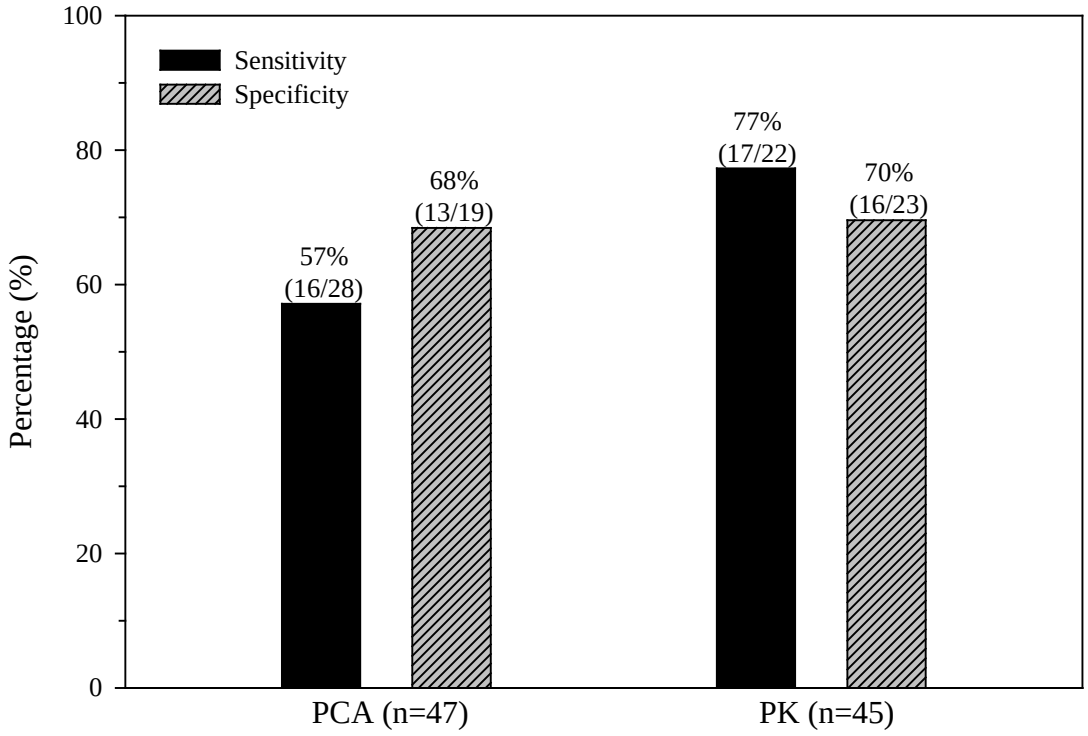

Figure 2.5. Clinical accuracy presented as percent sensitivity and specificity for patient samples analyzed by ELISA for ManLAM content after either PCA or PK treatment. Treatment with proteinase K improves the clinical sensitivity increases by ~20 % while the clinical specificity remains effectively unchanged.

treated samples (70% for PK compared to 68% for PCA). However, both methods measured ManLAM in some of the culture-negative samples, resulting in FPs. This may be due to the nonspecific adsorption of endogenous proteins present in the patient samples after treatment, but not in the control serum, which cross reacts with the labels, leading to unexpectedly high signals. It is important to note that all of the patient samples were from TB-suspect individuals, meaning that they were collected from patients presenting symptoms consistent with active TB infection in regions of the world where TB is endemic. We suspect a small fraction of the culture-negative samples may be missed by culture for two reasons.

First, a large number of individuals in the regions where the samples were collected are very likely to be latently infected with TB; in other words they are infected with TB bacilli, but are not actively infected.[1, 75] These patients would be negative from the SSM and bacterial culture test, but may have some level of bacterial loading in their bloodstream, leading to a measurable response in our assay and a positive diagnosis. Furthermore, ~10% of all TB infections are extrapulmonary. That is, Mtb enters the bloodstream and develops into active infections in the lymphatic system, larynx, spine, bone, or kidneys.[1, 76-79] Indeed, reports have shown that nonpulmonary manifestations of the disease cannot be detected by sputum sampling.[1, 8-11] Serum, to the contrary, is a reservoir of the products produced throughout the body, and several of the FPs for the detection of ManLAM are at levels well above the measurable LOD with either treatment method. To test these suspicions, a more in depth set of studies are needed which should also focus on nucleic acid amplification tests (NAATs) of the same serum samples to detect the presence of extrapulmonary TB.[15]

2.4 Conclusions

This work investigated the utility of PCA and PK treatment methods as a means to liberate ManLAM from complexation in human serum and, therefore, enhance its detection as a marker of active TB infection. Using either treatment method, the recovery of ManLAM is not quantitative (*i.e.*, >99.9%), but is significantly higher with PK compared to PCA. The effect of ManLAM recovery on the clinical accuracy of an ELISA test was also explored, using a small pilot set of patient samples in order to determine the relationship between recovery levels and clinical accuracy. Not surprisingly, higher levels of ManLAM using the PK treatment method resulted in a clear (~20%) improvement in the clinical sensitivity to 77%. Experiments aimed at optimizing the recovery of ManLAM with PK treatment are underway and we are working to establish linkages to serum specimens that used NAATs as part of the sample characterization.

2.5 References

1. World Health Organization, *Global Tuberculosis Report 2015*; **2015**.

2. Pai, M.; Minion, J.; Steingart, K.; Ramsay, A., New and Improved Tuberculosis Diagnostics: Evidence, Policy, Practice, and Impact. *Curr. Opin.Pulm. Med.* **2010,** *16* (3), 271-284.

3. Pai, N. P.; Vadnais, C.; Denkinger, C.; Engel, N.; Pai, M., Point-of-Care Testing for Infectious Diseases: Diversity, Complexity, and Barriers in Low-and Middle-Income Countries. *PLoS Med.* **2012,** *9* (9), e1001306.

4. Srivastava, S. K.; van Rijn, C. J. M.; Jongsma, M. A., Biosensor-Based Detection of Tuberculosis. *RSC Adv.* **2016,** *6* (22), 17759-17771.

5. Zumla, A.; Raviglione, M.; Hafner, R.; Fordham von Reyn, C., Tuberculosis. *N. Engl. J. Med.* **2013,** *368* (8), 745-755.

6. Steingart, K. R.; Henry, M.; Laal, S.; Hopewell, P. C.; Ramsay, A.; Menzies, D.; Cunningham, J.; Weldingh, K.; Pai, M., Commercial Serological Antibody Detection Tests for the Diagnosis of Pulmonary Tuberculosis: A Systematic Review. *PLoS Med.* **2007,** *4* (6), e202.

7. Steingart, K. R.; Ng, V.; Henry, M.; Hopewell, P. C.; Ramsay, A.; Cunningham, J.; Urbanczik, R.; Perkins, M. D.; Aziz, M. A.; Pai, M., Sputum Processing Methods to Improve the Sensitivity of Smear Microscopy for Tuberculosis: A Systematic Review. *Lancet Infect. Dis.* **2006,** *6* (10), 664-674.

8. Pai, M.; O'brien, R., New Diagnostics for Latent and Active Tuberculosis: State of the Art and Future Prospects. *Semin. Respir. Crit. Care Med.* **2008,** *29* (05), 560-568.

9. Perkins, M. D.; Cunningham, J., Facing the Crisis: Improving the Diagnosis of Tuberculosis in the HIV Era. *J. Infect. Dis.* **2007,** *196* (Supplement 1), S15-S27.

10. Norbis, L.; Alagna, R.; Tortoli, E.; Codecasa, L. R.; Migliori, G. B.; Cirillo, D. M., Challenges and Perspectives in the Diagnosis of Extrapulmonary Tuberculosis. *Exp. Rev. Anti-Infective Ther.* **2014,** *12* (5), 633-47.

11. Piccini, P.; Chiappini, E.; Tortoli, E.; de Martino, M.; Galli, L., Clinical Peculiarities of Tuberculosis. *BMC Infect. Dis.* **2014,** *14* (Suppl 1), S4.

12. Theron, G.; Pooran, A.; Peter, J.; van Zyl-Smit, R.; Mishra, H. K.; Meldau, R.; Calligaro, G.; Allwood, B.; Sharma, S. K.; Dawson, R., Do Adjunct Tuberculosis Tests, When combined with Xpert MTB/RIF, Improve Accuracy and the Cost of Diagnosis in a Resource-Poor Setting? *Eur. Respir. J.* **2012,** *40* (1), 161-168.

13. Wang, S.; Lifson, M. A.; Inci, F.; Liang, L.-G.; Sheng, Y.-F.; Demirci, U., Advances in Addressing Technical Challenges of Point-of-Care Diagnostics in Resource-Limited Settings. *Expert Rev. Mol. Diagn.* **2016,** *16* (4), 449-459.

14. McNerney, R.; Daley, P., Towards a Point-of-Care Test for Active Tuberculosis: Obstacles and Opportunities. *Nat. Rev. Microbiol.* **2011,** *9* (3), 204-213.

15. Honore-Bouakline, S.; Vincensini, J.; Giacuzzo, V.; Lagrange, P.; Herrmann, J., Rapid Diagnosis of Extrapulmonary Tuberculosis by PCR: Impact of Sample Preparation and DNA Extraction. *J. Clin. Microbiol.* **2003,** *41* (6), 2323-2329.

16. Abebe, F.; Holm-Hansen, C.; Wiker, H.; Bjune, G., Progress in Serodiagnosis of *Mycobacterium tuberculosis* Infection. *Scand. J. Immun.* **2007,** *66* (2-3), 176-191.

17. Reither, K.; Saathoff, E.; Jung, J.; Minja, L.; Kroidl, I.; Saad, E.; Huggett, J.; Ntinginya, E.; Maganga, L.; Maboko, L., Low Sensitivity of a Urine LAM-ELISA in the Diagnosis of Pulmonary Tuberculosis. *BMC Infect. Dis.* **2009,** *9* (1), 141.

18. Tucci, P.; González-Sapienza, G.; Marin, M., Pathogen-Derived Biomarkers for Active Tuberculosis Diagnosis. *Front. Microbiol.* **2014,** *5*, 549.

19. Chatterjee, D.; Khoo, K.-H., Mycobacterial Lipoarabinomannan: An Extraordinary Lipoheteroglycan with Profound Physiological Effects. *Glycobiology* **1998,** *8* (2), 113-120.

20. Lawn, S. D., Point-of-Care Detection of Lipoarabinomannan (LAM) in Urine for Diagnosis of HIV-associated Tuberculosis: A State of the Art Review. *BMC Infect. Dis.* **2012,** *12* (1), 103.

21. Sarkar, S.; Tang, X.; Das, D.; Spencer, J.; Lowary, T.; Suresh, M.; Nigou, J., A Bispecific Antibody Based Assay Shows Potential for Detecting Tuberculosis in Resource Constrained Laboratory Settings. *PLoS One* **2012,** *7* (2), e32340.

22. Hamasur, B.; Bruchfeld, J.; van Helden, P.; Källenius, G.; Svenson, S., A Sensitive Urinary Lipoarabinomannan Test for Tuberculosis. *PLoS One* **2015,** *10* (4), e0123457.

23. Drain, P.; Losina, E.; Coleman, S.; Giddy, J.; Ross, D.; Katz, J.; Walensky, R.; Freedberg, K.; Bassett, I., Diagnostic Accuracy of a Point-of-Care Urine Test for Tuberculosis Screening Among Newly-Diagnosed HIV-Infected Adults: A Prospective, Clinic-Based Study. *BMC Infect. Dis.* **2014,** *14* (1), 110.

24. Tessema, T. A.; Hamasur, B.; Bjune, G.; Svenson, S.; Bjorvatn, B., Diagnostic Evaluation of Urinary Lipoarabinomannan at an Ethiopian Tuberculosis Centre. *Scand. J. Infect. Dis.* **2001,** *33* (4), 279-284.

25. Kerkhoff, A. D.; Wood, R.; Vogt, M.; Lawn, S. D., Prognostic Value of a Quantitative Analysis of Lipoarabinomannan in Urine from Patients with HIV-Associated Tuberculosis. *PLoS One* **2014,** *9* (7), e103285.

26. De, P.; Amin, A. G.; Valli, E.; Perkins, M. D.; McNeil, M.; Chatterjee, D., Estimation of D-Arabinose by Gas Chromatography/Mass Spectrometry as Surrogate for Mycobacterial Lipoarabinomannan in Human Urine. *PLoS One* **2015,** *10* (12), e0144088.

27. Venisse, A.; Berjeaud, J. M.; Chaurand, P.; Gilleron, M.; Puzo, G., Structural Features of Lipoarabinomannan from Mycobacterium Bovis BCG. Determination of Molecular Mass by Laser Desorption Mass Spectrometry. *J. Biol. Chem.* **1993,** *268* (17), 12401-12411.

28. Chatterjee, D.; Bozic, C. M.; McNeil, M.; Brennan, P. J., Structural Features of the Arabinan Component of the Lipoarabinomannan of Mycobacterium Tuberculosis. *J. Biol. Chem.* **1991,** *266* (15), 9652-9660.

29. Torrelles, J. B.; Sieling, P. A.; Zhang, N.; Keen, M. A.; McNeil, M. R.; Belisle, J. T.; Modlin, R. L.; Brennan, P. J.; Chatterjee, D., Isolation of a Distinct Mycobacterium tuberculosis Mannose-capped Lipoarabinomannan Isoform Responsible for Recognition by CD1b-restricted T Cells. *Glycobiology* **2012,** *22* (8), 1118-27.

30. Arias-Bouda, L. M. P.; Nguyen, L. N.; Ho, L. M.; Kuijper, S.; Jansen, H. M.; Kolk, A. H., Development of Antigen Detection Assay for Diagnosis of Tuberculosis Using Sputum Samples. *J. Clin. Microbiol.* **2000,** *38* (6), 2278-2283.

31. Ortalo-Magne, A.; Dupont, M.-A.; Lemassu, A.; Andersen, A. B.; Gounon, P.; Mamadou, D., Molecular Composition of the Outermost Capsular Material of the Tubercle Bacillus. *Microbiology* **1995,** *141* (7), 1609-1620.

32. Crawford, A. C. Surface-enhanced Raman Scattering for the Reliable and Reproducible Detection of Disease Antigens in Biologically Relevant Media. Dissertation, The University of Utah, **2016**.

33. Chan, J.; Fan, X. D.; Hunter, S. W.; Brennan, P. J.; Bloom, B. R., Lipoarabinomannan, A Possible Virulence Factor Involved in Persistence of *Mycobacterium tuberculosis* Within Macrophages. *Infect. Immun.* **1991,** *59* (5), 1755-1761.

34. Moreno, C.; Mehlert, A.; Lamb, J., The Inhibitory Effects of Mycobacterial Lipoarabinomannan and Polysaccharides Upon Polyclonal and Monoclonal Human T Cell Proliferation. *Clin. Exp. Immunol.* **1988,** *74* (2), 206.

35. Glatman-Freedman, A.; Casadevall, A.; Dai, Z.; Jacobs, W. R.; Li, A.; Morris, S. L.; Navoa, J. A. D.; Piperdi, S.; Robbins, J. B.; Schneerson, R., Antigenic Evidence

of Prevalence and Diversity of Mycobacterium tuberculosis Arabinomannan. *J. Clin. Microbiol.* **2004,** *42* (7), 3225-3231.

36. Sada, E.; Aguilar, D.; Torres, M.; Herrera, T., Detection of Lipoarabinomannan as a Diagnostic Test for Tuberculosis. *J. Clin. Microbiol.* **1992,** *30* (9), 2415-2418.

37. Dorman, S., Advances in the Diagnosis of Tuberculosis: Current Status and Future Prospects. *Int. J. Tubercul. Lung. Dis.* **2015,** (19(5)), 504-516.

38. Sarkar, P.; Biswas, D.; Sindhwani, G.; Rawat, J.; Kotwal, A.; Kakati, B., Application of Lipoarabinomannan Antigen in Tuberculosis Diagnostics: Current Evidence. *Postgrad. Med. J.* **2014**.

39. Wood, R.; Racow, K.; Bekker, L.-G.; Middelkoop, K.; Vogt, M.; Kreiswirth, B.; Lawn, S., Lipoarabinomannan in Urine During Tuberculosis Treatment: Association with Host and Pathogen Factors and Mycobacteriuria. *BMC Infect. Dis.* **2012,** *12* (1), 47.

40. Sakamuri, R.; Price, D.; Lee, M.; Cho, S.; Barry, C.; Via, L.; Swanson, B.; Mukundan, H., Association of Lipoarabinomannan with High Density Lipoprotein in Blood: Implications for Diagnostics. *Tuberculosis* **2013,** *93* (3), 301-307.

41. Tessema, T.; Bjune, G.; Hamasur, B.; Svenson, S.; Bjorvatn, B.; Syre, H., Circulating Antibodies to Lipoarabinomannan in Relation to Sputum Microscopy, Clinical Features and Urinary Anti-lipoarabinomannan Detection in Pulmonary Tuberculosis. *Scand. J. Infect. Dis.* **2002,** *34* (2), 97-103.

42. Cox, J. A.; Lukande, R. L.; Kalungi, S.; Van Marck, E.; Van de Vijver, K.; Kambugu, A.; Nelson, A. M.; Colebunders, R.; Manabe, Y. C., Is Urinary Lipoarabinomannan the Result of Renal Tuberculosis? Assessment of the Renal Histology in an Autopsy Cohort of Ugandan HIV-Infected Adults. *PLoS One* **2015,** *10* (4), e0123323.

43. Laurentius, L. B.; Crawford, A. C.; Mulvihill, T. S.; Granger, J. H.; Robinson, R.; Spencer, J. S.; Chatterjee, D.; Hanson, K. E.; Porter, M. D., Importance of Specimen Pretreatment for the Low-level Detection of Mycobacterial Lipoarabinomannan in Human Serum. *Analyst* **2017,** *142* (1), 177-185.

44. Etienne, G.; Laval, F.; Villeneuve, C.; Dinadayala, P.; Abouwarda, A.; Zerbib, D.; Galamba, A.; Daffé, M., The Cell Envelope Structure and Properties of Mycobacterium smegmatis mc2155: Is There a Clue for the Unique Transformability of the Strain? *Microbiology* **2005,** *151* (6), 2075-2086.

45. He, Z.; De Buck, J., Cell Wall Proteome Analysis of Mycobacterium smegmatis Strain MC2 155. *BMC Microbiol.* **2010,** *10* (1), 1-10.

46. Crawford, A. C.; Laurentius, L. B.; Mulvihill, T. S.; Granger, J. H.; Spencer, J. S.; Chatterjee, D.; Hanson, K. E.; Porter, M. D., Detection of the Tuberculosis

Antigenic Marker Mannose-Capped Lipoarabinomannan in Pretreated Serum by Surface-enhanced Raman Scattering. *Analyst* **2017,** *142*, 186-196.

47. Engvall, E.; Perlmann, P., Enzyme-linked Immunosorbent Assay (ELISA) Quantitative Assay of Immunoglobulin G. *Immunochemistry* **1971,** *8* (9), 871-874.

48. Nilsson, B., Enzyme-linked Immunosorbent Assays. *Curr. Opin. Immunol.* **1990,** *2* (6), 898-904.

49. Lequin, R. M., Enzyme Immunoassay (EIA)/Enzyme-linked Immunosorbent Assay (ELISA). *Clin. Chem.* **2005,** *51* (12), 2415-8.

50. Ishikawa, E., Development and Clinical Application of Sensitive Enzyme Immunoassay for Macromolecular Antigens - A Review. *Clin. Biochem.* **1987,** *20* (6), 375-385.

51. Ludwiczak, P.; Brando, T.; Monsarrat, B.; Puzo, G., Structural Characterization of Mycobacterium tuberculosis Lipoarabinomannans by the Combination of Capillary Electrophoresis and Matrix-Assisted Laser Desorption/Ionization Time-of-Flight Mass Spectrometry. *Anal. Chem.* **2001,** *73* (10), 2323-2330.

52. Shi, L.; Zhou, R.; Liu, Z.; Lowary, T. L.; Seeberger, P. H.; Stocker, B. L.; Crick, D. C.; Khoo, K. H.; Chatterjee, D., Transfer of the First Arabinofuranose Residue to Galactan Is Essential for Mycobacterium Smegmatis Viability. *J. Bacteriol.* **2008,** *190* (15), 5248-55.

53. Malen, H.; Berven, F. S.; Softeland, T.; Arntzen, M. O.; D'Santos, C. S.; De Souza, G. A.; Wiker, H. G., Membrane and Membrane-associated Proteins in Triton-114 Extracts of Mycobacterium bovis BCG Identified Using a Combination of Gel-based and Gel-free Fractionation Strategies. *Proteomics* **2008,** *8*.

54. Burgess, R. R., Protein Precipitation Techniques. *Methods Enzymol.* **2009,** *463*, 331-342.

55. Pinto, M.; Morange, M.; Bensaude, O., Denaturation of Proteins During Heat Shock. In Vivo Recovery of Solubility and Activity of Reporter Enzymes. *J. Biol. Chem.* **1991,** *266* (21), 13941-13946.

56. Vermeer, A. W.; Norde, W., The Thermal Stability of Immunoglobulin: Unfolding and Aggregation of a Multi-domain Protein. *Biophys. J.* **2000,** *78* (1), 394-404.

57. Fujiwara, N.; Nakata, N.; Naka, T.; Yano, I.; Doe, M.; Chatterjee, D.; McNeil, M.; Brennan, P. J.; Kobayashi, K.; Makino, M., Structural Analysis and Biosynthesis Gene Cluster of an Antigenic Glycopeptidolipid from Mycobacterium Intracellulare. *J. Bacteriol.* **2008,** *190* (10), 3613-3621.

58. Petzold, C. J.; Stanton, L. H.; Leary, J. A., Structural Characterization of Lipoarabinomannans from Mycobacterium tuberculosis and Mycobacterium

smegmatis by ESI Mass Spectrometry. *J. Am. Soc. Mass Spectrom.* **2005,** *16* (7), 1109-1116.

59. Weber, P. L.; Gray, G. R., Structural and Immunochemical Characterization of the Acidic Arabinomannan of Mycobacterium smegmatis. *Carbohydr. Res.* **1979,** *74* (1), 259-278.

60. Hunter, S. W., Evidence for the Presence of a Phosphatidylinositol Anchor on the Lipoarabinomannan and Lipomannan of *Mycobacterium tuberculosis*. *J. Biol. Chem.* **1990,** *265* (16), 9272-9279.

61. Chatterjee, D.; Lowell, K.; Rivoire, B.; McNeil, M. R.; Brennan, P., Lipoarabinomannan of Mycobacterium tuberculosis. Capping with Mannosyl Residues in Some Strains. *J. Biol. Chem.* **1992,** *267* (9), 6234-6239.

62. Grubisha, D. S.; Lipert, R. J.; Park, H.-Y.; Driskell, J. D.; Porter, M. D., Femtomolar Detection of Prostate-specific Antigen: An Immunoassay Based on Surface-enhanced Raman Scattering and Immunogold Labels. *Anal. Chem.* **2003,** *75* (21), 5936-5943.

63. Lalkhen, A. G.; McCluskey, A., Clinical Tests: Sensitivity and Specificity. *Cont. Educ. Anaesth. Crit. Care Pain.* **2008,** *8* (6), 221-223.

64. Chiu, M. L.; Lawi, W.; Snyder, S. T.; Wong, P. K.; Liao, J. C.; Gau, V., Matrix Effects—A Challenge Toward Automation of Molecular Analysis. *JALA.* **2010,** *15* (3), 233-242.

65. Issaq, H. J.; Xiao, Z.; Veenstra, T. D., Serum and Plasma Proteomics. *Chem. Rev.* **2007,** *107* (8), 3601-3620.

66. Psychogios, N.; Hau, D. D.; Peng, J.; Guo, A. C.; Mandal, R.; Bouatra, S.; Sinelnikov, I.; Krishnamurthy, R.; Eisner, R.; Gautam, B., The Human Serum Metabolome. *PLoS One* **2011,** *6* (2), e16957.

67. Capon, B., Mechanism in Carbohydrate Chemistry. *Chem. Rev.* **1969,** *69* (4), 407-498.

68. BeMiller, J., Acid-catalyzed Hydrolysis of Glycosides. *Adv. Carbohydr. Chem.* **1967,** *22*, 25-108.

69. Tam, P.-H.; Lowary, T. L., Recent Advances in Mycobacterial Cell Wall Glycan Biosynthesis. *Curr. Opin. Chem. Biol.* **2009,** *13* (5), 618-625.

70. Kotani, S.; Kato, T.; Matsuda, T.; Kato, K.; Misaki, A., Chemical Structure of the Antigenic Determinants of Cell Wall Polysaccharide of Mycobacterium tuberculosis Strain H37Rv. *Biken J.* **1971,** *14* (4), 379-387.

71. Bajorath, J.; Saenger, W.; Pada Pal, G., Autolysis and Inhibition of Proteinase K, a Subtilisin-Related Serine Proteinase Isolated From the Fungus Tritirachium Album Limber. *Biochim. Biophys. Acta. Protein. Struct. Mol. Enzymol.* **1988,** *954* (1988), 176-182.

72. Hansen, J. N., Isolation of Higher Molecular Weight DNA from Bacillus Cereus T Using Proteinase K. *Prep. Biochem.* **1974,** *4* (6), 473-488.

73. Yang, H.; Amft, M.; GrundwÜrmer, J. M.; Li, X.; Grotemeyer, J., Primary Structures of Proteins Characterized by Proteinase K Digestion and Matrix-Assisted Laser Desorption/Ionization Mass Spectrometry. *J. Pept. Sci.* **1997,** *50* (5), 402-406.

74. Goldenberger, D.; Perschil, I.; Ritzler, M.; Altwegg, M., A Simple" Universal" DNA Extraction Procedure Using SDS and Proteinase K is Compatible with Direct PCR Amplification. *Genome Res.* **1995,** *4* (6), 368-370.

75. World Health Organization, WHO Warns Against the Use of Inaccurate Blood Tests for Active Tuberculosis. *Saudi Med. J.* **2011,** *32* (10), 1095-1096.

76. Peto, H. M.; Pratt, R. H.; Harrington, T. A.; LoBue, P. A.; Armstrong, L. R., Epidemiology of Extrapulmonary Tuberculosis in the United States, 1993–2006. *Clin. Infect. Dis.* **2009,** *49* (9), 1350-1357.

77. Lee, J. Y., Diagnosis and Treatment of Extrapulmonary Tuberculosis. *Tuberc. Respir. Dis.* **2015,** *78* (2), 47-55.

78. Daher, E. D. F.; da Silva Junior, G. B.; Barros, E. J. G., Renal Tuberculosis in the Modern Era. *Am. J. Trop. Med. Hyg.* **2013,** *88* (1), 54-64.

79. Eastwood, J. B.; Corbishley, C. M.; Grange, J. M., Tuberculosis and the Kidney. *J. Am. Soc. Nephrol.* **2001,** *12* (6), 1307-1314.

CHAPTER 3

VERSATILE APPROACH TO TUBERCULOSIS BIOMARKER DETECTION BY SURFACE-ENHANCED RESONANCE RAMAN SCATTERING

3.1 Introduction

Recent years have seen sharp growth in the use of surface-enhanced Raman scattering (SERS), with gold, silver, and a few other types of nanoparticles (NPs), as a detection methodology in immunoassays, as well as in a number of other bioanalysis areas.[1-3] Because the electromagnetic enhancement mechanism of SERS is sensitive to the size, composition, and degree of aggregation of these materials, and to the dielectric properties of the local environment, the development of an extensible, robust, and reproducible measurement is an immense challenge.[3-9] To address the challenges associated with improving the usability of SERS as an analytical technique, a number of research groups have developed highly ordered nanometric substrates (*e.g.*, 2-dimensional nanoparticle arrays, inverse opal structures, and nanolithographically produced 3-dimensional arrays such as pyramidal structures) to produce tunable and consistent enhancement factors.[10-12]

These nanofabricated SERS-enhancing substrates, however, suffer from several technical challenges.[13-16] First, fabricating these surfaces requires a high degree of technical

expertise and precise patterning hardware, and as such, can be a difficult and costly endeavor. Nanofabricated surfaces can also be affected in post processes, such as dicing and chemical etching. These processes can alter the carefully crafted surface structures and thus change the intended plasmonic properties.[13-16] Finally, forming surfaces with long-range order (*e.g.*, millimeters or centimeters) challenges the capabilities of current fabrication techniques.[13-16]

Herein, we seek to demonstrate how a chemically fabricated SERS-enhancing substrate can be used to increase the sensitivity of disease biomarker detection without the use of patterning processes. The basis for this enhancing surface arises from combining the enhancement effects typically associated with SERS with those of resonance Raman spectroscopy (RRS) in a phenomenon described as surface-enhanced resonance Raman spectroscopy (SERRS). With SERRS, the incoming excitation wavelength induces an electronic transition in the Ramanophore adsorbed on the gold substrate, which in this case is a layer of chemically modified cyanine 5 (Cy5).[12, 17-18] With SERS, large signal amplification arises from an electromagnetic enhancement mechanism due to the induction of localized surface plasmons in nanometric coinage metals (*i.e.*, gold and silver).[6, 8, 19]

Work previously performed in our laboratory centered on the optimization of relevant parameters, such as the use of gold nanoparticles with a tight size dispersity, reliable chemical functionalization, and the plasmonic interactions with the underlying gold surface, such that an enhancement factor of ~10^6 can be reproducibly obtained in an immunoassay using SERS.[20-22] Distinct from SERS, the enhancement mechanism associated with RRS and by extension, SERRS, arises when the excitation wavelength used during the measurement coincides with an electronic transition within the Ramanophore,

which increases the Raman scattering intensity by as much as another factor of 10^6.[12, 18] Previous work has realized single molecule detection using SERRS due to the multiplicative effects of electromagnetic and electronic enhancements to achieve reported enhancement factors as high as ~10^{14}.[12, 23] This Chapter details the fabrication and characterization of an enhancing substrate for a SERRS immunoassay. For this, a gold substrate is functionalized with a thiolated Cy5 adlayer, which has an electronic transition coinciding with the wavelength of the excitation source at 633 nm. An evaluation of this novel approach to immunoassays with respect to the sensitive detection of a disease biomarker indicative of active tuberculosis (TB) infection is also presented.

According to a recent report by the World Health Organization (WHO), it is estimated that 9.6 M people developed active TB infections in 2015, of which roughly one third were undiagnosed.[24] The cause for such a high level of undiagnosed patients largely reflects the difficulties in implementing existing testing methodologies (*i.e.*, sputum smear microscopy (SSM) and bacterial culture) in a point-of-need (PON) setting.[24-28] The current bacterial culture TB test requires a well-developed *in vitro* diagnostic laboratory infrastructure and skilled technicians and physicians to perform the test, has a long turnaround time, and is not capable of diagnosing extrapulmonary TB.[27, 29-30]

The challenges associated with developing an effective diagnostic approach for TB has caused a resurgence in developing tests to detect primary antigenic markers indicative of active infections. We recently described the development of a SERS immunoassay for the detection of mannose-capped lipoarabinomannan (ManLAM), a 17.3±5 kDa lipoglycan found in the cell wall of the *M. tuberculosis* bacteria.[31-34] Although the exact degree of branching is varied, ManLAM generally consists of a phosphatidylinositol mannoside

anchor linked with a mannose-capped region via an arabinomannan backbone (figure 3.1).[31, 34-36] We have also recently described how the incorporation of new handheld Raman spectrometers in the measurement hardware has the potential to facilitate the transition of this work from the research laboratory to a truly field-deployable platform by reducing the resource burden caused by complex and costly benchtop instrumentation (manuscript in preparation and Chapter 4). This Chapter continues to expand on this body of work by demonstrating the potential application of the SERRS immunoassay to quantitate levels of ManLAM in human serum. The potential utility of this new methodology in PON testing is also briefly discussed.

3.2 Experimental

3.2.1 Materials

Phosphate-buffered saline (PBS) packs (10 mM with 150 mM NaCl), borate buffer (BB) packs (50 mM), and dithiobis (succinimidyl propionate) (DSP) were purchased from Thermo Scientific. All buffers were prepared with 18.2 MΩ H_2O purified by a Barnstead ultrapure water system. Tween 20 (T20), StartingBlock™, 70% perchloric acid (PCA), potassium carbonate, and sodium chloride were obtained from Fisher Scientific. Bovine serum albumin (BSA), acetonitrile, and dimethyl sulfoxide were purchased from Sigma Aldrich. Octadecanethiol (ODT) and 2-aminoethanethiol (AET) were acquired from FLUKA. Deuterated 1-octadecane-d_{37}-thiol was obtained from C/D/N Isotopes. Polystyrene 24-well microplates and a two-component polydimethylsiloxane (PDMS) kit were purchased from Dow Corning. Solid PDMS transfer templates were made following package insert instructions. A UV-curable optical adhesive (#61) was obtained from

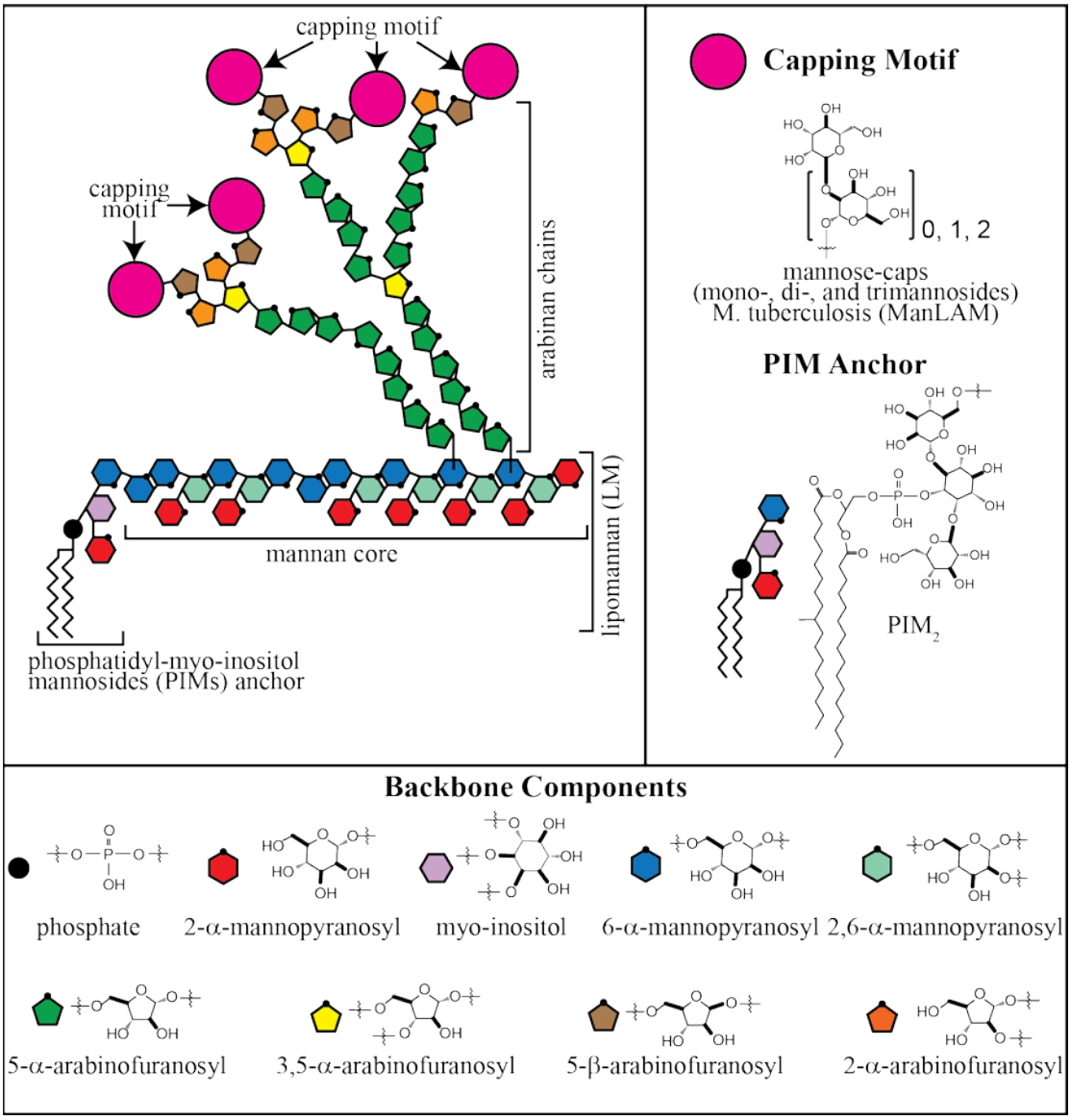

Figure 3.1. Generalized structure of lipoarabinomannan (LAM): (1) phosphatidylinositol mannoside (PIM_2) anchor, (2) mannan core, (3) arabinan side chains, and (4) capping motifs. The branching, capping agents, and overall molecular weight vary somewhat across different mycobacteria. Mannose-capped LAM (ManLAM) from *M. tuberculosis* is used throughout the work described herein.[37]

Norland and used per packaging instructions. Gold colloids (60 nm diameter, stock concentration of ~2 x10^{10} particles/mL) were acquired from BBI. Ethanol (200 proof) was purchased from Deacon Labs. Pooled AB human male serum, hereafter referred to as human serum, was obtained from Innovative Diagnostics, Inc. Mechanical-grade silicon wafers <1,1,1> were acquired from University Wafer. Gold shot (99.995% pure) was purchased from Alfa Aeser. Chrome-plated (99.9%) tungsten rods were acquired from Kurt J. Lesker Company.

The n-hydroxysuccinimide (NHS) ester of Cy5 was obtained from Lumiprobe and thiolated with AET following a procedure described elsewhere.[38-39] Glass microscope slides were purchased from Fisher Scientific and cut to 1x1 cm glass squares. The Raman reporter molecule (RRM), 5,5'-dithiobis (succinimidyl-2-nitrobenzoate) abbreviated as DSNB, was synthesized following procedures detailed elsewhere.[21] A polyclonal rabbit antibody for *M. tuberculosis* (Cat. No. 4601) was acquired from Virostat and used as the capture antibody. A monoclonal antibody specific to ManLAM (A194-01), was provided by Dr. Abraham Pinter at Rutgers University and used to selectively tag the capture ManLAM (see below). ManLAM was isolated and purified by Dr. Delphi Chatterjee at Colorado State University.[40-41]

3.2.2 Materials Fabrication and Sandwich Immunoassay Procedure

The general procedures for fabrication and functionalization of the substrates, extrinsic Raman labels (ERLs), and the sandwich immunoassay procedure, as overviewed in scheme 3.1, have been described in detail elsewhere.[2, 21, 42] In brief, template-stripped gold (TSG) was used as the supporting substrate. TSG was fabricated by coating a cleaned

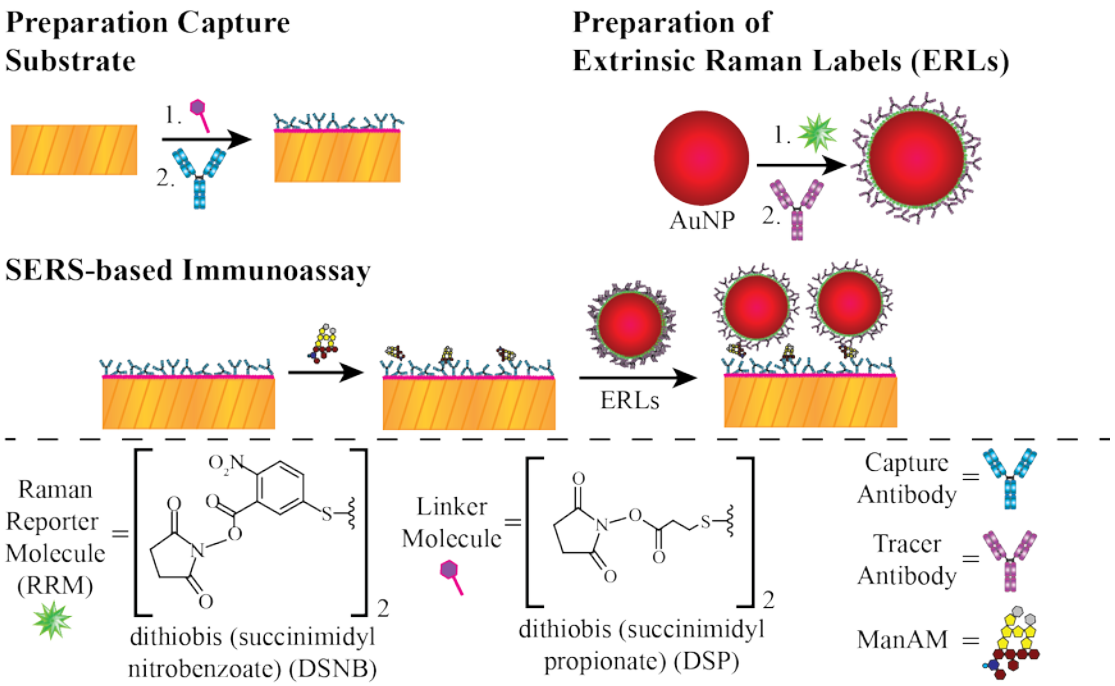

Scheme 3.1**.** Depicts the preparation of the extrinsic Raman labels (ERLs) and the active capture substrate, which are both prepared prior to performing the sandwich immunoassay for SERS readout. In brief, a sample is assayed for ManLAM content through sequential exposure to the capture substrate, followed by labeling with an ERL solution. The resulting nanoparticle-based sandwich is dried under ambient laboratory conditions and analyzed using a Raman microscope. The intensity of the signal arising from the Raman reporter molecule (RRM) on the ERL surface of the particle is used to indirectly determine the concentration of ManLAM in the sample.

silicon wafer with a 180-200 nm gold film using resistive evaporation at ≤ 0.1 nm/s. After cooling to room temperature, the wafers were removed from the evaporator and clean 1x1x0.1 cm glass squares were affixed to the surface using a UV-curable optical adhesive. The adhesive was cured with UV light for 3 h. Before use, the TSG substrates were carefully removed from the Si wafer, exposing the smooth gold film on the bottom side of the glass surface. Similarly, 25x75 mm glass microscope slides were coated with a ~200 nm gold film (10 nm chromium adhesion layer) at ≤0.1 nm/s.[43]

The clean gold surfaces were subsequently functionalized with a hydrophobic ODT adlayer by contact printing with a PDMS stamp that has a centered 2 mm hole. These stamps were immersed in an ethanolic solution of 1.0 mM ODT for 45 s, rinsed with ethanol, and dried with high purity nitrogen. The stamp was subsequently pressed onto the gold surface, creating a 2 mm diameter address of unmodified gold, surrounded by an ODT adlayer. This hydrophobic barrier defines the size of the capture address. Upon removing the PDMS stamp, the substrate was rinsed with EtOH and immersed in a 0.1 mM ethanolic DSP solution for 16 h. Finally, the samples were removed from the DSP solution, rinsed with EtOH, and dried with a stream of high purity nitrogen.

In the next step, substrates were individually arranged in the wells of a 24-well microplate. The substrates were functionalized by the addition of a 20 µL droplet of 10 µg/mL polyclonal anti-TB antibody (10 mM PBS) and then loaded into a humidity chamber. The humidity chamber was sealed and the antibody binding step proceeded for 60 min. After incubating, the substrates were rinsed with 10 mM PBS with 0.1% v/v Tween 20 (PBST), blocked with a 20 µL droplet of StartingBlock,™ and sealed in a humidity chamber for 60 min. The substrates were subsequently rinsed with 10 mM PBST and

exposed to antigen-containing solution (*i.e.*, 20 µL droplets of ManLAM spiked into either 10 mM PBS with 1% BSA (w/v) or human serum that subsequently underwent acid treatment), and the substrates were loaded in a humidity chamber and allowed to incubate for 3 h. To remove unbound or nonspecifically adsorbed antigen from the surface, the samples were rinsed with 2 mM BB with 0.1% v/v Tween 20 (BBT) with 150 mM NaCl, after which a 20 µL droplet of the ERL suspension was applied to each sample. As before, the samples were inverted in the humidity chamber and allowed to incubate overnight (~16 h). Finally, the unbound and nonspecifically adsorbed ERLs were rinsed from the surface with 2 mM BBT with 10 mM NaCl and allowed to dry under ambient laboratory conditions prior to Raman analysis.

The preparation of SERRS assay substrates, as shown in scheme 3.2, and assay procedure follow the same general outline as described above. However, the ODT-addressed TSG substrates were immersed in a 50 µM ethanolic thiol solution comprised of a 1:1 ratio of thiolated Cy5 and DSP as opposed to an ethanolic solution of only DSP. This result in the resonant Ramanophore forming an adlayer on the underlying gold substrate used in the assay. Further characterizations of the as-formed adlayers are described in section 3.3.1.

3.2.3 Preparation of Extrinsic Raman Labels

In the SERS immunoassay, the ERLs have two main functions: (1) to yield an intense Raman spectrum when irradiated with a suitable excitation source, and (2) to impart immunospecificity for the target biomarker.[2, 20-21] In the SERRS immunoassay presented herein, the gold NPs act as a specific label for the target biomarker through chemical

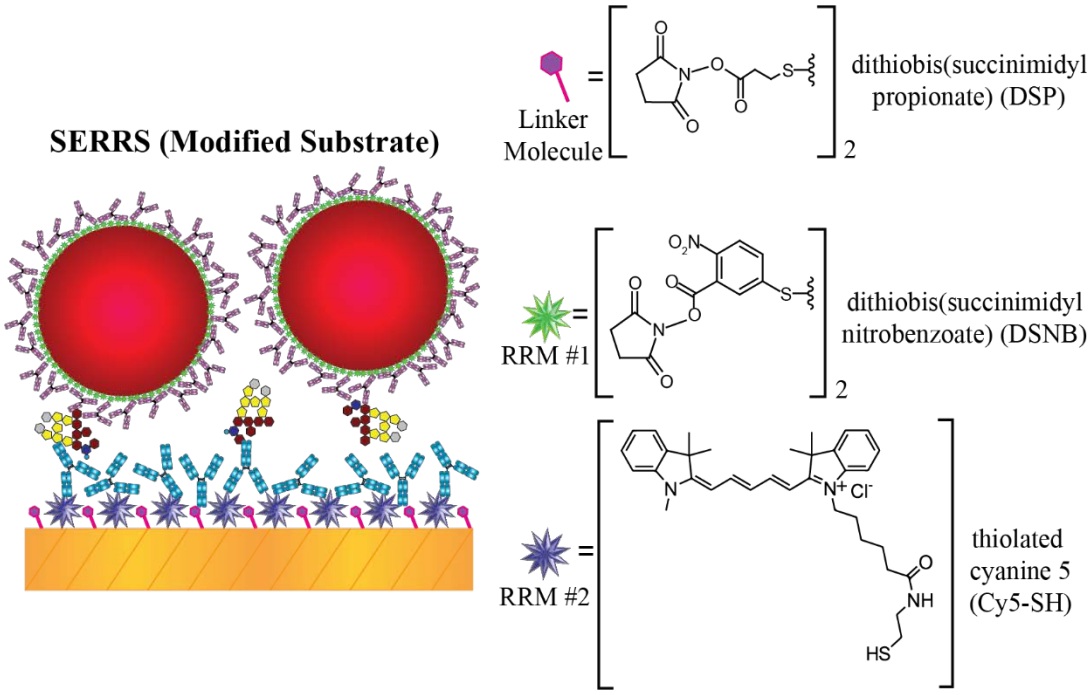

Scheme 3.2. Idealized scheme depicting the modification of a SERS assay (scheme 3.1) with the inclusion of a resonant Raman dye, thiolated cyanine 5, to make a surface-enhanced resonance Raman scattering (SERRS) immunoassay.

functionalization with a molecular recognition element, and also serve to enhance the signal of the resonance dye on the underlying assay substrate through plasmonic interactions when tagging the captured target.

The details concerning the reproducible preparation of ERLs have been described elsewhere.[2, 20-21] In brief, 1 mL of 60 nm gold colloids was combined with 40 µL of 50 mM BB to adjust the pH to 8.5; this suspension was then mixed with 13.7 µL of a 1.0 mM thiol solution DSNB in ACN. This solution was mixed through inversion for 30 s and then stored in a refrigerator at 2-8˚C for 90 min. Immunospecificity was imparted to the ERL through addition of 13.7 µL of a 100 µg/mL solution of the monoclonal A194-01 antibody in 10 mM PBS. This solution was briefly mixed by inversion for 30 s and stored at 2-8˚C for 90 min. The next step added 100 µL of a 10% BSA (w/v) solution in 2 mM BB at pH 8.5, which promoted colloidal stability and blocked unreacted binding sites. The ERL suspension was again mixed by inversion and stored at 2-8˚C for an additional 60 min. To remove excess functionalization reagents, the particles were centrifuged 3x for 10 min each at ~2000 *g*. The colorless supernatant was carefully removed from the ERL pellet after each centrifugation and the ERLs were re-suspended 2x with 1 mL of 1% BSA (w/v) in 2 mM BB at pH 8.5. The final resuspension concentrated the ERLs using 250 µL of 2% BSA (w/v) solution in 2 mM BB at pH 8.5. Finally, 25 µL of 10% NaCl (w/v) in H_2O was added to facilitate the colloidal stability.

3.2.4 Sample Treatment

Recent work has touched on the interactions that occur between ManLAM and endogenous serum proteins when spiked into human serum.[44-45] As such, ManLAM

samples prepared in human serum require a treatment step to release this marker for detection.[44] In brief, samples containing ManLAM were acidified to pH ~1 by the addition of 70% PCA. This process disrupts the complexed ManLAM by protein denaturation. Each sample was vortexed for 10 s and centrifuged at 12,000 *g* for 5 min to pellet the denatured proteins. After this step, the clear supernatant containing the liberated ManLAM was transferred to a separate microcentrifuge tube and neutralized to pH 7.5 by the addition of 2.0 M K_2CO_3. Finally, the samples were refrigerated at 2-8 º C for 60 min to precipitate $KClO_4$. For each sample, the clear ManLAM containing supernatant was transferred to a new microcentrifuge tube and the solutions were equilibrated to ambient laboratory conditions prior to running the assay.

3.2.5 Raman Scattering Analysis

The Raman spectra were collected using a Thermo Scientific DXR Raman microscope. The microscope was equipped with a HeNe laser (633 nm) with a measured power of 3.03±0.01 mW and a 50 mm slit aperture to the spectrograph. The samples were analyzed with 10x objective (numerical aperture of 0.25). The measured focal area of the laser on the sample surface was ~69 μm^2 giving a power density of ~0.04 $mW/\mu m^2$. Each spectrum was collected using a 0.3 s exposure time, and 3 exposures were averaged per spectrum. A total of 25 spectra with a uniform offset spacing of 125 µm were collected per sample, near the center of the address. For SERS, quantitation used the average peak height of the symmetric nitro stretch, $\nu_s(NO_2)$, of DSNB at 1336 cm^{-1}. For SERRS the peak for the polymethine bridge stretch, ν(C─C─C), of Cy5 at ~560 cm^{-1}, was used.[20, 46-48] For the adlayer characterizations (section 3.3.1) the laser power was increased to 7.02±0.01 mW

and the integration time was changed to 30 s.

3.2.6 Infrared Spectroscopy Analysis

Infrared external reflection spectra (IR-ERS) of the spontaneously adsorbed adlayers were collected using a modified Nicolet Magna 850 Fourier transform spectrometer equipped with a liquid nitrogen (LN_2)-cooled mercury cadmium telluride detector. Samples were prepared by immersion of gold-coated microscope slides in ethanolic solutions of DSP, 1:1 DSP:Cy5-SH (mole fraction), and Cy5-SH for 16 h. Spectra were collected using *p*-polarized light at an incident angle of 82° in a nitrogen atmosphere, and each spectrum was collected with a resolution of 4 cm^{-1} by co-adding 1024 scans of the sample surface. Reflection spectra are reported following equation 3.1.

$$-log\frac{R}{R_0} \tag{3.1}$$

where R is the sample spectrum and R_0 is the spectrum of a deuterated octadecanethiol-d_{37} reference sample.[43, 49]

3.2.7 Scanning Electron Microscopy (SEM) Analysis

Scanning electron microscopy (SEM) imaging was used to determine ERL surface densities on the completed assay substrates. Images were collected using a Hitachi S-4800 field emission scanning electron microscope. Each substrate was affixed to an SEM specimen mount to facilitate SEM analysis. The substrates were imaged 5 times at randomly selected locations about the address center. The images were taken at an acceleration voltage of 5 kV. Image J software (National Institutes of Health, Bethesda, MD) was used to analyze images and to enumerate particle density.

3.2.8 Data Analysis and Analytical Figures of Merit

Analytical sensitivity is used to gauge the performance of the two immunoassay formats, and is defined in two ways. First, analytical sensitivity can be categorized in terms of the limit of detection (LOD) (*i.e.,* the lowest concentration of ManLAM that produces an instrument response which is statistically different from a blank sample).[3, 50] Analytical sensitivity can also be described as the ability of the assay to resolve different concentrations of ManLAM (*i.e.,* an increase in sensitivity corresponds to an increase in the change in signal between different ManLAM concentrations).[51] The limit of the blank (LOB) and LOD are defined following the guidelines outlined by the Clinical and Laboratory Standards Institute, in the equations 3.2 and 3.3.[50, 52-53]

$$LOB = I_{Blank} + 1.645 \times \sigma_{Blank} \quad (3.2)$$

$$LOD = LOB + 1.645 \times \sigma_{x} \quad (3.3)$$

where I_{Blank} is the average signal of replicate blank measurements, σ_{Blank} is the standard deviation of the blank measurements, and σ_x is the standard deviation of the replicate measurements for the first sample that has an average measurement distinguishable from the blank at a 95% confidence interval. The LOB and LOD are converted from Raman signal in cts s^{-1} to concentration by dividing by the slope ((cts s^{-1})/(ng/mL)) of the fit line determined from the dose-response plot. The second definition of analytical sensitivity, concentration resolving power or the ability to differentiate separate ManLAM concentrations, can be described in two ways: (1) the slope of the linear fit line from dose-response plots of ManLAM, and (2) the signal-to-blank ratio (SBR) at a specified analyte concentration.[3, 51]

3.3 Results and Discussion

The following sections describe the results of a series of experiments designed to characterize the formation of the thiolated-Cy5 adlayer and to determine the performance of a SERRS substrate when applied to the detection of ManLAM, a biomarker indicative of active TB infection. These sections describe (1) the characterization of DSP, mixed DSP:Cy5-SH, and Cy5-SH adlayers on gold using IR-ERS and Raman scattering; (2) the effectiveness of the SERRS substrate in the detection of ManLAM and the potential for its broader application in disease diagnostics; (3) an in-depth analysis using SEM and Raman scattering to assess the basis of the improvements in ManLAM detection; and (4) a discussion of possible approaches to further improve the use of this methodology.

3.3.1 Characterization of Cy5-based Enhancing Surface

This section describes the characterization of the three adlayers by IR-ERS and Raman scattering. Figure 3.2 presents the resulting IR-ERS spectra from 900 to 1900 cm^{-1}. Band assignments are listed in table 3.1. Spectral features indicative of the terminal NHS group are particularly apparent for the DSP-based adlayer.[43] These include the carbonyl stretch, ν(C=O), of the ester linkage at 1812 cm^{-1}, the symmetric carbonyl stretch, ν_s(C=O), at 1785 cm^{-1}, and the asymmetric carbonyl stretch, ν_a(C=O), at 1747 cm^{-1} of the NHS group.[43, 54] Other features consistent with the adlayer composition include the symmetric CNC stretch, ν_s(C-N-C), at 1372 cm^{-1}, the asymmetric CNC stretch, ν_a(C-N-C), at 1216 cm^{-1}, and the C-O stretch, ν(N-C-O), at 1082 cm^{-1}.[43, 54] There are, in comparison, only a few distinct bands present in the spectra to differentiate the two Cy5-containing adlayers.[55-56] The most notable observation is the significant reduction in the strength of

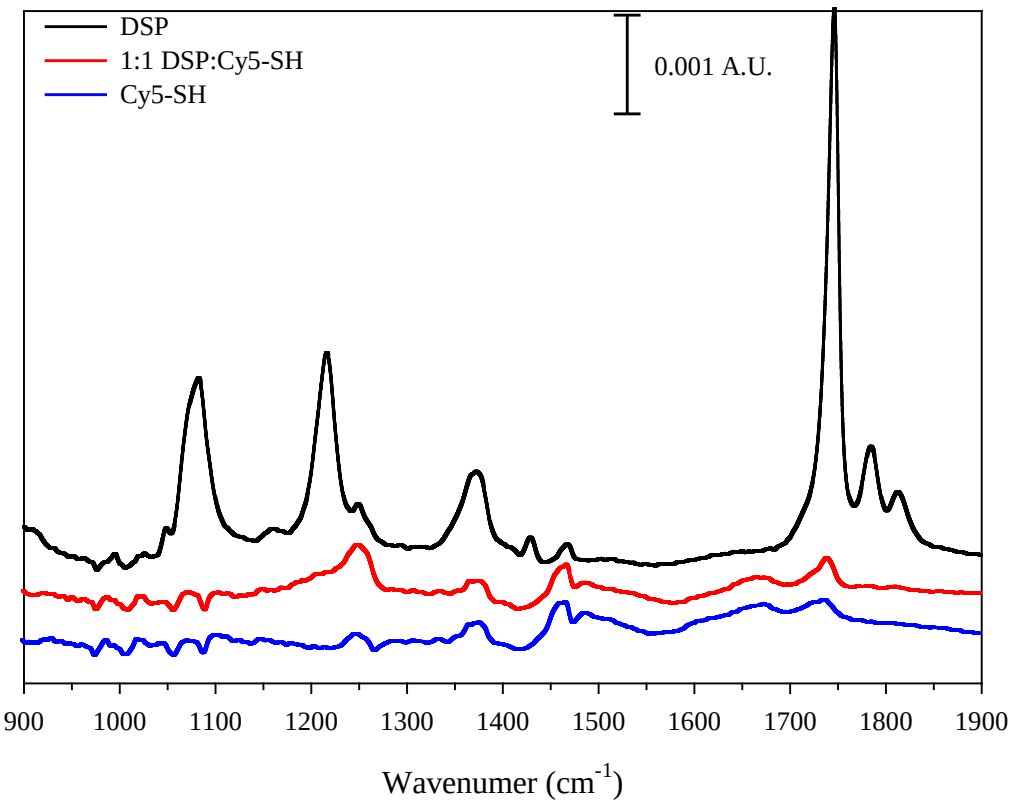

Figure 3.2. Infrared external reflection spectra for planar gold substrates functionalized using ethanolic solutions of DSP, 1:1 DSP:Cy5-SH (mole fraction), and Cy5-SH.

Table 3.1**.** Infrared band assignments and peak positions for gold substrates coated using ethanolic solutions of DSP, 1:1 DSP:Cy5-SH (mole fractions), and Cy5-SH.[43, 54-56]

Mode Assignment	Description	Peak Position (cm^{-1})		
		DSP	DSP:Cy5-SH	Cy5-SH
ν(C═O)	carbonyl stretch of ester	1812	–	–
ν_s(C═O)	NHS symmetric carbonyl stretch	1785	–	–
ν_a(C═O)	NHS asymmetric carbonyl stretch	1747	1739	1737
$\delta(CH_2)$	methylene scissors	1467 and 1429	1467	1467
$\delta(CH_2)$ and ν(C═C)	methylene scissors and ring modes	–	1467-1460	1467-1460
ν_s(C─N─C)	NHS symmetric CNC stretch	1372	1363	1369
ν_a(C─N─C)	NHS asymmetric CNC stretch	1216	–	–
ν(C─O)	succinimide NCO stretch	1082	1072	1072

the asymmetric carbonyl stretch in the DSP:Cy5-SH adlayer, indicating that there is very little, if any, of the DSP present in this adlayer. The absence of bands clearly assignable to the modes of Cy5 in either spectrum point to the likelihood that the thiolated Cy5 molecules in the adlayer are chemisorbed with the extended aromatic ring structure in the plane of the gold surface.[56]

Figure 3.3 shows Raman spectra for the mixed and thiolated-Cy5 adlayer samples. The DSP adlayer was indistinguishable from that of an uncoated substrate. Table 3.2 lists the band assignments for the vibrational modes of the two adlayers.[48, 55, 57-58] The two spectra confirm the formation of the expected adlayers (*e.g.*, the aromatic ring stretches at 1598 cm^{-1}, 1355 cm^{-1}, 935 cm^{-1}, 800 cm^{-1}) and the C-C-C stretch of the polymethine bridge at 560 cm^{-1}. Both spectra also have a band at ~320 cm^{-1}, which is assigned to the gold thiolate stretching mode, ν(Au-S), which is consistent with the expected chemisorption of aromatic thiols on gold.[59-60] More so, and in agreement with the IR-ERS measurements, the intensity of the Raman spectra of the two coatings are roughly the same, indicating there is very little, if any, DSP present in the mixed adlayer.

An example of the spectral responses for the immunoassays based on both SERS and SERRS for ManLAM (50 ng/mL) spiked into human serum and then PCA treated, is presented in figure 3.4. The SERS response is composed of only features due to the DSNB adlayer formed on the ERL used to tag captured ManLAM. The band assignments for these features are listed in table 3.2. The most prominent Raman bands include the symmetric nitro stretch, $\nu_s(NO_2)$, at 1336 cm^{-1}, and the aromatic ring breathing modes, ν(C═C), at 1556 cm^{-1}.[21] A very weak ν(Au-S) band at 320 cm^{-1} is also present.[59-60] The baseline-corrected peak height of the $\nu_s(NO_2)$, the strongest band in the observed spectra, is used

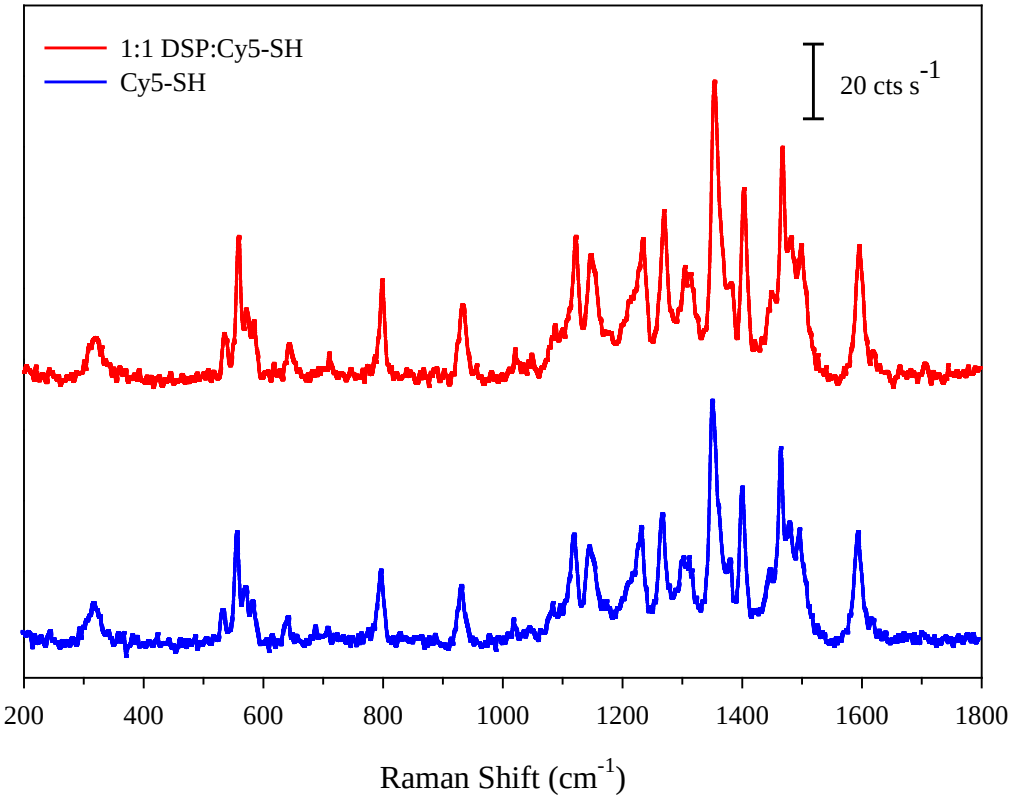

Figure 3.3. Raman spectra for samples prepared using ethanolic solutions of 1:1 DSP:Cy5-SH (mole fraction) and Cy5-SH that was coated on smooth gold substrates.

Table 3.2**.** Raman band assignments and peak positions for the Ramanophores, Cy5-SH and DSNB, used in the SERRS and SERS immunoassays.[48, 55, 57-60]

Mode Assignment	Description	Peak Position (cm^{-1})	
		1:1 DSP:Cy5-SH	DSNB
ν(C═N) and ν(C─C) Breathing	C-N stretch overlapped with aromatic ring vibrations	1598	–
ν(C─C) Breathing	aromatic ring modes	–	1566
ν(C═C)	aromatic ring vibrations (broad)	1470	–
ν(C─C─C)	polymethine bridge stretch	1405	–
ν(C─C) and δ(C─H)	aromatic ring modes overlapped with C-H bending	1355	
$\nu_s(NO_2)$	symmetric nitro stretch	–	1336
ν(C─C)	aromatic ring modes	1306	
ν(C─N)	quinoline stretch	1271	–
δ(C─H)	in plane bend	1236, 1149 and 1123	–
ν(C─N─O) and ring modes	succinimidyl NCO stretch and aromatic ring modes	–	1079
ν(C─C)	ring vibrations (broad)	1022, 935, 800	–
$\delta(NO_2)$	nitro scissoring		851
δ(C─H)	out-of-plane bend	644	–
ν(C─C─C)	polymethine bridge stretch	560	–
ν(Au-S)	gold-sulfur stretching mode	319	328

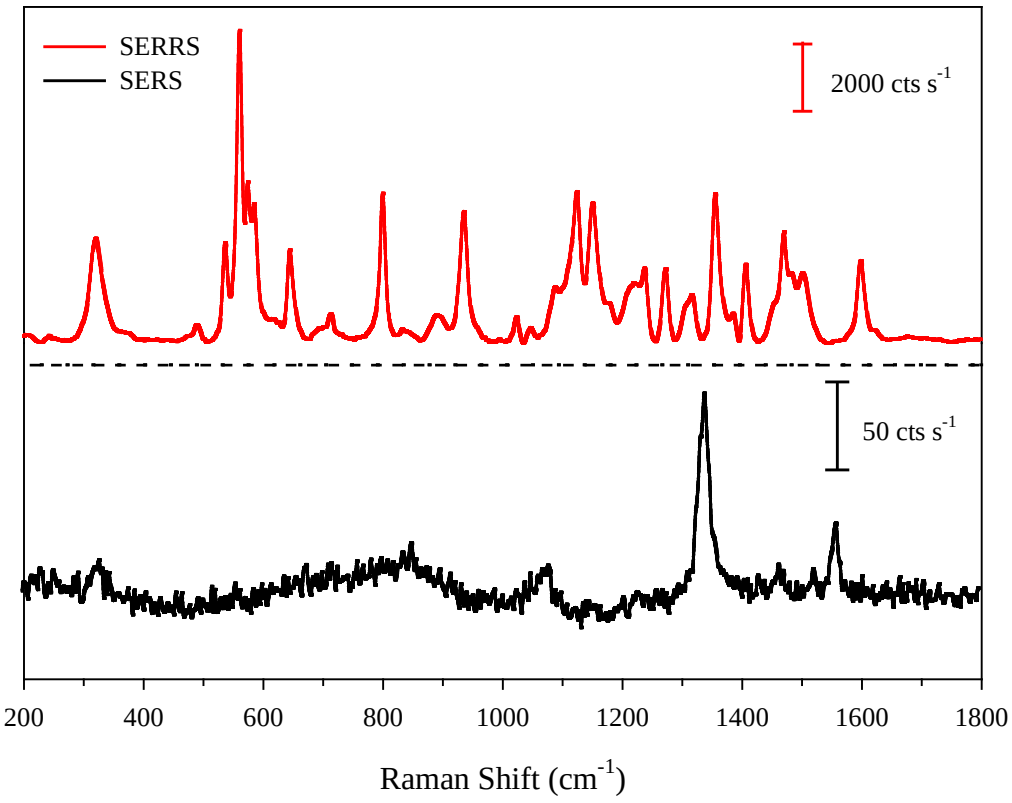

Figure 3.4. Raman spectra collected from 50 ng/mL ManLAM spiked in human serum, which has been subsequently pretreated. The top is a spectrum for the surfaced-enhanced resonance Raman scattering (SERRS) assay (Cy5-SH functionalized substrate) sample, and the bottom spectrum is for the surface-enhanced Raman scattering (SERS) assay (DSNB-modified particles) sample. The peak heights of the 560 cm^{-1} and 1336 cm^{-1} peaks were used to quantify the SERRS and SERS signal responses, respectively. The SERRS assay signal is ~80x greater for equivalent samples analyzed under the same parameters.

for antigen quantitation.

` The SERRS response is markedly different, with only the bands indicative of Cy5 present, as measured by preparing the capture substrate according to the procedure in scheme 3.2. Using the same pretreated 50 ng/mL sample described previously, the spectrum closely matches that in figure 3.3. The prominent bands include those indicative of the aromatic ring structure at 1598 cm^{-1}, 1355 cm^{-1}, 935 cm^{-1}, 800 cm^{-1}, the polymethine bridge stretches at 1405 cm^{-1} and 560 cm^{-1}, and the gold thiolate stretch at 320 cm^{-1}. The peak for the polymethine stretch at 560 cm^{-1} is used for antigen quantification and, in this case, is nearly 80x more intense than the 1336 cm^{-1} peak from the SERS immunoassay analyzed using the same collection parameters (*e.g.*, integration time, number of spectra collected, and power density at the sample surface).

3.3.2 Detection of ManLAM in Multiple Sample Matrices

This set of experiments compared the performance of the SERRS and SERS immunoassays when analyzing the same samples. This was accomplished using samples composed of ManLAM spiked in an innocuous sample matrix, a solution of 10 mM PBS with 150 mM NaCl containing 1% w/v BSA at pH 7.4.[44] Figure 3.5 shows the spectra collected from the SERRS and SERS assays for ManLAM spiked into PBS (1% v/v BSA) at 0.5, 1.0, 5.0, and 10.0 ng/mL, and a blank consisting of only buffer. In both cases, the strength of the signal for the RRM increases with ManLAM concentration. However, the strengths of the two sets of signal are markedly different, with the SERRS responses consistently and significantly higher at a given concentration. From a preliminary analysis of the data, we estimate the limit of detection to be 0.5 and 5 ng/mL, for the SERRS and

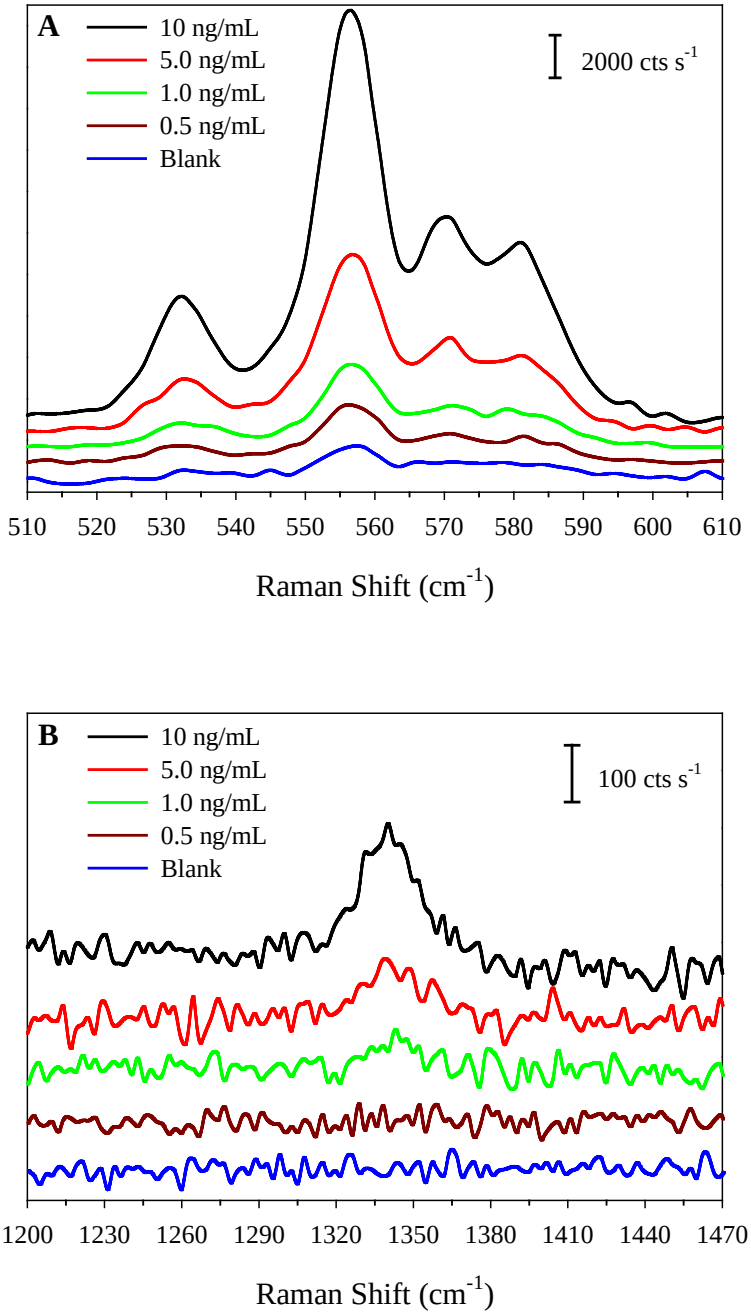

Figure 3.5**.** Spectra for (A) SERRS and (B) SERS immunoassays for ManLAM spiked in 10 mM PBS with 1% BSA (pH 7.4).

SERS immunoassays, respectively.

A more in-depth perspective of the differences in the two sets of measurements is presented by plotting the intensities of the $\nu_s(NO_2)$ at 1336 cm^{-1} and ν(C-C-C) at 560 cm^{-1} as a function of the analytical concentration of ManLAM in the sample for the SERS- and SERRS-style immunoassays, respectively. Figure 3.6 presents the dose-response plots based on the data in figure 3.5. The signal intensity increases linearly from the blank (0 ng/mL ManLAM) to the 10 ng/mL ManLAM sample. Interestingly the LOD for the SERRS immunoassay (0.8 ng/mL) is ~5x lower than the SERS assay (4.9 ng/mL). A comparison of the slopes of the two linear fits, however, shows that there is a larger difference between the SERRS [2395 (cts s^{-1})/(ng/mL)] and SERS [16 (cts s^{-1})/(ng/mL)] assays in analytical sensitivity. This difference represents an increase in the resolving power of the SERRS assay (*i.e.*, the ability to resolve differences in ManLAM concentrations) by a factor of ~150x. It is important to note that, at the lower concentrations, the associated error bars are smaller than the data points, as shown in figure 3.6. The next set of experiments contrasted the two types of immunoassays using human serum as a much more complex sample matrix.[44-45, 61-63]

Samples prepared by spiking ManLAM into human serum were used to determine the performance of the SERRS immunoassay in a complex sample matrix. Previous work in our laboratory has described the initial development of a PCA sample treatment procedure to liberate ManLAM so it can be detected effectively in such matrices.[44-45] Like the experiments summarized in figures 3.5 and 3.6, these samples were examined by SERRS and SERS. Figure 3.7 shows the spectra collected from the SERRS and SERS assays for the samples prepared in human serum. As before, the spectral intensities increase

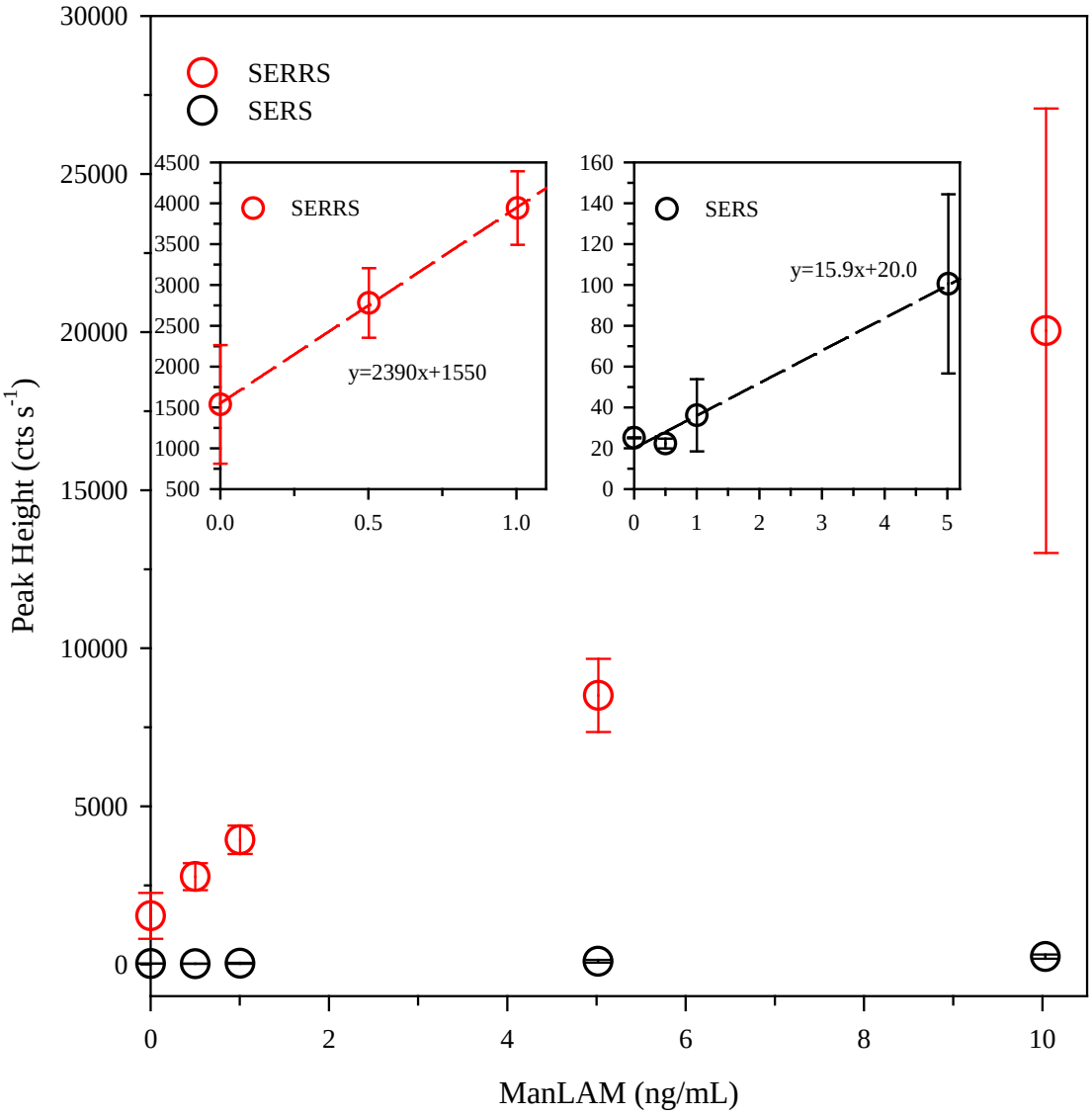

Figure 3.6. Dose-response plots for ManLAM spiked into clean sample matrix, 10 mM phosphate-buffered saline with 150 mM NaCl at a pH of 7.4, analyzed using both SERS (DSNB-modified particles) and SERRS (Cy5-modified substrate). SERRS represents an improvement in sensitivity (ratio of the fit lines) of 150x. The determined limits of detection are 0.8 ng/mL and 4.9 ng/mL for SERRS and SERS immunoassays, respectively. The average and standard deviation arise from 3 replicate samples each. At low concentrations, the error bars are smaller than the data points.

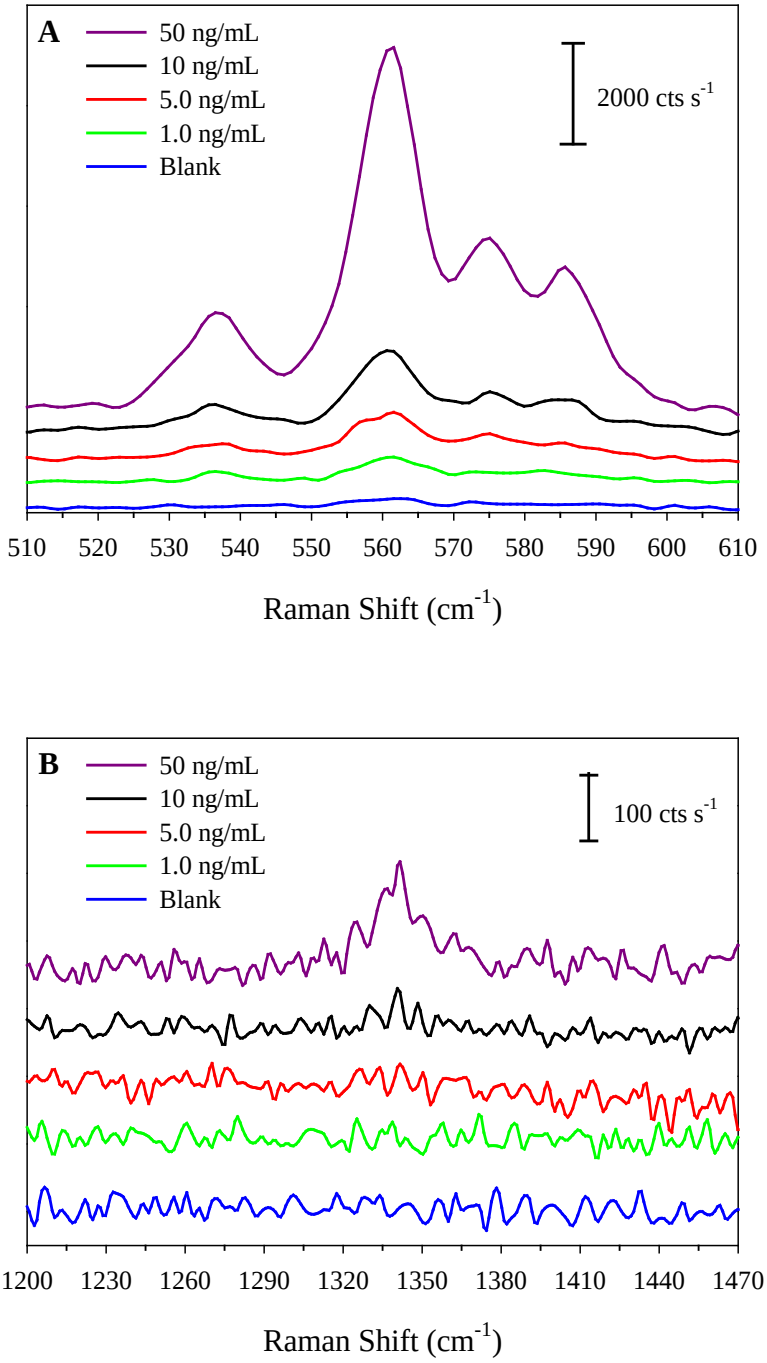

Figure 3.7. Spectra for (A) SERRS and (B) SERS immunoassays for ManLAM spiked into human serum that was subsequently PCA treated.

with the concentration of ManLAM in the sample, but not nearly at the levels for the buffer matrix (figure 3.5). This is attributed to the labile nature of the arabinan sidechains with respect to acid hydrolysis and the potential for incomplete protein decomplexation, as examined in depth in Chapter 2.[31, 36, 44-45, 64] A preliminary analysis of the data suggests the LOD for the SERRS assay is unchanged (1 ng/mL), but the LOD for the SERS has deteriorated significantly to as high as 50 ng/mL

For an-indepth analysis, figure 3.8 shows dose-response plots for pretreated ManLAM samples analyzed using both assay formats. Using linear best fits to these data, the estimated LOD for the SERRS assay (1.1 ng/mL) is on par with the same assay performed in a buffer (0.8 ng/mL). The SERS assay functions more poorly with an LOD of 10 ng/mL. The average LOD improvement for SERRS from replicate assays is 9.3±0.1. It can also be seen that the SERRS assay retains a much higher level of concentration resolving power, 38x greater with SERRS, compared to the SERS assay. To gain insight into the origin of the improved performance with SERRS, experiments were carried out to determine the signal per ERL (described below) for the two assays.

3.3.3 Origin of Observed Increase in Assay Performance

In looking more deeply into the differences in the strength of the signals in the SERRS and SERS assays, the two sets of responses were examined on a per particle level by measuring the surface concentration of ERLS at each ManLAM concentration by examining SEM images, as shown in figure 3.9. Each image reveals the presence of nanometrically sized objects that have a size and shape consistent with the footprints of the ERLs. Moreover, the number of ERLS in the images increases with increasing ManLAM

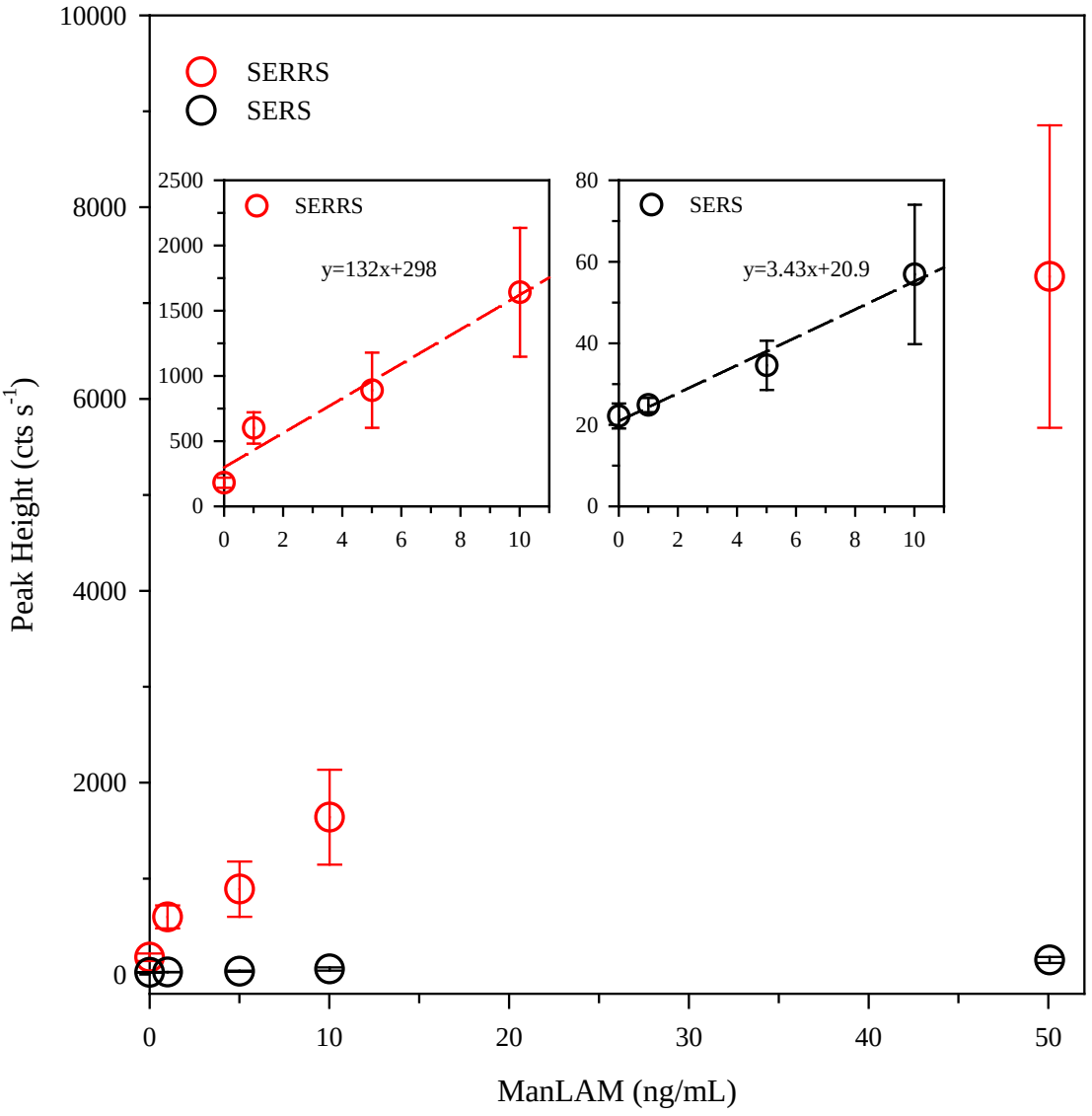

Figure 3.8**.** Dose-response plots for ManLAM spiked in a complex sample matrix, pooled AB human male serum, followed by a pretreatment method, and analyzed using both SERS (DSNB-modified particles) and SERRS (Cy5-modified substrate). SERRS represents an improvement in sensitivity (ratio of the fit line) of ~39x. The limits of detection are ~1.08 ng/mL for the SERRS and ~10.0 ng/mL for the SERS assays. In this regard, the SERRS assay is ~10x more sensitive than the SERS assay. The average and standard deviation are calculated from 3 replicate samples each.

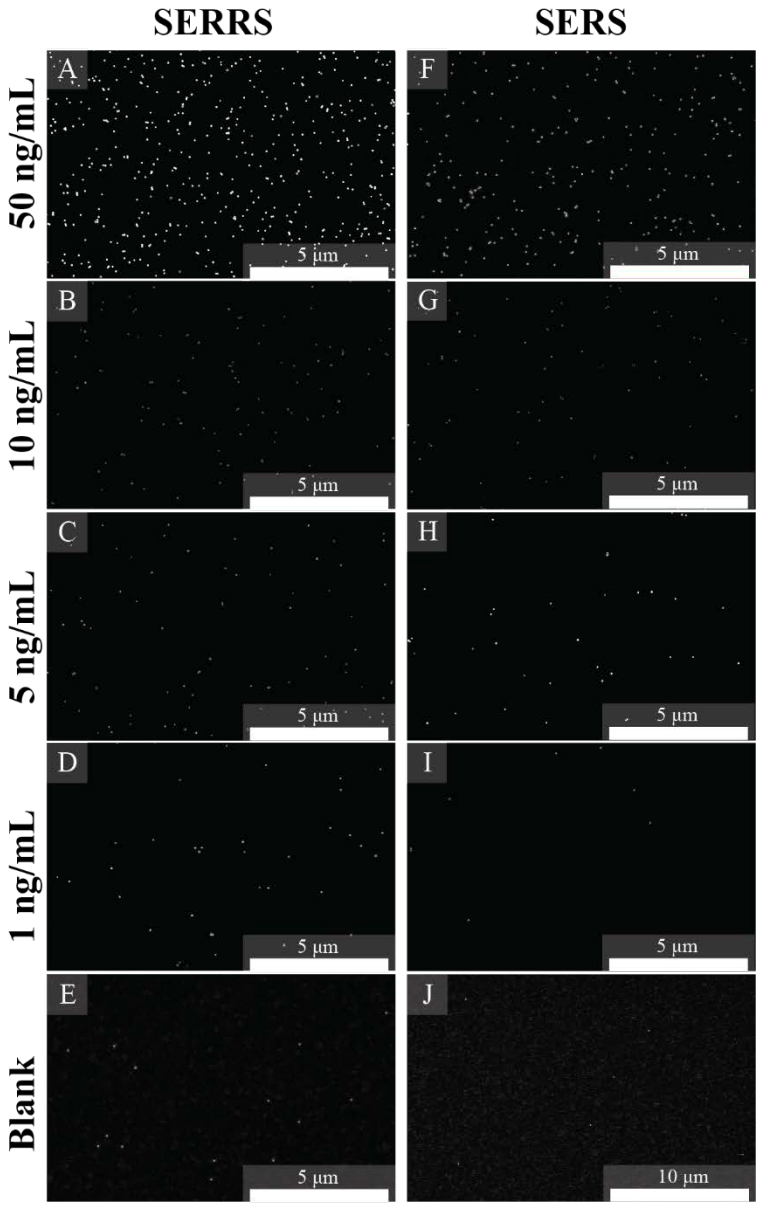

Figure 3.9. Representative scanning electron micrographs of the completed assay surfaces for samples containing 50, 10, 5.0, 1.0, and 0.0 ng/mL ManLAM in serum followed by acid treatment, by SERRS (A-E) and SERS (F-J). The increase in the size of the image for (J) reflects the lower level of nonspecifically adsorbed ERLs on the SERS substrate.

concentration. There are also a larger number of bound particles for the SERRS assays relative to the SERS assays. As expected, the particle surface concentrations, obtained using Image J software increase with ManLAM concentration, as listed in table 3.3. The number of particles on the SERRS substrates are consistently higher than the number found on the SERS substrate at each concentration analyzed. Assuming that the particle densities determined from the blank samples can be attributed to the nonspecific adsorption of ERLs in both the SERRS and SERS assays, the particle densities of the blank samples can be subtracted from the particle densities determined at the higher concentrations of ManLAM (*i.e.*, 1.0 to 50 ng/mL). This analysis indicates that there is an average increase in particle density of 2.02±0.76 ERLs/μm^2 for the SERRS immunoassay substrates. While this begins to explain the observed increase in analytical sensitivity for the SERRS immunoassay, the higher particle density (~2x) alone is insufficient to account for the observed increase in analytical sensitivity (~39x).

To determine the other contributions to the increased analytical sensitivity, these results were then combined with the Raman responses from each measurement and the area irradiated by the focused laser light in order to calculate the signal per ERL. Using the measured area of the focused laser light on the sample surface (69 um^2), the signal strengths in figure 3.7, and the data in table 3.3, it is possible to calculate the signal per ERL.[65-66] Figure 3.10 shows a dose-response plot of the ERLS on the surface at each ManLAM concentration for the SERRS and SERS assay. Even though there are large differences in Raman signal, when analyzing the number of ERLS on the surface, the assays have the same analytical sensitivity within a 95% confidence interval.[67] From an analysis of the data using the samples in which the resulting Raman signal is significantly higher than the

Table 3.3. Measured ERL surface density as a function of the ManLAM concentration in the sample. The average and standard deviation arise from an SEM analysis of 3 replicate samples at each concentration.

Concentration ManLAM (ng/mL)	Measured Particle Density (ERL/μm^2)	
	SERS	SERRS
50	2.38±0.24	4.39±0.77
10	0.73±0.12	1.18±0.36
5	0.36±0.06	0.74±0.05
1	0.09±0.01	0.38±0.02
0	0.02±0.01	0.16±0.02

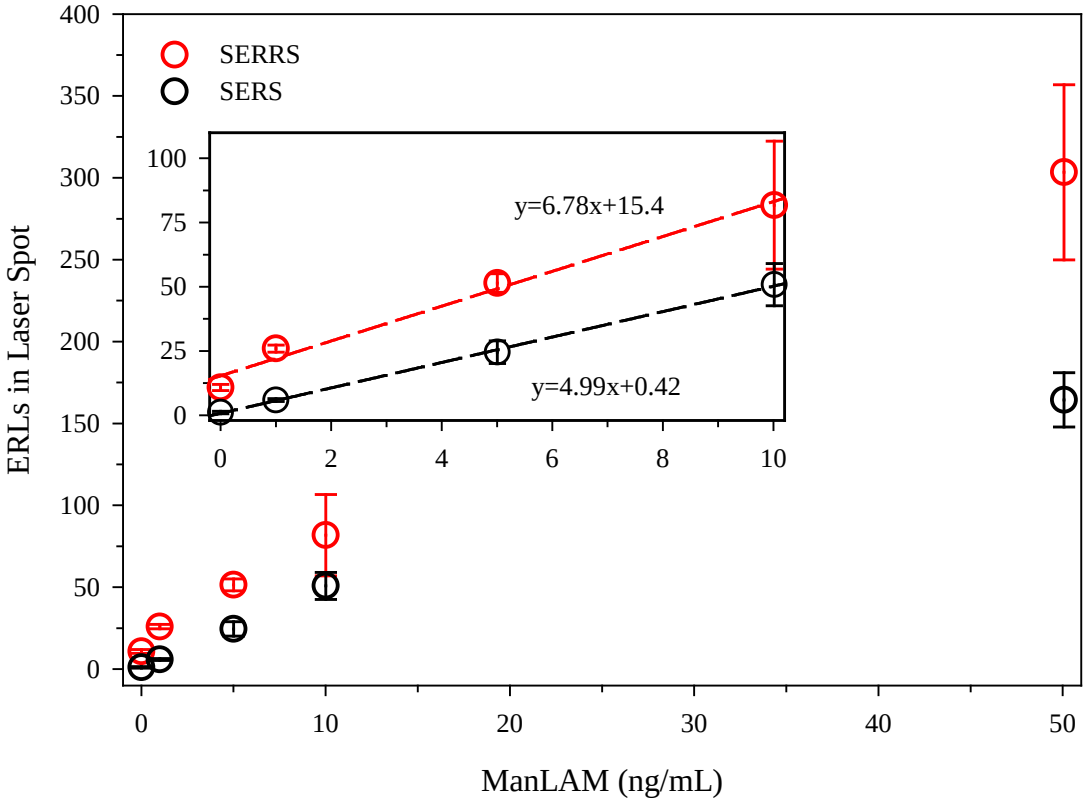

Figure 3.10. Dose-response plots for ManLAM spiked into human serum, followed by PCA treatment, presented as the average number of ERLs interrogated by the laser, for both SERS (DSNB-modified particles) and SERRS (Cy5-modified substrate) assays. SERRS represents an improvement in sensitivity (ratio of the fit line) of 1.4x. The average and standard deviation arise from a combined Raman and SEM analysis of 3 replicate samples at each concentration.

instrument noise, the average signal per binding event is 21±6 and 1.0±0.1 for the SERRS and SERS assays, respectively. This corresponds to a ~21x increase in signal for the SERRS assay relative to the SERS assay format. Taking into account the ~2x increase in particle density for the SERRS assay and the increase in signal per binding event, the calculated improvement in sensitivity for the SERRS immunoassay is 42x greater than that for the SERS immunoassay, which agrees well with the observed improvement in analytical sensitivity (39x) for the SERRS assay.

Furthermore, these data suggest that when working with an instrument capable of sufficiently sampling a larger part of the substrate, the use of this novel SERRS substrate will provide an increase in sensitivity of at least 21x compared to SERS when both assays are performing under ideal conditions. Discrepancies are likely due to the assumption that the particles are homogeneously and randomly distributed on the assay surface and the potential bias induced by undersampling the surface due to the small laser spot size used in the Raman analysis.[68] Experiments to ascertain the dispersity of ERLs across the immunoassay substrates, as well as an investigation into the impact of improved sampling methods, are currently underway. However, the experiments described herein have demonstrated the improved sensitivities in the detection of a biomarker indicative of TB infection, summarized in table 3.4, with the introduction of a novel chemically derived SERRS substrate, and additionally, have addressed the potential extensibility of this platform as an analytical tool.

Table 3.4. Determined limit of detection (LOD), analytical sensitivity, slope of dose-response plot, and signal-to-blank ratio (SBR), calculated at 10 ng/mL for the assay in buffer and 50 ng/mL for the assay in human serum.

method	10 mM PBS with 1% BSA (pH 7.4)			Human Serum		
	LOD (ng/mL)	Sensitivity (cts s^{-1})/(ng/mL)	SBR	LOD (ng/mL)	Sensitivity (cts s^{-1})/(ng/mL)	SBR
SERS	4.83	15.9	9.87	10.0	3.43	6.85
SERRS	0.79	2390	13.0	1.0	132	40.4

3.4 Conclusions

We have described the development of a novel chemically fabricated SERRS substrate for the detection of disease biomarkers. We detailed a series of measurements and experiments that: (1) characterized thiolated-Cy5 modified immunoassay substrates as a component in a novel highly sensitive SERS-enhancing substrate; (2) assessed the performance of this new SERRS immunoassay compared to a traditional SERS assay with respect to the detection of ManLAM, a biomarker indicative of active TB infections; and (3) determined the improvement in analytical sensitivity derived directly from the increased particle density on the SERRS substrates and the intrinsic signal amplification per binding event of this new SERRS immunoassay relative to the traditional SERS immunoassay. This work suggests that the advancement of this novel SERRS immunoassay may provide a relatively simple method to detect biomarkers of interest at extremely low levels. These new capabilities of this detection strategy may improve disease diagnostics and thus help to improve positive patient outcomes. To further understand the underpinnings of this new detection strategy, future work will focus on the detailed analysis of the dispersion of nanoparticle labels on the immunoassay surface and the further implication of under sampling during surface-based measurements. This ongoing work will be reported elsewhere.

3.5 References

1. Bantz, K.; Meyer, A.; Wittenberg, N.; Im, H.; Kurtuluş, Ö.; Lee, S.; Lindquist, N.; Oh, S.-H.; Haynes, C., Recent Progress in SERS Biosensing. *Phys. Chem. Chem. Phys.* **2011,** *13* (24), 11551-11567.

2. Porter, M. D.; Lipert, R.; Siperko, L.; Wang, G.; Narayanan, R., SERS as a Bioassay Platform: Fundamentals, Design, and Applications. *Chem. Soc. Rev.* **2008,** *37* (5), 1001-1011.

3. Granger, J. H.; Schlotter, N. E.; Crawford, A. C.; Porter, M. D., Prospects for Point-of-Care Pathogen Diagnostics Using Surface-enhanced Raman Scattering (SERS). *Chem. Soc. Rev.* **2016,** *45* (14), 3865-3882.

4. Moskovits, M., Surface-Enhanced Spectroscopy. *Rev. Mod. Phys.* **1985,** *57* (3), 783-826.

5. Kneipp, K.; Moskovits, M.; Kneipp, H., *Surface-enhanced Raman Scattering: Physics and Applications*. Springer: **2006**; Vol. 103.

6. Stiles, P.; Dieringer, J.; Shah, N.; Van Duyne, R., Surface-Enhanced Raman Spectroscopy. *Annu. Rev. Anal. Chem.* **2008,** *1* (1), 601-626.

7. Okamoto, T.; Yamaguchi, I., Optical Absorption Study of the Surface Plasmon Resonance in Gold Nanoparticles Immobilized onto a Gold Substrate by Self-assembly Yechnique. *J. Phys. Chem. B* **2003,** *107* (38), 10321-10324.

8. Schatz, G. C.; Van Duyne, R. P., Electromagnetic Mechanism of Surface-Enhanced Spectroscopy. *Handb. Vib. Spectrosc.* **2002**.

9. Kelly, K. L.; Coronado, E.; Zhao, L. L.; Schatz, G. C., The Optical Properties of Metal Nanoparticles: The Influence of Size, Shape, and Dielectric Environment. *J. Phys. Chem. B* **2003,** *107* (3), 668-677.

10. Fan, M.; Andrade, G. F.; Brolo, A. G., A Review on the Fabrication of Substrates for Surface enhanced Raman Spectroscopy and Their Applications in Analytical Chemistry. *Anal. Chim. Acta* **2011,** *693* (1), 7-25.

11. Kumar, G. P., Plasmonic Nano-Architectures for Surface enhanced Raman Scattering: A Review. *J. Nanophotonics* **2012,** *6* (1), 064503-1-064503-20.

12. McNay, G.; Eustace, D.; Smith, W. E.; Faulds, K.; Graham, D., Surface-enhanced Raman Scattering (SERS) and Surface-enhanced Resonance Raman Scattering (SERRS): A Review of Applications. *Appl. Spectrosc.* **2011,** *65* (8), 825-837.

13. Sharma, B.; Cardinal, M. F.; Kleinman, S. L.; Greeneltch, N. G.; Frontiera, R. R.; Blaber, M. G.; Schatz, G. C.; Van Duyne, R. P., High-performance SERS substrates: Advances and challenges. *MRS Bull.* **2013,** *38* (8), 615-624.

14. Sharma, B.; Frontiera, R.; Henry, A.-I.; Ringe, E.; Van Duyne, R., SERS: Materials, Applications, and the Future. *Mater. Today* **2012,** *15* (1-2), 16-25.

15. Kleinman, S. L.; Frontiera, R. R.; Henry, A.-I.; Dieringer, J. A.; Van Duyne, R. P., Creating, Characterizing, and Controlling Chemistry with SERS Hot Spots. *Phys. Chem. Chem. Phys.* **2013,** *15* (1), 21-36.

16. Yan, B.; Thubagere, A.; Premasiri, W. R.; Ziegler, L. D.; Dal Negro, L.; Reinhard, B. M., Engineered SERS Substrates with Multiscale Signal Enhancement: Nanoparticle Cluster Arrays. *ACS Nano* **2009,** *3* (5), 1190-1202.

17. Stacy, A.; Van Duyne, R., Surface Enhanced Raman and Resonance Raman spectroscopy in a Non-aqueous Electrochemical Environment: Tris (2, 2′-bipyridine) Ruthenium (II) Adsorbed on Silver from Acetonitrile. *Chem. Phys. Lett.* **1983,** *102* (4), 365-370.

18. McCreery, R. L., *Raman Spectroscopy for Chemical Analysis*. John Wiley & Sons, Inc.: New York, **2000**.

19. Haynes, C. L.; McFarland, A. D.; Duyne, R. P. V., Surface-enhanced Raman spectroscopy. *Anal. Chem.* **2005,** *77* (17), 338 A-346 A.

20. Driskell, J. D.; Lipert, R. J.; Porter, M. D., Labeled Gold Nanoparticles Immobilized at Smooth Metallic Substrates: Systematic Investigation of Surface Plasmon Resonance and Surface-enhanced Raman Scattering. *J. Phys. Chem. B* **2006,** *110* (35), 17444-17451.

21. Grubisha, D. S.; Lipert, R. J.; Park, H.-Y.; Driskell, J. D.; Porter, M. D., Femtomolar Detection of Prostate-specific Antigen: An Immunoassay Based on Surface-enhanced Raman Scattering and Immunogold Labels. *Anal. Chem.* **2003,** *75* (21), 5936-5943.

22. Park, H.-Y.; Driskell, J. D.; Kwarta, K. M.; Lipert, R. J.; Porter, M. D.; Schoen, C.; Neill, J. D.; Ridpath, J. F., Ultrasensitive Imunoassays Based on Surface-Enhanced Raman Scattering by Immunogold Labels. In *Surface-Enhanced Raman Scattering - Physics and Applications,* Kneipp, K.; Moskovits, M.; Kneipp, H., Eds. Springer-Verlag Berlin: Heidelberg, **2006**; pp 427-446.

23. Nie, S.; Emory, S. R., Probing Single Molecules and Single Nanoparticles by Surface-enhanced Raman Scattering. *Science* **1997,** *275* (5303), 1102-1106.

24. World Health Organization, *Global Tuberculosis Report 2015*; **2015**.

25. Pai, N. P.; Vadnais, C.; Denkinger, C.; Engel, N.; Pai, M., Point-of-Care Testing for Infectious Diseases: Diversity, Complexity, and Barriers in Low-and Middle-Income Countries. *PLoS Med.* **2012,** *9* (9), e1001306.

26. Levy, H., A Reevaluation of Sputum Microscopy and Culture in the Diagnosis of Pulmonary Tuberculosis. *Chest* **1989,** *95* (6), 1193-1197.

27. Norbis, L.; Alagna, R.; Tortoli, E.; Codecasa, L. R.; Migliori, G. B.; Cirillo, D. M., Challenges and Perspectives in the Diagnosis of Extrapulmonary Tuberculosis. *Exp. Rev. Anti-Infective Ther.* **2014,** *12* (5), 633-47.

28. Steingart, K. R.; Ng, V.; Henry, M.; Hopewell, P. C.; Ramsay, A.; Cunningham, J.; Urbanczik, R.; Perkins, M. D.; Aziz, M. A.; Pai, M., Sputum Processing Methods to Improve the Sensitivity of Smear Microscopy for Tuberculosis: A Systematic Review. *Lancet Infect. Dis.* **2006,** *6* (10), 664-674.

29. Perkins, M. D.; Cunningham, J., Facing the Crisis: Improving the Diagnosis of Tuberculosis in the HIV Era. *J. Infect. Dis.* **2007,** *196* (Supplement 1), S15-S27.

30. Piccini, P.; Chiappini, E.; Tortoli, E.; de Martino, M.; Galli, L., Clinical Peculiarities of Tuberculosis. *BMC Infect. Dis.* **2014,** *14* (Suppl 1), S4.

31. Venisse, A.; Berjeaud, J. M.; Chaurand, P.; Gilleron, M.; Puzo, G., Structural Features of Lipoarabinomannan from Mycobacterium Bovis BCG. Determination of Molecular Mass by Laser Desorption Mass Spectrometry. *J. Biol. Chem.* **1993,** *268* (17), 12401-12411.

32. Chatterjee, D.; Khoo, K.-H., Mycobacterial Lipoarabinomannan: An Extraordinary Lipoheteroglycan with Profound Physiological Effects. *Glycobiology* **1998,** *8* (2), 113-120.

33. Chan, J.; Fan, X. D.; Hunter, S. W.; Brennan, P. J.; Bloom, B. R., Lipoarabinomannan, A Possible Virulence Factor Involved in Persistence of *Mycobacterium tuberculosis* Within Macrophages. *Infect. Immun.* **1991,** *59* (5), 1755-1761.

34. Chatterjee, D.; Lowell, K.; Rivoire, B.; McNeil, M. R.; Brennan, P., Lipoarabinomannan of Mycobacterium tuberculosis. Capping with Mannosyl Residues in Some Strains. *J. Biol. Chem.* **1992,** *267* (9), 6234-6239.

35. Mishra, A. K.; Driessen, N. N.; Appelmelk, B. J.; Besra, G. S., Lipoarabinomannan and Related Glycoconjugates: Structure, Biogenesis and Role in Mycobacterium tuberculosis Physiology and Host–Pathogen Interaction. *FEMS Microbiol. Rev.* **2011,** *35* (6), 1126-1157.

36. Chatterjee, D.; Bozic, C. M.; McNeil, M.; Brennan, P. J., Structural Features of the Arabinan Component of the Lipoarabinomannan of Mycobacterium Tuberculosis. *J. Biol. Chem.* **1991,** *266* (15), 9652-9660.

37. Crawford, A. C. Surface-enhanced Raman Scattering for the Reliable and Reproducible Detection of Disease Antigens in Biologically Relevant Media. Dissertation, The University of Utah, **2016**.

38. Hermanson, G. T., *Bioconjugate Techniques*. Academic Press: **2013**.

39. Yakes, B. J. Advanced Detection and Separation Methods: Developments in Surface-enhanced Raman Scattering Readout immunoassays and Electrochemically Modulated Liquid Chromatography. Graduate, Iowa State University, Ames, Iowa, **2007**.

40. Shi, L.; Zhou, R.; Liu, Z.; Lowary, T. L.; Seeberger, P. H.; Stocker, B. L.; Crick, D. C.; Khoo, K. H.; Chatterjee, D., Transfer of the first arabinofuranose residue to galactan is essential for Mycobacterium smegmatis viability. *J. Bacteriol.* **2008,** *190* (15), 5248-55.

41. Torrelles, J. B.; Sieling, P. A.; Zhang, N.; Keen, M. A.; McNeil, M. R.; Belisle, J. T.; Modlin, R. L.; Brennan, P. J.; Chatterjee, D., Isolation of a Distinct Mycobacterium tuberculosis Mannose-capped Lipoarabinomannan Isoform Responsible for Recognition by CD1b-restricted T Cells. *Glycobiology* **2012,** *22* (8), 1118-27.

42. Granger, J.; Granger, M.; Firpo, M.; Mulvihill, S.; Porter, M., Toward Development of a Surface-enhanced Raman Scattering (SERS)-based Cancer Diagnostic Immunoassay Panel. *Analyst* **2013,** *138* (2), 410-416.

43. Lim, C. Y.; Owens, N. A.; Wampler, R. D.; Ying, Y.; Granger, J. H.; Porter, M. D.; Takahashi, M.; Shimazu, K., Succinimidyl Ester Surface Chemistry: Implications of the Competition between Aminolysis and Hydrolysis on Covalent Protein Immobilization. *Langmuir* **2014,** *30* (43), 12868-12878.

44. Laurentius, L. B.; Crawford, A. C.; Mulvihill, T. S.; Granger, J. H.; Robinson, R.; Spencer, J. S.; Chatterjee, D.; Hanson, K. E.; Porter, M. D., Importance of Specimen Pretreatment for the Low-level Detection of Mycobacterial Lipoarabinomannan in Human Serum. *Analyst* **2017,** *142* (1), 177-185.

45. Crawford, A. C.; Laurentius, L. B.; Mulvihill, T. S.; Granger, J. H.; Spencer, J. S.; Chatterjee, D.; Hanson, K. E.; Porter, M. D., Detection of the Tuberculosis Antigenic Marker Mannose-Capped Lipoarabinomannan in Pretreated Serum by Surface-enhanced Raman Scattering. *Analyst* **2017,** *142*, 186-196.

46. Driskell, J. D.; Kwarta, K. M.; Lipert, R. J.; Porter, M. D.; Neill, J. D.; Ridpath, J. F., Low-level Detection of Viral Pathogens by a Surface-enhanced Raman Scattering Based Immunoassay. *Anal. Chem.* **2005,** *77* (19), 6147-6154.

47. Yang, J. P.; Callender, R., The Resonance Raman Spectra of Some Cyanine Dyes. *J. Raman Spectrosc.* **1985,** *16* (5), 319-321.

48. Kneipp, K.; Kneipp, H.; Rentsch, M., SERS on a 1, 1′-diethyl-2, 2′ Cyanine dye Adsorbed on Colloidal Silver. *J. Mol. Struct.* **1987,** *156* (3-4), 331-340.

49. Dluhy, R., Infrared Spectroscopy of Biophysical Monomolecular Films at Interfaces: Theory and Applications. *Appl. Spectrosc. Rev.* **2000,** *35* (4).

50. Armbruster, D. A.; Pry, T., Limit of Blank, Limit of Detection and Limit of Quantitation. *Clin. Biochem. Rev.* **2008,** *29* (Suppl 1), S49-S52.

51. Skoog, D. A.; Holler, F. J.; Nieman, T. A., *Principles of Instrumental Analysis*. Cengage Learning: **1998**.

52. EP17-A, N., Protocols for the Determination of Limits of Detection and Limits of Quantitation. *CLISI.* **2004,** *5*.

53. Moretti, M.; Sisti, D.; Rocchi, M. B.; Delprete, E., CLSI EP17-A Protocol: A Useful Tool for Better Understanding the Low End Performance of Total Prostate-Specific Antigen Assays. *Clin. Chim. Acta* **2011,** *412* (11), 1143-1145.

54. Frey, B. L.; Corn, R. M., Covalent Attachment and Derivatization of Poly (L-lysine) Monolayers on Gold Surfaces as Characterized by Polarization− Modulation FT-IR Spectroscopy. *Anal. Chem.* **1996,** *68* (18), 3187-3193.

55. Iwata, K.; Weaver, W. L.; Gustafson, T. L., Spontaneous Raman Spectra of the Cyanine Dye DODCI and its Six Analogs Using Titanium: Sapphire Laser Excitation. *J. Phys. Chem.* **1992,** *96* (25), 10219-10224.

56. Menéndez, G. O.; Cortés, E.; Grumelli, D.; De Leo, L. P. M.; Williams, F. J.; Tognalli, N. G.; Fainstein, A.; Vela, M. E.; Jares-Erijman, E. A.; Salvarezza, R. C., Self-Assembly of Thiolated Cyanine Aggregates on Au (111) and Au Nanoparticle Surfaces. *Nanoscale* **2012,** *4* (2), 531-540.

57. Wang, X.; Wen, H.; He, T.; Zuo, J.; Xu, C.; Liu, F.-C., Enhancement Mechanism of SERS from Cyanine Dyes Adsorbed on Ag 2 O Colloids. *Spectrochim. Acta, Part A* **1997,** *53* (14), 2495-2504.

58. Neves, T. B.; Andrade, G. F., SERS Characterization of the Indocyanine-Type Dye IR-820 on Gold and Silver Nanoparticles in the Near Infrared. *J. Spectrosc.* **2015,** *2015*.

59. Carron, K. T.; Hurley, L. G., Axial and Azimuthal Angle Determination with Surface-enhanced Raman Spectroscopy: Thiophenol on Copper, Silver, and Gold Metal Surfaces. *J. Phys. Chem.* **1991,** *95* (24), 9979-9984.

60. Bürgi, T., Properties of the Gold–Sulphur Interface: From Self-Assembled Monolayers to Clusters. *Nanoscale* **2015,** *7* (38), 15553-15567.

61. Psychogios, N.; Hau, D. D.; Peng, J.; Guo, A. C.; Mandal, R.; Bouatra, S.; Sinelnikov, I.; Krishnamurthy, R.; Eisner, R.; Gautam, B., The Human Serum Metabolome. *PLoS One* **2011,** *6* (2), e16957.

62. Wishart, D. S.; Jewison, T.; Guo, A. C.; Wilson, M.; Knox, C.; Liu, Y.; Djoumbou, Y.; Mandal, R.; Aziat, F.; Dong, E., HMDB 3.0—The Human Metabolome Database in 2013. *Nucleic Acids Res.* **2012**, gks1065.

63. Tate, J.; Ward, G., Interferences in Immunoassay. *Clin. Biochem. Rev.* **2004,** *25* (2), 105-120.

64. Ludwiczak, P.; Brando, T.; Monsarrat, B.; Puzo, G., Structural Characterization of Mycobacterium tuberculosis Lipoarabinomannans by the Combination of Capillary Electrophoresis and Matrix-Assisted Laser Desorption/Ionization Time-of-Flight Mass Spectrometry. *Anal. Chem.* **2001,** *73* (10), 2323-2330.

65. Magnes, J.; Odera, D.; Hartke, J.; Fountain, M.; Florence, L.; Davis, V., Quantitative and Qualitative Study of Gaussian beam Visualization Techniques. *arXiv.org, e-Print Arch., Phys.* **2006**.

66. Khosrofian, J. M.; Garetz, B. A., Measurement of a Gaussian Laser Beam Diameter Through the Direct Inversion of Knife-Edge Data. *Appl. Opt.* **1983,** *22* (21), 3406-3410.

67. Harris, D. C., *Quantitative Chemical Analysis*. Macmillan: **2010**.

68. Crawford, A. C.; Skuratovsky, A.; Porter, M. D., Sampling Error: Impact on the Quantitative Analysis of Nanoparticle-Based Surface-Enhanced Raman Scattering Immunoassays. *Anal. Chem.* **2016,** *88* (12), 6515-6522.

CHAPTER 4

HANDHELD RAMAN INSTRUMENTATION FOR QUANTITATIVE TUBERCULOSIS BIOMARKER DETECTION: FEASIBILITY AND IMPLICATIONS FOR POINT-OF-NEED INFECTIOUS DISEASE DIAGNOSTICS

4.1 Introduction

The development of point-of-need (PON) diagnostic tests for the detection of disease biomarkers, chemical and biowarfare agents, and environmental contaminants has emerged as a global research effort.[1-5] The goal is to translate the diagnostic strength of today's advanced *in vitro* diagnostic tests (*e.g.,* the enzyme-linked immunosorbent immunoassay (ELISA) and the nucleic acid amplification test (NAAT)) to modalities that can be used beyond the confines of the formal laboratory or clinical setting.[1] Many of the existing diagnostic tests require secure sample transportation systems, a modern laboratory infrastructure, and highly trained personnel, limiting their PON applicability.[1, 6-8] In order to reduce the burden of infectious disease, particularly in resource-limited regions of the world, the development of PON testing methodologies that can overcome the limitations of conventional testing is a key first step in the fight against infectious disease.[1, 7, 9-10]

The so called "dip stick" tests, like those for human immunodeficiency virus (HIV)

detection, are among the most recognized PON diagnostic platforms.[11] These tests are typically designed for qualitative purposes (*i.e.*, yes/no visual readout), which limits their overall utility, particularly with respect to disease staging and monitoring response to treatment.[11-12] To overcome this limitation, a new generation of quantitative and increasingly sensitive PON testing architectures are being developed featuring small electronic readers.[1, 13] This Chapter examines the utility of a handheld Raman spectrometer as a means to assess the potential of, and identify the design needs for, moving immunoassays based on surface-enhanced Raman scattering (SERS) readout to PON use.

In response to the growing importance of PON tests, the World Health Organization (WHO) has put forward criteria by which nascent PON diagnostic methods can be qualified. The *ASSURED* criteria was first developed to frame the characteristics of an ideal PON test for sexually transmitted infections, but has since been applied to include tests for a number of diseases.[14-15] *ASSURED* stands for affordable, sensitive, specific, user-friendly, rapid, equipment free, and deliverable to those in need. While the equipment-free metric originally focused on assays that relied on visual readout, this element of the *ASSURED* criteria has been revised to include backpack portable instrumentation to take advantage of more quantitative spectrophotometric, electrochemical, and magnetoresistive detection modalities.[1, 7, 16-20] Nonetheless, approaches that use an electronic reader must still meet all of the other elements of the criteria. This Chapter expands on our work aimed at applying SERS detection to tuberculosis (TB) diagnostics to determine how this methodology begins to meet the *ASSURED* metrics and identify the next step necessary to move forward.[21]

TB is but one of many examples where today's diagnostic test capabilities fail to

meet the *ASSURED* criteria with respect to deployment in resource-limited regions of the world.[7, 9, 22] According to the *Global Tuberculosis Report 2015* published by the WHO, TB now ranks as the world's deadliest infectious disease.[9] It is estimated that 9.6 million people developed active TB infections in 2015. Of those, approximately 1 in 7 cases proved to be fatal. More so, the report projects that 1 in every 3 individuals who develop TB remains undiagnosed/unreported due to limitations in existing testing methodologies, access to effective healthcare, economic barriers, and social stigma.[1, 9] Bacterial culture using patient sputum is the TB diagnostics gold standard.[9, 23] However, this test takes several weeks to complete and requires a well-developed laboratory infrastructure with highly skilled clinicians.[1, 9, 22, 24] Tests based on sputum are also ineffective in diagnosing extrapulmonary TB infections, which account for ~10% of the TB cases worldwide.[9]

These shortcomings have triggered a refocusing of TB diagnostics to include the use of primary antigenic biomarkers indicative of infection. As part of our interest in this area, we recently detailed the development of an immunoassay based on SERS for the detection of mannose-capped LAM (ManLAM), a major component of the bacterial cell wall of *M. tuberculosis*.[21, 25] LAM, a 17.3±5 kDa lipoglycan, consists of a mannosyl phosphatidylinositol anchor, an arabinomannan backbone, and a mannose-capping motif.[5, 22-25] The broad range observed in molecular weight for LAM is indicative of the variability in the branching of the side chains, capping, and branching of the backbone.[26] Importantly, the composition of the capping motif differs across mycobacteria. Phospho-myo-inositol-capped LAM (PILAM) is from *M. smegmatis*, an often-used nonpathogenic simulant for *M. tuberculosis*.[5, 27-39] PILAM is commonly applied as a simulant for ManLAM in the development of TB assays because: (1) the two bacteria have very similar

genotypes, giving rise to similar cell walls resulting in the shared core structure of PILAM and ManLAM; (2) *M. smegmatis* is a relatively fast growing bacteria and can be readily prepared in copious amounts; and (3) *M. smegmatis* is nonpathogenic and can be handled without the biosafety facilities required for *M. tuberculosis*.[30-39] Herein, PILAM (see figure 4.1 for a generalized structure) will be used as a simulant for ManLAM in an assessment of a TB diagnostic test analyzed using a handheld Raman spectrometer.

Two of our recent reports have examined the development and preliminary clinical accuracy of a sandwich immunoassay for PILAM and ManLAM using SERS detection.[21, 25] This chapter delineates the potential utility of this immunoassay platform (scheme 4.1) within the framework of a PON diagnostic test. Our earlier work also showed that this platform requires less sample and smaller amounts of reagents when compared to immunoassays like ELISA.[21, 25, 40-41] Moreover, the large signal enhancement factor for SERS (Scheme 4.1), which derives in part from the plasmonic coupling between the gold nanoparticle-based labels and underlying gold capture surface, enables the measurement of PILAM and ManLAM at low limits of detection (LOD).[16, 21, 25, 42] Several other characteristics point to the potential value of SERS with respect to field deployability. First, the use of long wavelength excitation sources (*e.g.*, 633 nm) minimizes background fluorescence from other constituents in the sample matrix.[41] Second, Raman scattering is relatively insensitive to environmental factors like temperature and humidity and to the impact of oxygen and other fluorescence quenchers.[43-44] These insensitivities also facilitate archiving the completed assays for further analysis and record keeping purposes.

However, assay development is only the first step in moving this platform towards an effective PON test. Clinically informative test results should be obtained in near real

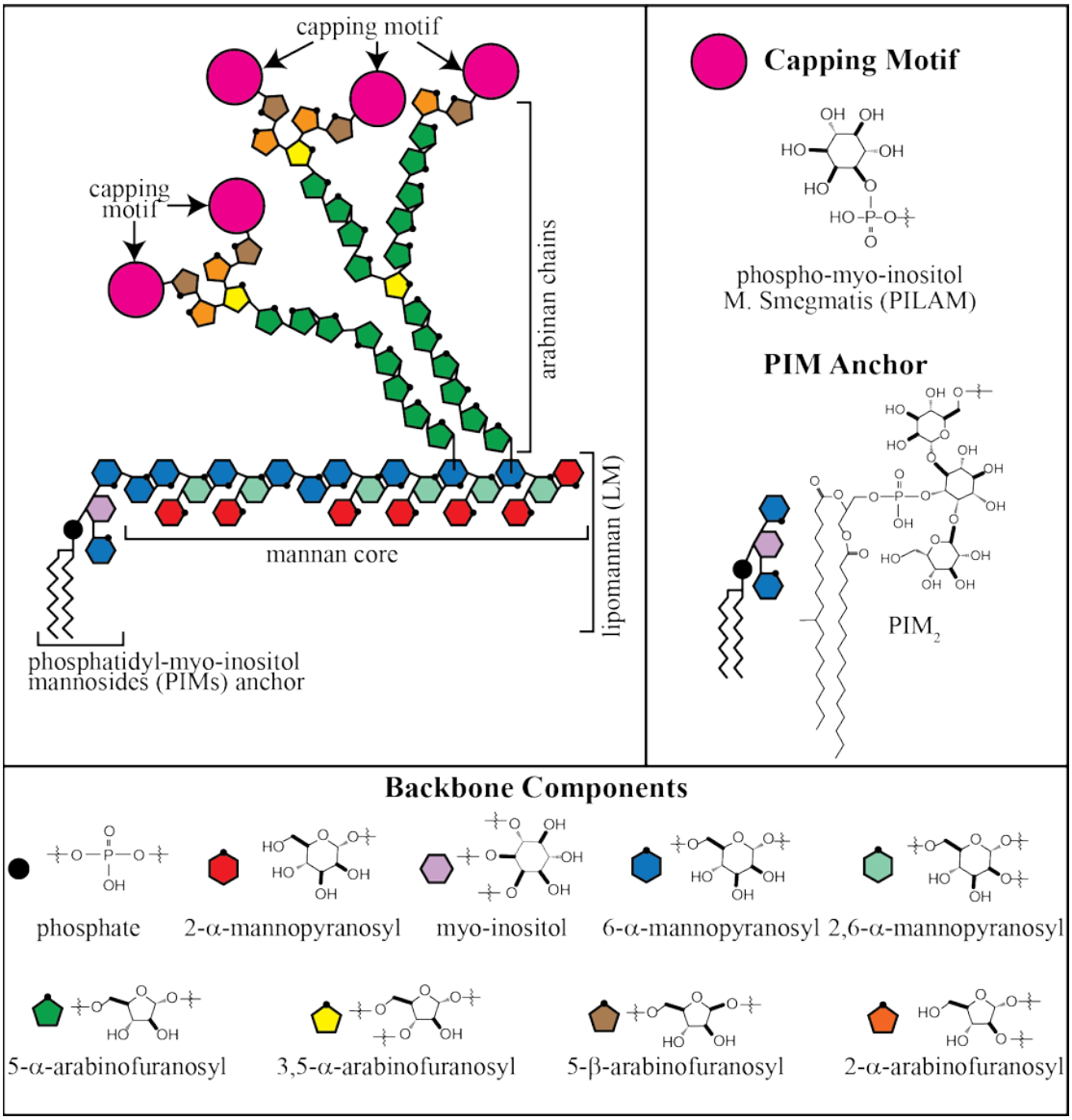

Figure 4.1. The general structure of phosphoinositol-capped lipoarabinomannan including the: (1) phosphatidylinositol mannoside (PIM_2) anchor, (2) mannan core, (3) arabinan side chains, and (4) capping motifs.[45]

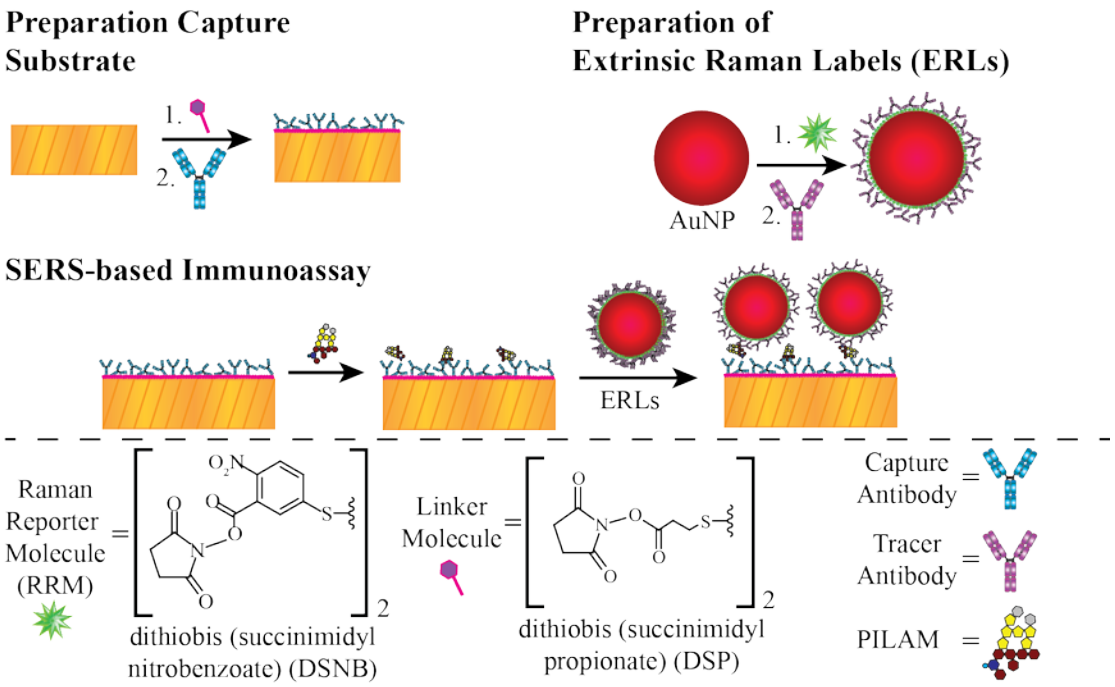

Scheme 4.1. Outline of the processes and procedures used in the surface-enhanced Raman scattering (SERS)-based immunoassay. Both the extrinsic Raman labels (ERL), which have a 60 nm gold nanoparticle (AuNP) core, and gold capture substrate are prepared prior to running the assay.

time, particularly in a forward operating setting (*e.g.*, at remote worksites or mobile clinics). To this end, handheld Raman spectrometers have been employed for quality control in the pork industry, and to screen for threats from explosives.[46-48] However, the handheld Raman instrumentation used in these settings is typically limited to determining the presence of given compound by comparison to a preloaded spectral library. There are few reports beyond that by Zheng *et al.*, which used a handheld Raman spectrometer for the semiquantitative detection.[13, 49-50] In this case, the detection of a fungicide by labeling samples in four groups: no risk, low risk, risk, and high risk, used this type of portable reader beyond a qualitative capacity.[13, 49-50]

This Chapter expands on the current state of PON diagnostics with SERS by investigating the feasibility of applying a handheld Raman spectrometer as an electronic optical reader for the immunoassay shown in scheme 4.1 to quantitatively detect PILAM.[13, 21, 25, 51] It describes the testing of a SERS immunoassay designed to detect PILAM spiked into human serum with a handheld Raman spectrometer, followed by a series of comparative experiments on the analytical figures of merit (*i.e.*, analytical sensitivity and LODs) for benchtop and handheld Raman spectrometers. It concludes with a brief discussion of the challenges associated with moving this approach forward as a potential tool in PON diagnostics.

4.2 Experimental

4.2.1 Materials

Phosphate-buffered saline (PBS) packs (pH 7.4 with 10 mM PBS and 150 mM NaCl), borate buffer (BB) packs (pH 8.5 with 50 mM BB), and dithiobis (succinimidyl

propionate) (DSP) were purchased from Thermo Scientific. All buffers were prepared with 18.2 MΩ H_2O supplied by a Barnstead ultrapure water system. Tween 20 (T20), StartingBlock™, perchloric acid (70%), potassium carbonate, glass microscope slides, and sodium chloride were obtained from Fisher Scientific. Bovine serum albumin (BSA) and acetonitrile were acquired from Sigma Aldrich. Octadecanethiol (ODT) was obtained from Fluka. Polystyrene 24-well microplates and a two-component polydimethylsiloxane (PDMS) kit were purchased from Dow Corning. Solid PDMS transfer templates were made following the package insert instructions. A UV-curable optical adhesive (#61) was obtained from Norland. Colloidal gold (60 nm diameter) at a stock concentration of 2 $x10^{10}$ particles/mL was acquired from NanoPartz. Ethanol (200 proof) was purchased from Deacon Labs. Pooled AB human male serum was obtained from Innovative Research, Inc. Test-grade silicon wafers <1,1,1> were acquired from University Wafer. Gold shot (99.995% pure) was purchased from Alfa Aesar. The Raman reporter molecule (RRM) 5,5'-dithiobis (succinimidyl-2-nitrobenzoate) (DSNB) was synthesized in house per procedures detailed elsewhere.[42] PILAM and its associated monoclonal capture and tracer antibody (CS906.7) were provided by Dr. Delphi Chatterjee and associates at Colorado State University.[52]

4.2.2 Preparation of Extrinsic Raman labels (ERLs)

The following sections elaborate more fully on the processes shown in scheme 4.1. The fabrication and surface functionalization of ERLs have been detailed elsewhere.[40, 42] In brief, a suspension of 60 nm gold colloids was incubated in a 10 μM solution of DSNB and 2 mM BB. This suspension was subsequently agitated by inversion mixing for 30 s

and stored at 2-8˚C for 90 min. This step forms a DSNB-derived thiolate monolayer on the gold nanoparticles that acts as an RRM and as a coating for the adsorption of monoclonal anti-PILAM tracer antibodies.

The next step imparted immunospecificity to the ERLs by the addition of monoclonal anti-PILAM antibodies solubilized in PBS and 0.1% T20 (v/v) (PBST) to the colloidal suspension at a final concentration of 1.0 μg/mL. This suspension was also briefly mixed by inversion and stored at 2-8˚C for 60 min. The particles were then blocked by the addition of a 10% (w/v) BSA solution (2 mM BB) to reach a final BSA concentration of 1% (w/v). The suspension is again agitated by inversion mixing for 30 s and stored at 2-8˚C for 60 min. This step coated the particles with BSA, which acts to combat the nonspecific adsorption of the ERLs in the antigen labeling step.

To remove excess reagents, the particles were centrifuged 3x for 10 min at ~2000 *g* to precipitate the ERLs, and the colorless supernatant is carefully removed. Between the first and second centrifugation steps, the ERLs were resuspended in 1 mL of 1% BSA (w/v) (2 mM BB); the final cleanup step concentrated the ERLs in 0.25 mL of 2% BSA (w/v) (2 mM BB). Finally, a 1.71 M aqueous solution of NaCl was used to adjust the final NaCl concentration in the suspension to 150 mM.

4.2.3 Substrate Fabrication and General Immunoassay Procedure

The procedures for fabrication of the assay and for performing the immunoassay have been described in detail elsewhere.[25, 53] In brief, template-stripped gold (TSG) served as the solid support for the immunoassay. To fabricate TSG, a clean silicon wafer (100 mm diameter) was coated with a thin (180-200 nm) gold film via resistive evaporation at a rate

≤ 1 Å/s. After cooling to room temperature, the wafers were removed from the evaporator and clean 1x1 cm glass squares cut from microscope slides were affixed across the surface using an optical adhesive. The adhesive was cured under UV light for 3 h. When needed, the TSG substrates were carefully detached from the Si wafer, exposing the smooth gold film on the bottom side of the glass squares.

Next, the freshly exposed gold surfaces were functionalized with a hydrophobic ODT monolayer by contact printing with a PDMS stamp with a 2 mm diameter hole centered in the stamp. These stamps were immersed in an ethanolic solution of 1.0 mM ODT for ~45 s, and then removed and dried with a gentle stream of high purity nitrogen. The dried stamp was gently pressed into conformal contact with the gold surface, creating a 2-mm diameter address of unmodified gold surrounded by an ODT hydrophobic barrier that confined aqueous solutions within its boundaries in all subsequent assay procedures. After removing the stamp, the substrate was rinsed with EtOH and immersed in a 0.1 mM ethanolic solution of DSP for 16 h. Finally, the samples were removed from the DSP solution, rinsed with EtOH, and dried with a stream of high purity nitrogen.

The next step arranged the modified TSG substrates in the bottom of a 24-well microplate, which was then loaded into a humidity chamber. The substrates were functionalized by means of a 20 µL droplet of 2.5 µg/mL (10 mM PBST) monoclonal anti-PILAM antibody at the center of each address. The humidity chamber was then sealed for 60 min.[54] The substrates were subsequently rinsed with 10 mM PBST, blocked with a 20 µL droplet of StartingBlock™, and incubated for 60 min in the humidity chamber. The substrates were again rinsed with 10 mM PBST and exposed to the antigen-containing solutions [*i.e.*, 20 µL droplets of PILAM-spiked human serum which underwent the PCA

treatment procedure (section 4.2.4)] for 120 min. The next rinse step used 2 mM BB with 0.1% T20 (BBT) with 150 mM NaCl, after which captured antigens were labeled for 16 h with a 20 µL droplet of the ERL suspension. Finally, unbound ERLs were rinsed off the surface with 2 mM BBT with 10 mM NaCl. The completed assay substrates were dried under ambient laboratory conditions and analyzed.

4.2.4 Sample Treatment

The complexation of PILAM with other human serum constituents requires sample pretreatment to release PILAM for low level detection.[21, 25] Procedurally, these samples were acidified to pH ~1 by the addition of a small amount of 70% perchloric acid. Acidification liberates PILAM from complexation by protein denaturation and causes most of the serum proteins to precipitate via noncovalent aggregation.[55-57] The acidified sample was then vortexed for 10 s and centrifuged at ~12,000 *g* for 5 min to form a pellet of denatured proteins and other poorly soluble materials. After centrifugation, a known volume of the clear PILAM-containing supernatant was transferred to a new microcentrifuge tube and neutralized to pH ~7.5 by the addition of a small volume of 2.0 M K_2CO_3. The samples were sequentially stored at 2-8 º C for 60 min to precipitate $KClO_4$, after which the PILAM containing supernatant was transferred to another new microcentrifuge tube. The samples were returned to ambient laboratory temperature before analysis.

4.2.5 Raman Analysis

The completed assay substrates were analyzed using two different benchtop Raman and one handheld Raman spectrometers to evaluate the utility of a handheld Raman spectrometer for PON diagnostics. A summary of the analysis parameters for the three instruments is shown in table 4.1**.** The substrates were first analyzed using a modified NanoRaman instrument (Concurrent Analytical). With this instrument, the output from a HeNe (633 nm) laser is fiber optically coupled to a spectrograph consisting of an f/2.0 Czerny Turner imaging spectrometer (6-8 cm^{-1} nm resolution) and a thermoelectrically cooled (0°C) Kodak™ charged coupled device (CCD). The laser is focused through an objective lens (numerical aperture of 0.68) onto the sample surface. The diameter of the laser spot on the sample surface is ~30 µm and the measured power at the sample surface is 3.02±0.05 mW (*i.e.,* the power density of 4.27±0.07 $x10^{-3}$ $mW/\mu m^2$).

The SERS spectra were collected using 1.0 s integration times at 10 different locations about the center of the address with ~150 µm offset between each location. After baseline correction, the intensity of the symmetric nitro stretch, $\nu_s(NO_2)$, at 1336 cm^{-1} of the RRM on the ERLs was used for analyte quantification. These same substrates were analyzed using a handheld Raman spectrometer (Tactic ID, B&W TEK™). This easy-to-use handheld instrument has a 785 nm excitation source (diode laser) and a linear CCD array detector. The spectral resolution is ~7 cm^{-1}. As shown in figure 4.2, this instrument has a point-and-shoot configuration and uses a firmly mounted sample holder to place a planar sample at a set focal distance for excitation and scattered light collection. Double-sided tape was used to affix the substrates to the sample holder so that the approximate center of the sample could be interrogated. Due to the large spot size (~100 µm) and to

Table 4.1. Comparison of the collection parameters and assay results for multiple instruments used to analyze samples.

Instrument	**NanoRaman**	**Tactic ID**	**DXR**	
Excitation Wavelength (nm)	633	785	633	780
DSNB Scattering Wavelength for $\nu_s(NO_2)$ of RRM (nm)	691	877	691	871
Measured Focal Area (μm^2) $^{\alpha}$	707	7854$^{\alpha}$	69.2 (ellipsoid)	25.1 (ellipsoid)
Power Density ($mW/\mu m^2$) $^{\beta}$	4.27 x10^{-3}	2.41 x10^{-2}	0.101	0.106
Spectral Resolution (cm^{-1})$^{\alpha}$	6-8	9-10	5.2-8.8	4.7-8.7
Data Spacing (cm^{-1} per point)$^{\gamma}$	1.6-2.3*	4	~1	~1
LOD (pg/mL)	32	179	609**	2958**
Slope of Dose Response Plot (cts)/(ng/mL)	3473±146	646±39	~556	~45
Signal-to-blank Ratio at 1 ng/mL	68±35	15±12	–	–

$^{\alpha}$manufacturer specification.
$^{\beta}$measured at sample surface.
$^{\gamma}$manufacturer-specified wavenumber (cm^{-1}) per data point.
*Interpolated to 1 cm^{-1}.
**Calculated from instrument noise.

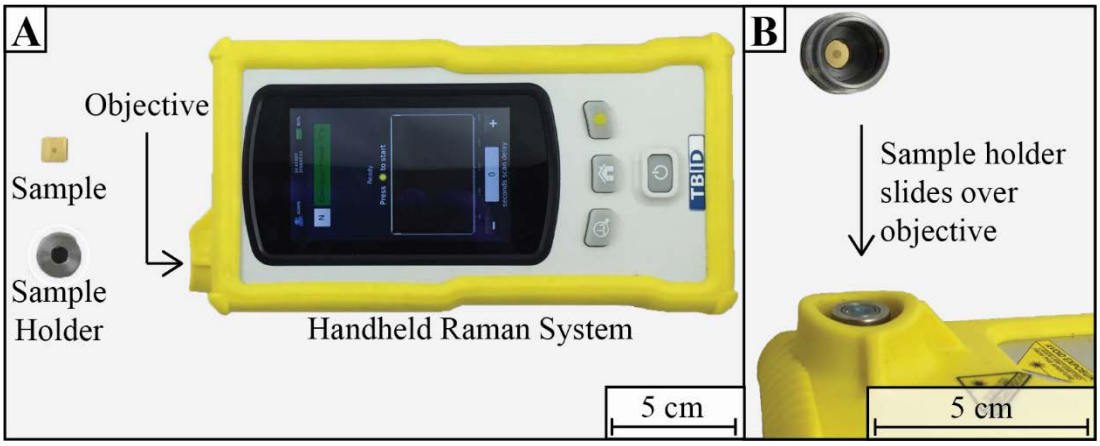

Figure 4.2. Digital images of: (A) the handheld Raman instrument and components needed for sample measurement, and (B) the sample mounted to the adapter with the sample address centered in the adapter.

mirror the desired simple “point-and-shoot” application for PON testing, only one location on each sample was analyzed using a collection time of 65 s. The laser power measured at the sample was 189±1 mW, which translates to a power density of 2.41±0.01 $x10^{-2}$ $mW/\mu m^2$.

In completing the hardware assessment, a subset of these samples was analyzed using a Thermo Scientific DXR Raman microscope in order to directly compare how differences in excitation wavelength effect the spectral response and, therefore, assay performance. This instrument has interchangeable 633 and 780 nm laser sources. The microscope was configured such that the measured power density at the sample surface at both excitation wavelengths was nearly identical, ~0.101 and ~0.106 mW/um^2 for the 633 and 780 nm sources, respectively. Spectra were collected from each sample following a 11x11 grid pattern with 50 μm spacing (121 equally spaced locations), using three 1.0 s exposures per location.

4.2.6 External Reflectance UV-Vis Spectroscopy

The localized surface plasmon resonance (SPR) associated with the ERLs upon completion of the assay was measured by external reflection UV-Vis spectroscopy using the method described by Driskell *et al*.[58] In brief, spectra were obtained using a Perkin Elmer Lambda 650 UV-Vis spectrometer equipped with a Universal Reflectance Accessory. The spectra for each sample were collected using *p*-polarized light at an angle of incidence of 58°. The spectra were collected at a resolution of 2 nm and an integration time of 0.24 s/nm. The extinction measurement is given in equation 4.1.

$$-\log\frac{R}{R_0} \tag{4.1}$$

where R is the reflectance of the sample and R_0 is the reflectance of a bare TSG sample.

4.2.7 Analytical Figures of Merit

For comparative purposes, two key metrics, LOD and analytical sensitivity, were used to define the performance of the three instruments. The LOD is the lowest concentration of PILAM that produces a signal statistically distinguishable from instrument noise or from the signal from a blank serum sample, a sample that contains no PILAM. The LOD concentration is calculated from the average signal of the blank plus three times its standard deviation.[42] Analytical sensitivity describes how well differences in the concentration of PILAM can be resolved. That is, an increase in analytical sensitivity corresponds to an increase in the difference in signal from different PILAM concentrations. Herein, the analytical sensitivity is described in two ways: (1) the signal-to-blank ratio (SBR) for a given PILAM concentration, and (2) the slope of the linear fit line from a dose-response plot.

4.3 Results and Discussion

This section presents the results from experiments designed to evaluate the performance of a first generation handheld Raman spectrometer as applied to disease diagnostics. It describes: (1) measurements of completed PILAM immunoassays using a benchtop Raman spectrometer to serve as a point of reference for assessment of the performance of the handheld unit; (2) the effectiveness of handheld Raman instrumentation for the detection of PILAM; (3) a brief discussion of the challenges faced in implementing

handheld Raman instrumentation for disease detection; and (4) the potential for its application in future disease diagnostic measurements.

4.3.1 SERS Measurements

To establish a comparative set of figures of merit, a benchtop Raman instrument, NanoRaman, designed specifically for highly sensitive Raman analysis, was used. Figure 4.3 shows SERS responses from this instrument after acid treatment of PILAM-spiked serum samples prepared at 0.025, 0.05, 0.1, 0.5, 1.0 and 5.0 ng/mL of PILAM. The spectrum for an acid-treated serum blank is also included. The spectra have the bands indicative of the DSNB coating of the ERLS: ν(C=C) at 1559 cm^{-1}, $\nu_s(NO_2)$ at 1336 cm^{-1}, ν(C-O), at 1153 cm^{-1}, and ν(N-C-O) at 1079 cm^{-1}.[42, 59-60] All of these band intensities increase with PILAM concentration.[42, 59-60] A cursory examination of the spectra in the inset points to an LOD for PILAM of approximately 25 pg/mL.

The performance of the assay is more fully analyzed through the dose-response plot shown in figure 4.4, which was generated by graphing the average intensity for three replicate assays of the $\nu_s(NO_2)$ at 1336 cm^{-1} as a function of the spike-in concentration (0-5 ng/mL) of PILAM. The calculated LOD for PILAM in pretreated serum is 32 pg/mL (1.8 pM). The SBR at 1 ng/mL of PILAM is 68 and the slope of the linear fit line is 3740 (cts)/(ng/mL).

Spectra collected for the same sample spike-in concentrations analyzed using the handheld spectrometer (figure 4.2) are presented in figure 4.5. As evident, the strength of the signal for these measurements is about 20% those in figure 4.3, and indicates an LOD for PILAM between 0.1 and 0.5 ng/mL. The corresponding dose-response plot

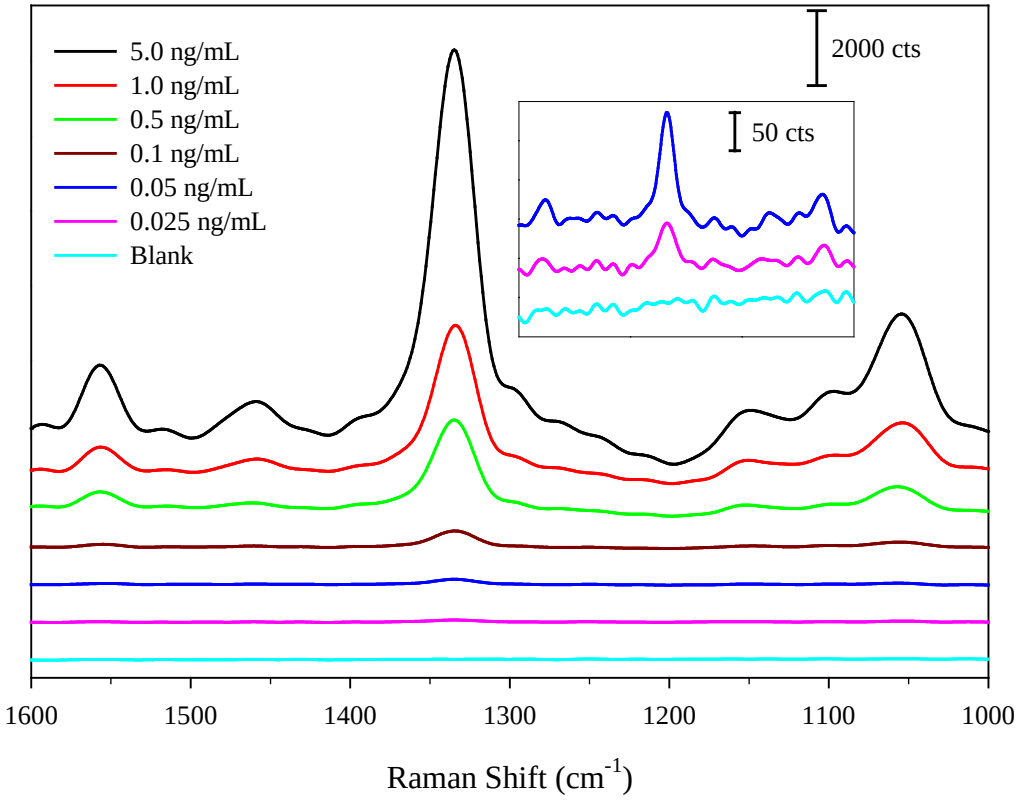

Figure 4.3. Representative SERS spectra collected using a benchtop Raman instrument, NanoRaman, for PILAM-spiked human serum samples after PCA treatment. The spectra are vertically offset for clarity.

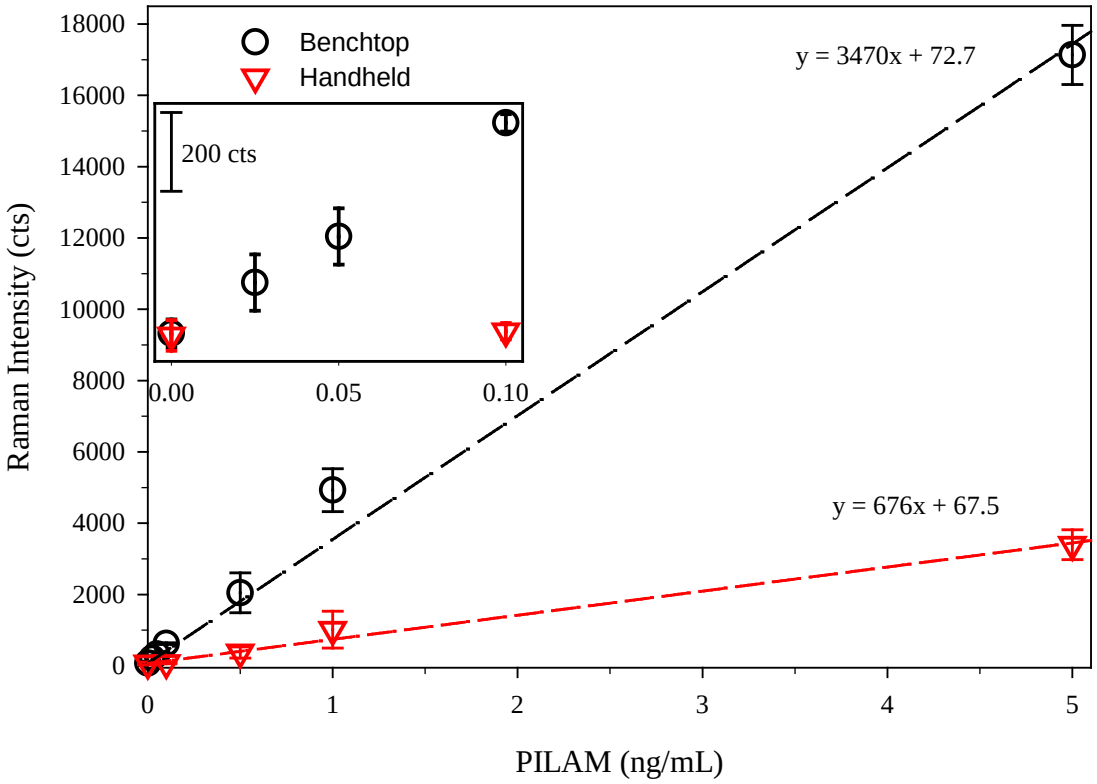

Figure 4.4. Dose-response plot for PILAM-spiked human serum that underwent PCA treatment to remove interferents. The samples were analyzed using a benchtop Raman instrument with a 633 nm source and a handheld unit with a 785 nm source. The calculated limit of detections (LOD) is 32 pg/mL (~1.8 pM) and 180 pg/mL (~10 pM), respectively. The average and standard deviation for the plot are based on 3 separate assays. The error bars are smaller than the data points at lower concentration.

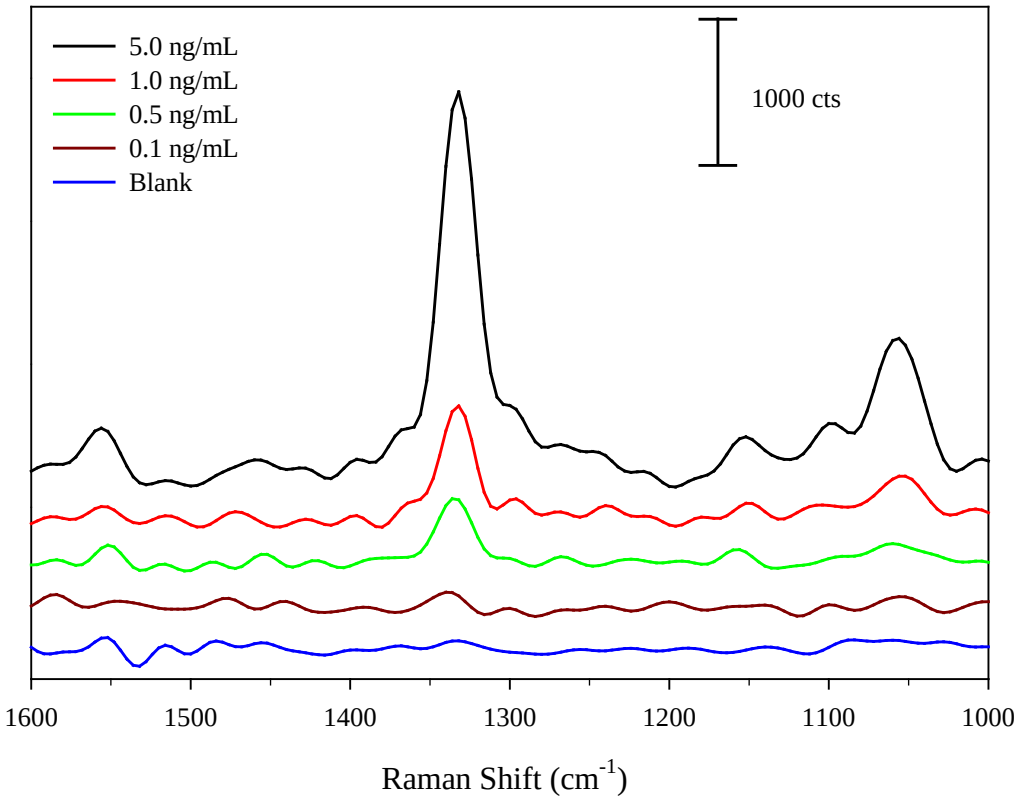

Figure 4.5. Representative SERS spectra for PILAM-spiked human serum samples after PCA treatment collected using a handheld instrument.

generated from three replicate assays is shown in figure 4.4. In this case, the LOD for PILAM was 180 pg/mL (10 pM), only ~20% of that for the benchtop instrument. Moreover, the SBR at 1.0 ng/mL is 15, which is ~4.5 times less than that for the benchtop instrument. And, the slope of the linear fit line, 676 (cts)/(ng/mL), is 5.6 times lower than the slope obtained with the benchtop instrument. All three analytical figures of merit for the handheld unit are only a factor of ~5 off those for the benchtop system.

The potential utility of the handheld unit can be framed based on our earlier work on the detection of PILAM and ManLAM.[21, 25] That work used the same procedures, materials and benchtop Raman spectrometer employed to collect the data in figure 4.3, and showed that (1) the LOD for ManLAM (~2 ng/mL) is 200x greater than that for PILAM (~10 pg/L), and (2) the detectable levels of ManLAM in 21 of the 24 TB-positive (culture confirmed) patient samples was ≥10 ng/mL (see table 1 in reference 25).[25] If we assume the 200x difference in detectability between ManLAM and PILAM found with the benchtop Raman spectrometer can be applied to the handheld Raman spectrometer, an LOD for ManLAM of ~36 ng/mL can be projected using this portable unit. While only a qualitative assessment, and one that remains to be tested experimentally, it appears that the handheld Raman spectrometer would have the same clinical specificity as the benchtop instrument and only a 30 % drop in clinical sensitivity.[25, 61]

There is one additional metric to mention: measurement reproducibility. The reproducibility for replicate measurements made with the handheld instrument is greater than that of the benchtop instrument, particularly for higher concentration samples. Typical values for the coefficient of variance (CV) of 10% can be readily achieved with the handheld instrument. The CV when analyzing samples with the benchtop instrument

ranges from 5-40%. Laboratory-based instruments typically have high numerical aperture objectives to focus the excitation source down to a very small spot (≤30 μm) on the sample surface. This is done both to create a higher power density on the sample surface and to achieve a higher collection efficiency of the scattered signal, in order to maximize the signal from a given sample. Our laboratory recently showed that while high signals at low particle coverages can be obtained in this type of immunoassay, using a very small measurement area defines the CV, the sampling error, of the measurement of randomly disperse ERLs on surface.[62] Moreover, this type of sampling error becomes more problematic at low surface concentrations, and degrades the LOD.[45, 62]

As part of the approach to realize portability, handheld instrumentation often forgoes bulky high numerical aperture objectives and simply utilizes a high power output diode laser source in order to maintain a high power density at the sample surface of a much larger focal area (*e.g.*, ~100-120 μm in diameter). The larger measurement area inherently lowers the sampling error, which improves the uncertainty in the measurement and, as a consequence, may ultimately lead to improved LODs.[62]

4.3.2. Moving Toward PON Detection

Among the chief concerns when using a handheld Raman system is power consumption. To be effective for field deployment, the battery must provide power for a display/interface system, laser, spectrometer, onboard computer, and other components in an easily transportable form factor. This imposes a few key limitations that affect the performance of the instrument. First, the more sensitive, thermoelectrically cooled detectors require too much power to operate using a battery for long periods. Additionally,

several types of laser sources (*e.g.*, HeNe laser at 633 nm), apart from being rather bulky, can also draw relatively high power. Handheld spectrometer designers and manufacturers therefore favor the use of more energy efficient diode lasers that emit at longer wavelengths (*e.g.*, 780 and 785 nm).

A number of reports have examined the impact of excitation wavelength on the achievable enhancement factor (EF) in SERS measurement and, therefore, the overall sensitivity of the measurement.[58, 63] More to the point, we have shown EF is also dependent on the extent of the plasmonic coupling between the ERL and planar gold capture surface and how the SPR of the system changes the optimal wavelength for making the immunoassay measurements.[58, 63] That work demonstrated that the EF is highest when the maximum SPR falls midway between the excitation wavelength (λ_{ex}) and the wavelength of the scattered radiation (λ_{sc}).[58]

Figure 4.6 presents the extinction spectrum measured by the reflectance of a completed PILAM assay sample. The extinction maximum is at 618 nm, which represents a shift of nearly 80 nm from that of 60 nm gold nanoparticles suspended in 2 mM borate buffer (extinction maximum of 540 nm).[58, 63] The relevant λ_{ex} and λ_{sc} values associated with both the bench top instrument and handheld unit are marked as vertical solid and dashed lines, respectively. The extinction maximum for the reflectance measurement is shifted from the optimal wavelength (*i.e.*, the midpoint between λ_{ex} and λ_{sc}) by 44 nm and 213 nm for the benchtop and handheld spectrometers, respectively. Previous work has shown that shifts of 50 nm can decrease the EF by 10-130x.[58] By measuring the extinction maximum by reflectance UV-Vis for assay samples performed using multiple particle sizes (30-80 nm) and assuming a constant gap distance, it is possible to determine the optimal particle

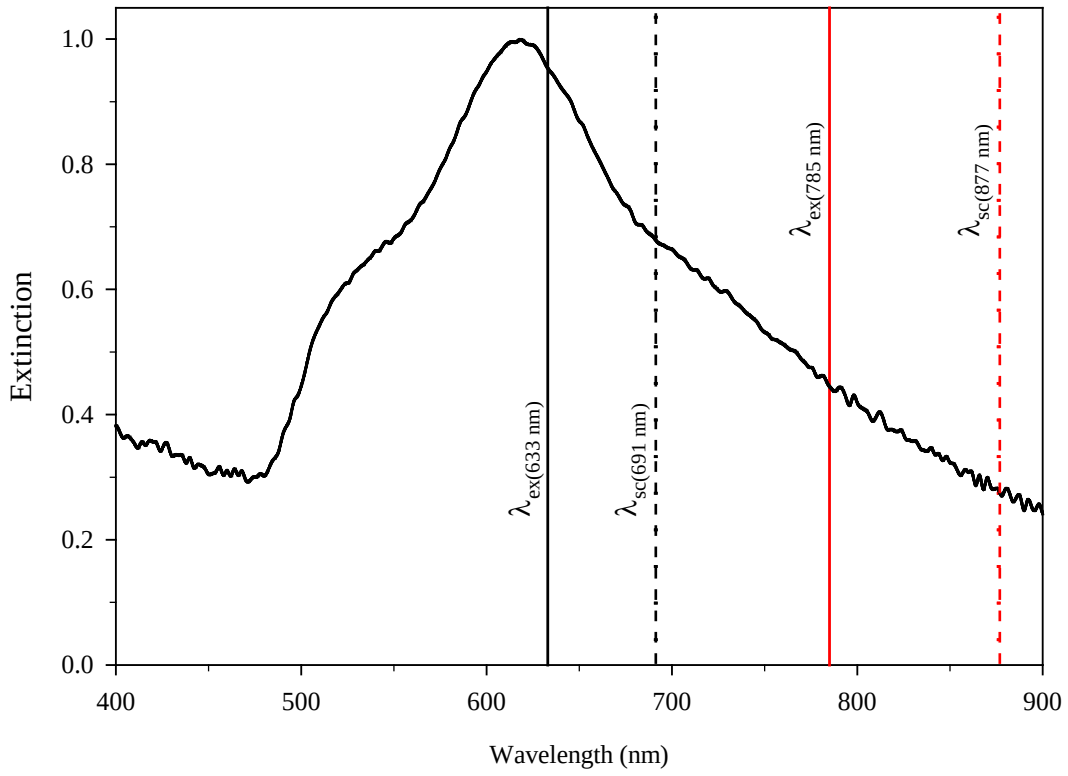

Figure 4.6. Extinction spectrum measured by reflectance UV-Vis for a 50 ng/mL of PILAM sample from a completed immunoassay. The solid vertical lines represent the excitation wavelengths (λ_{ex}), 633 nm (black) and 785 nm (red). The other set of dashed vertical lines are for the scattering (λ_{sc}) wavelengths for the $\nu_s(NO_2)$ band at 1336 cm^{-1} of the DSNB-based RRM on the ERLS for the two different excitation sources. The spectrum was collected in a reflection mode at an angle of incidence of 58° with *p*-polarized light.

size to maximize the EF for the two Raman systems (figure 4.7). To optimize the assay for this handheld system would require the use of ~190 nm gold particles, which is above the usable particle sizes typically associated with SERS immunoassays, due to a level of sedimentation and the resulting increase in nonspecific particle adsorption.[45]

This situation is further compounded by the underlying wavelength dependence of Raman scattering in which the scattering intensity (I) is inversely proportional to the excitation source wavelength (λ_{ex}) to the fourth power, equation 4.2, separate from the plasmonics of the system.[64-66]

$$I \propto \frac{1}{\lambda_{ex}{}^4} \tag{4.2}$$

Thus, samples analyzed with the handheld using 785 nm excitation should experience a signal drop of nearly 60% compared to excitation at 633 nm due solely to the longer excitation wavelength. However, this holds true only if all other measurement parameters (*e.g.*, power density, collection efficiency, and integration time) for the two instruments are matched.

To more fully examine the impact of analyzing samples using the handheld instrument, it is necessary to measure the samples when using the two different excitation wavelengths under an equivalent set of instrumental conditions. For this, we used a Raman microscope that has interchangeable 633 and 780 nm excitation sources. The following comparative experiments were run setting all of the instrument parameters as closely matched as possible *(e.g.*, collection time, number of integrations, and measured power density of 0.101 and 0.106 mW/cm^2 for the 633 and 780 nm sources, respectively). The first experiment measured the Raman spectrum of a glassy carbon substrate. The spectra

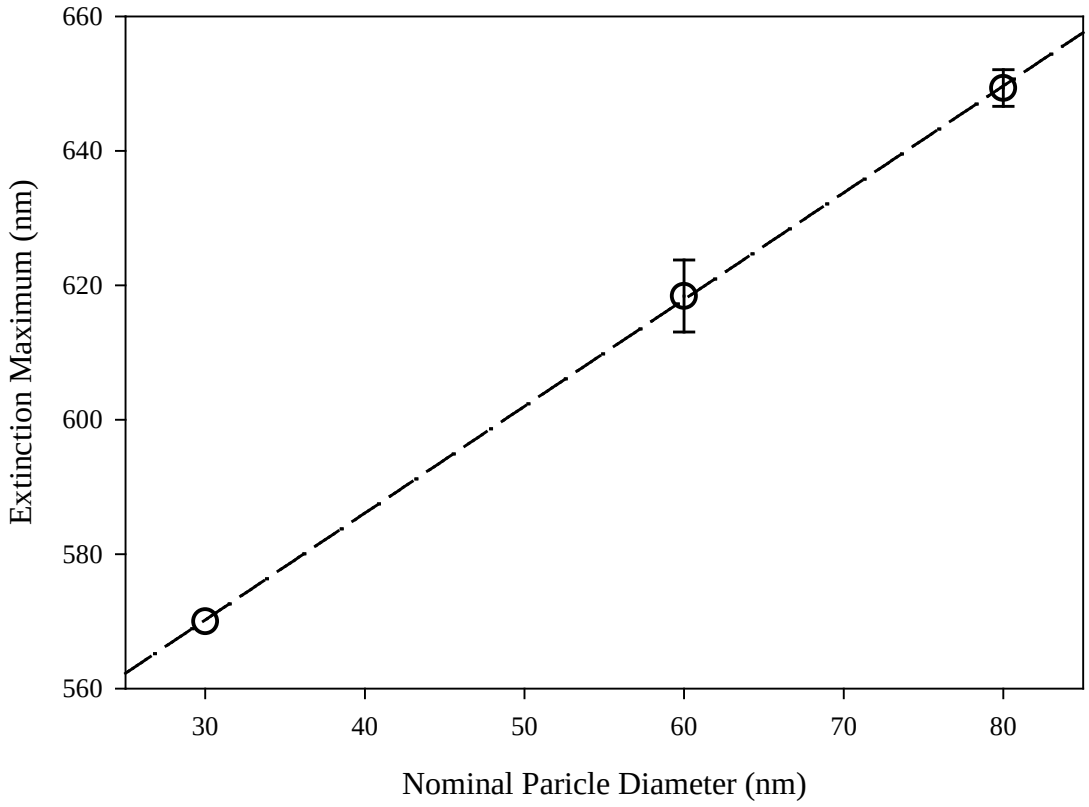

Figure 4.7. Plot of the measured reflectance extinction maxima as a function of the as-received gold nanoparticle diameters used in the fabrication of the ERLs.

for both excitation wavelengths are shown in figure 4.8. The two expected features, indicative of the D and G bands at ~1330 cm^{-1} and ~1600 cm^{-1}, respectively, of a glassy carbon surface, are evident.[67-70] The lower signal strengths with longer wavelength excitation are consistent with expectations. The theoretical decrease of the D band should be 58%, based on the difference in excitation wavelength; however, the measured drop is ~80%, 235±7 to 47±3 cts for the 633 and 780 nm sources, respectively. This is attributed to a difference in throughput of the instrument and the efficiency of the detector at the two wavelengths. Taking the intensity ratio of the D and G bands collected using the two excitation sources gives an increase in signal of 4.96±0.05x using the 633 nm source relative to the 780 nm source. This increase in signal will be used as a wavelength correction factor in dissecting the data in the next experiment.

Figure 4.9 shows representative spectra for completed PILAM assay samples analyzed under closely matched collection parameters with both the 633 and 780 nm excitation sources. As expected, the signal indicative of the $\nu_s(NO_2)$ at 1336 cm^{-1} increases as a function of initial PILAM, concentration and those collected at 780 nm are significantly less than those 633 nm. The $\nu_s(NO_2)$ intensity at the different PILAM concentrations are summarized in figure 4.10. The signal with 633 nm excitation, the more optimal plasmonic enhancement condition, is nearly 10 times stronger than that at 780 nm. However, after accounting for the difference in excitation wavelength per figure 4.9, the improvement in signal with the 633 nm source is ~5x, due to the more favorable plasmonics. If we project this improvement in the comparative measurement using the two different excitation sources with the Raman microscope, the LOD for PILAM improves to ~37 pg/mL. This means with respect to the analysis of the patient samples discussed

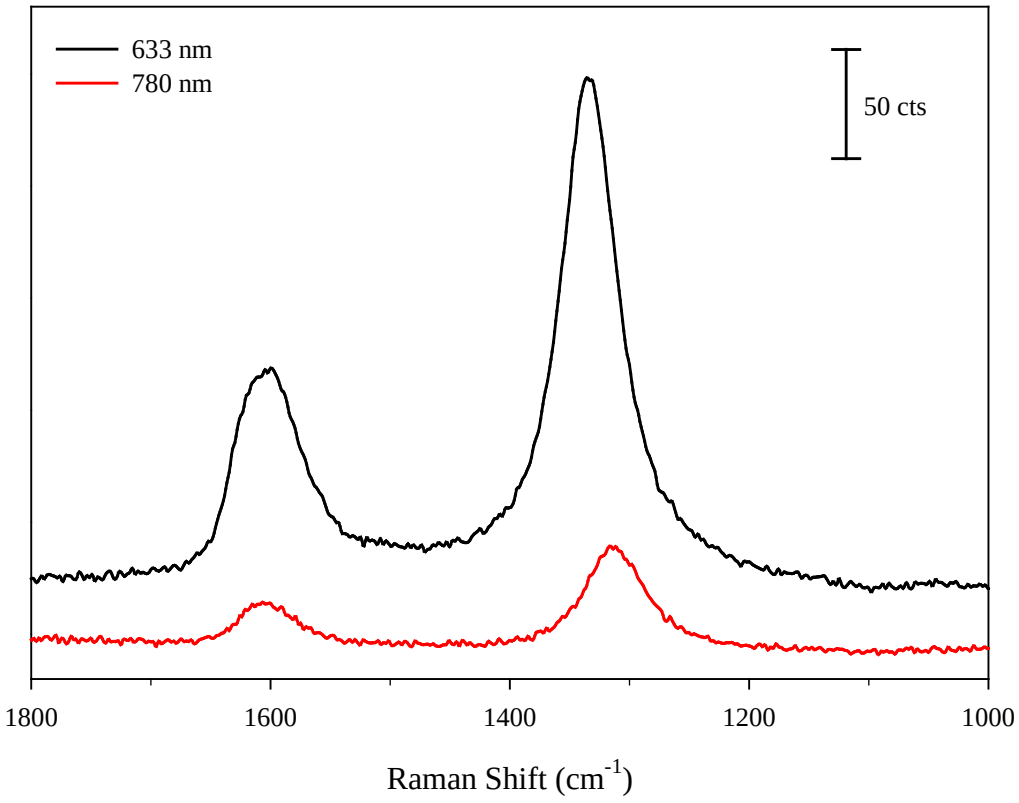

Figure 4.8. Raman spectra for a glassy carbon GC sample analyzed using a Raman microscope under closely matched conditions using 633 and 780 nm excitation sources. The spectra show the expected D and G bands at ~1330 cm^{-1} and ~1600 cm^{-1} characteristic of an amorphous carbon surface. The signal strength for the D band with the 633 nm source was 235 cts compared to 47 cts for the 780 nm source.

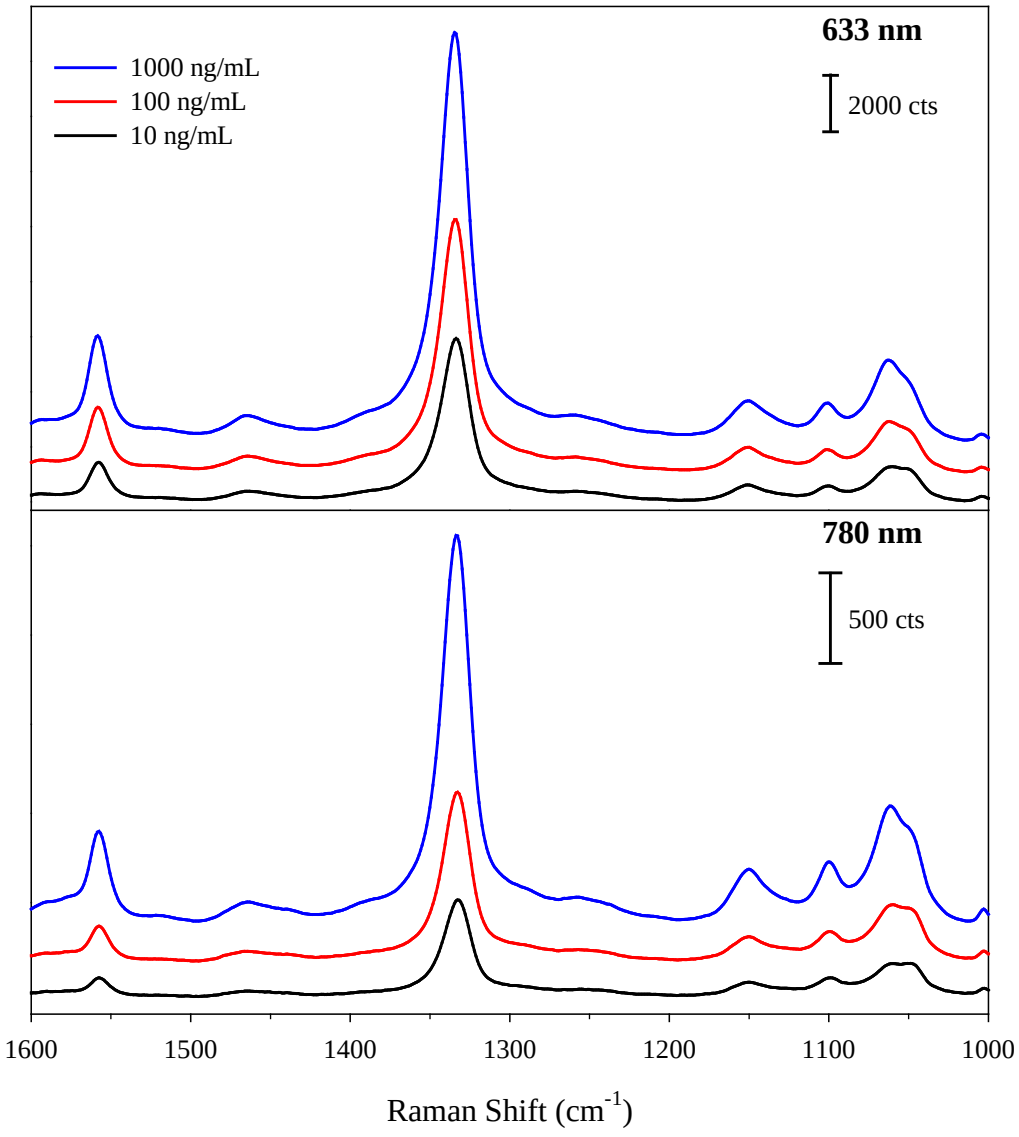

Figure 4.9. Spectra for the same PILAM assay samples analyzed with a Raman microscope under matched conditions using excitation source wavelengths 633 nm and 780 nm. The signal strength of the $\nu_s(NO_2)$ obtained with the 633 nm source is 9.5 ± 2.3 times greater than those with the 780 nm source.

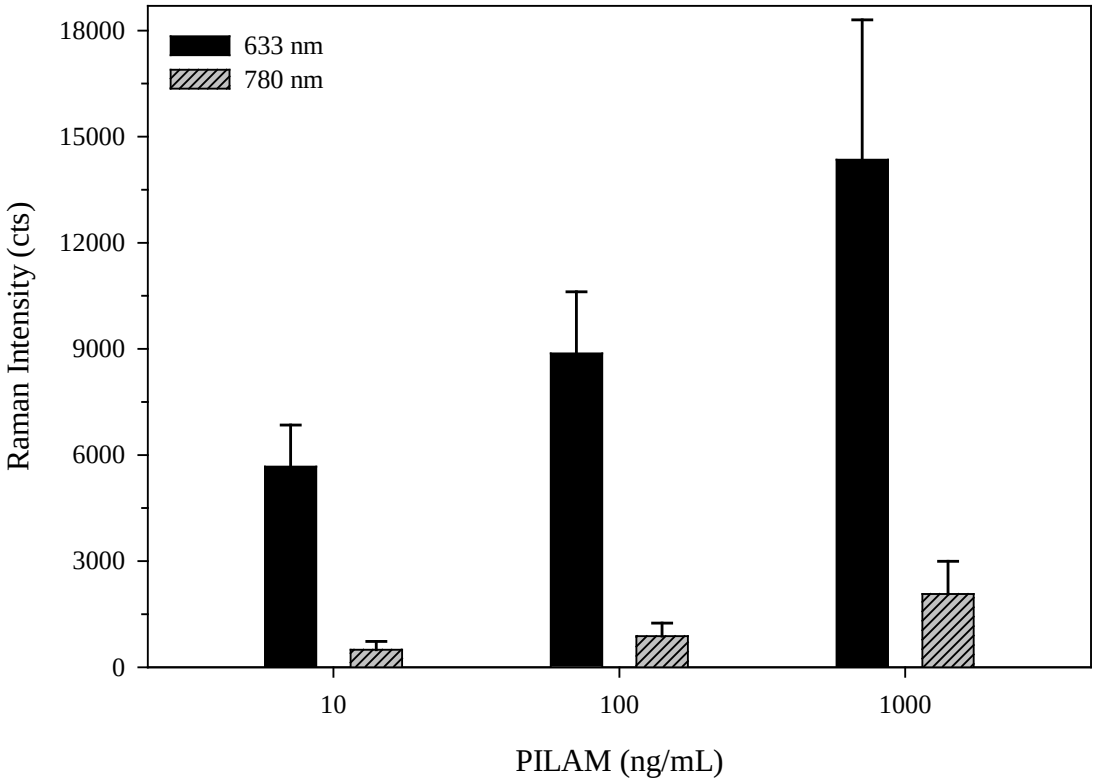

Figure 4.10. Plot of signal intensity of $\nu_s(NO_2)$ relative to PILAM concentration for the same samples analyzed with a Raman microscope under closely matched conditions using excitation source wavelengths of 633 nm and 780 nm. The signal obtained with the 633 nm source is 9.5 ± 2.3 times greater than that obtained with a 780 nm source

previously, when using the handheld unit the LOD for ManLAM becomes ~7.4 ng/mL, which would give it the same diagnostic accuracy as the benchtop instrument in our previous work.[25] These results begin to demonstrate the potential utility of handheld Raman spectrometers for effectively diagnosing infectious diseases like TB. It is also important to recognize that there are other factors that should be considered for more comprehensive studies, including data acquisition time and the laser output stability.

4.4 Conclusions

This Chapter described a series of comparative experiments to gauge the potential utility of a handheld Raman spectrometer as a component in moving a SERS immunoassay toward PON applications. While focused on the detection of PILAM, a simulant for a biomarker for active TB infection, the combined weight of the data indicates that realization of this capability with ManLAM is possible in the not-too-distant future, especially when designing a portable instrument and support software for the explicit purpose of optimizing the plasmonics central to the assay reviewed in scheme 4.1. This work begins to establish the ground rules for such an effort.

There are a number of other challenges to overcome before this transition can become reality. These include further studies to validate the clinical utility of the assay through extensive tests on several types of TB-positive specimens, including those from patients who are both TB-positive and HIV-positive and those with extrapulmonary TB. Other factors include the marked reduction in the time required at present to complete the assay and the design of reagent packaging, in terms of stability and cost. Importantly, this work sets the stage to begin to more fully exploit the extensibility and multiplexing

potential of this platform for biomarkers of other diseases, biowarfare agents, and environmental pathogens.[6, 16, 25, 40, 48, 71-73] Studies along these lines are underway in our and several other laboratories.

4.5 References

1. Pai, N. P.; Vadnais, C.; Denkinger, C.; Engel, N.; Pai, M., Point-of-Care Testing for Infectious Diseases: Diversity, Complexity, and Barriers in Low-and Middle-Income Countries. *PLoS Med.* **2012,** *9* (9), e1001306.

2. Dumlao, M.; Sinues, P. M.-L.; Nudnova, M.; Zenobi, R., Real-time Detection of Chemical Warfare Agent Simulants in Forensic Samples Using Active Capillary Plasma Ionization with Benchtop and Field-Deployable Mass Spectrometers. *Anal. Methods* **2014,** *6* (11), 3604-3609.

3. Gałuszka, A.; Migaszewski, Z. M.; Namieśnik, J., Moving your Laboratories to the Field–Advantages and Limitations of the Use of Field Portable Instruments in Environmental Sample Analysis. *Environ. Res.* **2015,** *140*, 593-603.

4. Grimme, J.; King, T.; Jo, K. D.; Cropek, D.; Timperman, A. T., Development of Fieldable Lab-on-a-Chip Systems for Detection of a Broad Array of Targets From Toxicants to Biowarfare Agents. *J. Nanotechnol. Eng. Med.* **2013,** *4* (2), 020904-1-8.

5. He, Z.; De Buck, J., Cell Wall Proteome Analysis of Mycobacterium smegmatis Strain MC2 155. *BMC Microbiol.* **2010,** *10* (1), 1-10.

6. Granger, J. H.; Schlotter, N. E.; Crawford, A. C.; Porter, M. D., Prospects for Point-of-Care Pathogen Diagnostics Using Surface-enhanced Raman Scattering (SERS). *Chem. Soc. Rev.* **2016,** *45* (14), 3865-3882.

7. McNerney, R.; Daley, P., Towards a Point-of-Care Test for Active Tuberculosis: Obstacles and Opportunities. *Nat. Rev. Microbiol.* **2011,** *9* (3), 204-213.

8. Wang, S.; Lifson, M. A.; Inci, F.; Liang, L.-G.; Sheng, Y.-F.; Demirci, U., Advances in Addressing Technical Challenges of Point-of-Care Diagnostics in Resource-Limited Settings. *Expert Rev. Mol. Diagn.* **2016,** *16* (4), 449-459.

9. World Health Organization, *Global Tuberculosis Report 2015*; **2015**.

10. Drain, P.; Losina, E.; Coleman, S.; Giddy, J.; Ross, D.; Katz, J.; Walensky, R.; Freedberg, K.; Bassett, I., Diagnostic Accuracy of a Point-of-Care Urine Test for Tuberculosis Screening Among Newly-Diagnosed HIV-Infected Adults: A Prospective, Clinic-Based Study. *BMC Infect. Dis.* **2014,** *14* (1), 110.

11. Paltiel, A. D.; Walensky, R. P., Home HIV Testing: Good News But Not a Game Changer. *Ann. Intern. Med.* **2012,** *157* (10), 744-746.

12. Pai, N. P.; Balram, B.; Shivkumar, S.; Martinez-Cajas, J. L.; Claessens, C.; Lambert, G.; Peeling, R. W.; Joseph, L., Head-to-Head Comparison of Accuracy of a Rapid Point-of-Care HIV Test with Oral Versus Whole-Blood Specimens: A Systematic Review and Meta-Analysis. *Lancet Infect. Dis.* **2012,** *12* (5), 373-380.

13. Zheng, J.; Pang, S.; Labuza, T. P.; He, L., Semi-Quantification of Surface-enhanced Raman Scattering Using a Handheld Raman Spectrometer: A Feasibility Study. *Analyst* **2013,** *138* (23), 7075-7078.

14. Peeling, R. W.; Holmes, K. K.; Mabey, D.; Ronald, A., Rapid Tests for Sexually Transmitted Infections (STIs): The Way Forward. *Sex Transm. Infect.* **2006,** *82* (suppl 5), v1-v6.

15. Mabey, D.; Peeling, R. W.; Ustianowski, A.; Perkins, M. D., Tropical Infectious Diseases: Diagnostics for the Developing World. *Nat. Rev. Microbiol.* **2004,** *2* (3), 231-240.

16. Granger, J.; Granger, M.; Firpo, M.; Mulvihill, S.; Porter, M., Toward Development of a Surface-enhanced Raman Scattering (SERS)-based Cancer Diagnostic Immunoassay Panel. *Analyst* **2013,** *138* (2), 410-416.

17. Hossain, A.; Canning, J.; Ast, S.; Rutledge, P. J.; Yen, T. L.; Jamalipour, A., Lab-in-a-Phone: Smartphone-Based Portable Fluorometer for pH Measurements of Environmental Water. *IEEE Sens. J.* **2015,** *15* (9), 5095-5102.

18. Choi, J.; Gani, A. W.; Bechstein, D. J.; Lee, J.-R.; Utz, P. J.; Wang, S. X., Portable, One-Step, and Rapid GMR Biosensor Platform with Smartphone Interface. *Biosens. Bioelectron.* **2016,** *85*, 1-7.

19. Wu, G.; Zaman, M. H., Low-cost Tools for Diagnosing and Monitoring HIV Infection in Low-resource Settings. *Bull. W. H. O.* **2012,** *90* (12), 914-920.

20. Pai, M.; Minion, J.; Sohn, H.; Zwerling, A.; Perkins, M. D., Novel and Improved Technologies for Tuberculosis Diagnosis: Progress and Challenges. *Clin. Chest Med.* **2009,** *30* (4), 701-716.

21. Laurentius, L. B.; Crawford, A. C.; Mulvihill, T. S.; Granger, J. H.; Robinson, R.; Spencer, J. S.; Chatterjee, D.; Hanson, K. E.; Porter, M. D., Importance of Specimen Pretreatment for the Low-level Detection of Mycobacterial Lipoarabinomannan in Human Serum. *Analyst* **2017,** *142* (1), 177-185.

22. Norbis, L.; Alagna, R.; Tortoli, E.; Codecasa, L. R.; Migliori, G. B.; Cirillo, D. M., Challenges and Perspectives in the Diagnosis of Extrapulmonary Tuberculosis. *Exp. Rev. Anti-Infective Ther.* **2014,** *12* (5), 633-47.

23. Pai, M.; O'brien, R., New Diagnostics for Latent and Active Tuberculosis: State of the Art and Future Prospects. *Semin.Respir.Crit. Care Med.* **2008,** *29* (05), 560-568.

24. Levy, H., A Reevaluation of Sputum Microscopy and Culture in the Diagnosis of Pulmonary Tuberculosis. *Chest* **1989,** *95* (6), 1193-1197.

25. Crawford, A. C.; Laurentius, L. B.; Mulvihill, T. S.; Granger, J. H.; Spencer, J. S.; Chatterjee, D.; Hanson, K. E.; Porter, M. D., Detection of the Tuberculosis Antigenic Marker Mannose-Capped Lipoarabinomannan in Pretreated Serum by Surface-enhanced Raman Scattering. *Analyst* **2017,** *142*, 186-196.

26. De, P.; Amin, A. G.; Valli, E.; Perkins, M. D.; McNeil, M.; Chatterjee, D., Estimation of D-Arabinose by Gas Chromatography/Mass Spectrometry as Surrogate for Mycobacterial Lipoarabinomannan in Human Urine. *PLoS One* **2015,** *10* (12), e0144088.

27. Etienne, G.; Laval, F.; Villeneuve, C.; Dinadayala, P.; Abouwarda, A.; Zerbib, D.; Galamba, A.; Daffé, M., The Cell Envelope Structure and Properties of Mycobacterium smegmatis mc2155: Is There a Clue for the Unique Transformability of the Strain? *Microbiology* **2005,** *151* (6), 2075-2086.

28. Mishra, A. K.; Driessen, N. N.; Appelmelk, B. J.; Besra, G. S., Lipoarabinomannan and Related Glycoconjugates: Structure, Biogenesis and Role in Mycobacterium tuberculosis Physiology and Host–Pathogen Interaction. *FEMS Microbiol. Rev.* **2011,** *35* (6), 1126-1157.

29. Cao, B.; Williams, S. J., Chemical Approaches for the Study of the Mycobacterial Glycolipids Phosphatidylinositol mannosides, Lipomannan and Lipoarabinomannan. *Nat. Prod. Rep.* **2010,** *27* (6), 919-947.

30. Chatterjee, D.; Khoo, K.-H., Mycobacterial Lipoarabinomannan: An Extraordinary Lipoheteroglycan with Profound Physiological Effects. *Glycobiology* **1998,** *8* (2), 113-120.

31. Petzold, C. J.; Stanton, L. H.; Leary, J. A., Structural Characterization of Lipoarabinomannans from Mycobacterium tuberculosis and Mycobacterium smegmatis by ESI Mass Spectrometry. *J. Am. Soc. Mass Spectrom.* **2005,** *16* (7), 1109-1116.

32. Venisse, A.; Berjeaud, J. M.; Chaurand, P.; Gilleron, M.; Puzo, G., Structural Features of Lipoarabinomannan from Mycobacterium Bovis BCG. Determination of Molecular Mass by Laser Desorption Mass Spectrometry. *J. Biol. Chem.* **1993,** *268* (17), 12401-12411.

33. Khoo, K.-H.; Douglas, E.; Azadi, P.; Inamine, J. M.; Besra, G. S.; Mikušová, K.; Brennan, P. J.; Chatterjee, D., Truncated Structural Variants of Lipoarabinomannan in Ethambutol Drug-Resistant Strains of Mycobacterium smegmatis: Inhibition of Arabinan Biosynthesis by Ethambutol. *J. Biol. Chem.* **1996,** *271* (45), 28682-28690.

34. Singh, A. K.; Reyrat, J. M., Laboratory Maintenance of Mycobacterium smegmatis. *Curr. Prot. Microbio.* **2009**, 10C. 1.1-10C. 1.12.

35. Maura, R. B.; Férnandez, S.; Reyes, G.; Perez, J. L.; Reyes, F.; de los Angeles García, M.; Fariñas, M.; Infante, J. F.; Tirado, Y.; Puig, A., Evaluation of the Potential of Mycobacterium Smegmatis as Vaccine Candidate Against Tuberculosis by in Silico and in Vivo Studies. *VacciMonitor* **2010,** *19* (1), 20-26.

36. Reyrat, J. M.; Kahn, D., Mycobacterium smegmatis: An Absurd Model for Tuberculosis? *Trends Microbiol.* **2001,** *9* (10), 472-474.

37. Mohan, A.; Padiadpu, J.; Baloni, P.; Chandra, N., Complete Genome Sequences of a Mycobacterium smegmatis Laboratory Strain (MC2 155) and Isoniazid-Resistant (4XR1/R2) Mutant Strains. *Genome Announcements* **2015,** *3* (1).

38. Akinola, R. O.; Mazandu, G. K.; Mulder, N. J., A Systems Level Comparison of Mycobacterium tuberculosis, Mycobacterium leprae and Mycobacterium smegmatis Based on Functional Interaction Network Analysis. *J. Bacteriol. Parasitol.* **2014,** *2013*.

39. Waagmeester, A.; Thompson, J.; Reyrat, J.-M., Identifying Sigma Factors in Mycobacterium Smegmatis by Comparative Genomic Analysis. *Trends Microbiol.* **2005,** *13* (11), 505-509.

40. Driskell, J. D.; Kwarta, K. M.; Lipert, R. J.; Porter, M. D.; Neill, J. D.; Ridpath, J. F., Low-level Detection of Viral Pathogens by a Surface-enhanced Raman Scattering Based Immunoassay. *Anal. Chem.* **2005,** *77* (19), 6147-6154.

41. Porter, M. D.; Lipert, R.; Siperko, L.; Wang, G.; Narayanan, R., SERS as a Bioassay Platform: Fundamentals, Design, and Applications. *Chem. Soc. Rev.* **2008,** *37* (5), 1001-1011.

42. Grubisha, D. S.; Lipert, R. J.; Park, H.-Y.; Driskell, J. D.; Porter, M. D., Femtomolar Detection of Prostate-specific Antigen: An Immunoassay Based on Surface-enhanced Raman Scattering and Immunogold Labels. *Anal. Chem.* **2003,** *75* (21), 5936-5943.

43. Park, H.-Y.; Driskell, J. D.; Kwarta, K. M.; Lipert, R. J.; Porter, M. D.; Schoen, C.; Neill, J. D.; Ridpath, J. F., Ultrasensitive Imunoassays Based on Surface-Enhanced Raman Scattering by Immunogold Labels. In *Surface-Enhanced Raman Scattering - Physics and Applications*, Kneipp, K.; Moskovits, M.; Kneipp, H., Eds. Springer-Verlag Berlin: Heidelberg, **2006**; pp 427-446.

44. Ni, J.; Lipert, R. J.; Dawson, G. B.; Porter, M. D., Immunoassay Readout Method Using Extrinsic Raman Labels Adsorbed on Immunogold Colloids. *Anal. Chem.* **1999,** *71* (21), 4903-4908.

45. Crawford, A. C. Surface-enhanced Raman Scattering for the Reliable and Reproducible Detection of Disease Antigens in Biologically Relevant Media. Dissertation, The University of Utah, **2016**.

46. Jentzsch, P. V.; Ramos, L. A.; Ciobotă, V., Handheld Raman Spectroscopy for the Distinction of Essential Oils Used in the Cosmetics Industry. *Cosmetics* **2015,** *2* (2), 162-176.

47. Schmidt, H.; Sowoidnich, K.; Kronfeldt, H.-D., A Prototype Hand-Held Raman Sensor for the in situ Characterization of Meat Quality. *Appl. Spectrosc.* **2010,** *64* (8), 888-894.

48. Roy, E. G.; Dentinger, C.; Robotham, C. In *Detection of Homemade Explosives Using Raman Excitation at 1064 nm*, **2015**; pp 94540U-94540U-5.

49. Carron, K.; Cox, R., Qualitative Analysis and the Answer Box: A Perspective on Portable Raman Spectroscopy. *Anal. Chem.* **2010,** *82* (9), 3419-3425.

50. Watson, M.; Buller, S.; Carron, K., Spectrometer. Google Patents: **2015**.

51. Schechinger, M.; Marks, H.; Locke, A.; Choudhury, M.; Coté, G. In *Optimization of Surface Enhanced Raman Scattering (SERS) Assay for the Transition From Benchtop to Handheld Raman Systems*. Proc. SPIE 10072, Optical Diagnostics and Sensing XVII: Toward Point-of-Care Diagnostics. **2017**, pp 1007203-1.

52. Gaylord, H.; Brennan, P. J.; Young, D. B.; Buchanan, T. M., Most *Mycobacterium leprae* Carbohydrate-Reactive Monoclonal Antibodies are Directed to Lipoarabinomannan. *Infect. Immun.* **1987,** *55* (11), 2860-2863.

53. Hegner, M., Ultralarge Atomically Flat Template-Stripped Au Surfaces for Scanning Probe Microscopy. *Surf. Sci.* **1993,** *291* (1-2), 39-46.

54. Lim, C. Y.; Owens, N. A.; Wampler, R. D.; Ying, Y.; Granger, J. H.; Porter, M. D.; Takahashi, M.; Shimazu, K., Succinimidyl Ester Surface Chemistry: Implications of the Competition between Aminolysis and Hydrolysis on Covalent Protein Immobilization. *Langmuir* **2014,** *30* (43), 12868-12878.

55. Goto, Y.; Takahashi, N.; Fink, A. L., Mechanism of Acid-induced Folding of Proteins. *Biochemistry* **1990,** *29* (14), 3480-3488.

56. Rajalingam, D.; Loftis, C.; Xu, J. J.; Kumar, T. K. S., Trichloroacetic Acid-induced Protein Precipitation Involves the Reversible Association of a Stable Partially Structured Intermediate. *Protein Sci.* **2009,** *18* (5), 980-993.

57. Sivaraman, T.; Kumar, T.; Jayaraman, G.; Yu, C., The Mechanism of 2, 2, 2-trichloroacetic Acid-induced Protein Precipitation. *J. Protein Chem.* **1997,** *16* (4), 291-297.

58. Driskell, J. D.; Lipert, R. J.; Porter, M. D., Labeled Gold Nanoparticles Immobilized at Smooth Metallic Substrates: Systematic Investigation of Surface Plasmon Resonance and Surface-enhanced Raman Scattering. *J. Phys. Chem. B* **2006,** *110* (35), 17444-17451.

59. Moore, D. S.; McGrane, S. D., Comparative Infrared and Raman Spectroscopy of Energetic Polymers. *J. Mol. Struct.* **2003,** *661*, 561-566.

60. Lewis, I. R.; Daniel Jr, N. W.; Griffiths, P. R., Interpretation of Raman Spectra of Nitro-Containing Explosive Materials. Part I: Group Frequency and Structural Class Membership. *Appl. Spectrosc.* **1997,** *51* (12), 1854-1867.

61. Lalkhen, A. G.; McCluskey, A., Clinical Tests: Sensitivity and Specificity. *Cont. Educ. Anaesth. Crit. Care Pain.* **2008,** *8* (6), 221-223.

62. Crawford, A. C.; Skuratovsky, A.; Porter, M. D., Sampling Error: Impact on the Quantitative Analysis of Nanoparticle-Based Surface-Enhanced Raman Scattering Immunoassays. *Anal. Chem.* **2016,** *88* (12), 6515-6522.

63. Park, H.-Y.; Driskell, J.; Kwarta, K.; Lipert, R.; Porter, M.; Schoen, C.; Neill, J.; Ridpath, J.; Kneipp, K.; Moskovits, M.; Kneipp, H., *Surface-enhanced Raman Scattering: Physics and Applications*. Springer: **2006**; Vol. 103, p 427-446.

64. Stiles, P.; Dieringer, J.; Shah, N.; Van Duyne, R., Surface-Enhanced Raman Spectroscopy. *Annual Review of Analytical Chemistry* **2008,** *1* (1), 601-626.

65. McFarland, A. D.; Young, M. A.; Dieringer, J. A.; Van Duyne, R. P., Wavelength-Scanned Surface-Enhanced Raman Excitation Spectroscopy. *J. Phys. Chem. B* **2005,** *109* (22), 11279-11285.

66. McCreery, R. L., *Raman Spectroscopy for Chemical Analysis*. Wiley-Interscience: **2005**; Vol. 225.

67. Chu, P. K.; Li, L., Characterization of Amorphous and Nanocrystalline Carbon Films. *Mater. Chem. Phys.* **2006,** *96* (2), 253-277.

68. Hodkiewicz, J., Characterizing Carbon Materials with Raman Spectroscopy. *Thermo Sci. App. Note* **2010,** *51946*.

69. Solopova, N.; Dubrovinskaia, N.; Dubrovinsky, L., Raman Spectroscopy of Glassy Carbon Up to 60 GPa. *Appl. Phys. Lett.* **2013,** *102* (12), 121909.

70. Wang, Y.; Alsmeyer, D. C.; McCreery, R. L., Raman Spectroscopy of Carbon Materials: Structural Basis of Observed Spectra. *Chem. Mater.* **1990,** *2* (5), 557-563.

71. Graham, D.; Goodacre, R., Chemical and Bioanalytical Applications of Surface Enhanced Raman Scattering Spectroscopy. *Chem. Soc. Rev.* **2008,** *37* (5), 883-884.

72. Wang, G.; Park, H.-Y.; Lipert, R. J.; Porter, M. D., Mixed Monolayers on Gold Nanoparticle Labels for Multiplexed Surface-Enhanced Raman Scattering Based Immunoassays. *Anal. Chem.* **2009,** *81* (23), 9643-9650.

73. Laing, S.; Gracie, K.; Faulds, K., Multiplex in Vitro Detection using SERS. *Chem. Soc. Rev.* **2016,** *45* (7), 1901-1918.

CHAPTER 5

CONCLUSION

5.1 Conclusion and Future Perspectives

The effective diagnosis of infectious diseases continues to challenge the scientific and medical community. Despite the reemergence of some infectious diseases (*e.g.*, Tuberculosis (TB), Zika, and Ebola viruses) beyond their endemic regions, people in upper-income economies are typically less impacted by their effects due to the availability of testing redundancies and access to high quality medical care.[1-6] However, the impact of infectious diseases in lower-income economies, particularly in areas that overlap with endemic regions, is devastating. TB is now the deadliest infectious disease on the planet, accounting for 1.37 million deaths in 2015 alone.[6] While effective treatment regimens (*i.e.*, antibiotics) are in hand, the inadequacies of existing detection technologies (*e.g.,* sputum smear microscopy and bacterial culture) result in nearly one-third of all infected people remaining undiagnosed.[6-10] Efforts to ease the burden of disease associated with TB have resulted in a refocusing on the research and development of new and highly sensitive detection strategies. While continuing to push the boundaries of knowledge, these technological advancements are of little use if, in the end, they are inaccessible to those at the point of need (PON). For example, the past decade has seen the development of

incredibly sensitive nucleic acid amplification tests for TB, but these tests are often costly, time consuming, and require a sophisticated laboratory infrastructure and skilled technical staff.[6, 8, 11-13] In addition, limited accessibility by the patient population and differing attitudes towards healthcare only add to the problem.[6, 13-14]

To clearly frame the challenges in meeting this shortfall in effective PON diagnostic tests, the World Health Organization has formulated the *ASSURED* (affordable, sensitive, specific, user-friendly, rapid, equipment-free, and delivered to those in need) guidelines to direct the development and implementation of PON methodologies.[15-16] Using TB diagnostics and the detection of phospho-*myo*-inositol-capped LAM (PILAM), and mannose-capped LAM (ManLAM) as a model system, this Dissertation has focused on approaches towards meeting the challenges faced in modern infectious disease diagnostics, while also attempting to drive the eventual transition of laboratory-based detection methods toward PON applications within the *ASSURED* framework.

Chapter 2 built on previous studies in our laboratory investigating the underpinnings of effective sample treatment methods to improve the detection of ManLAM.[17-18] In this work, two separate sample treatment methods, perchloric acid (PCA) and proteinase K (PK), were used to investigate the recovery of the TB antigenic marker, ManLAM, from human serum. We showed that while the PCA treatment is ideal from the perspective of speed and cost, recovery of ManLAM was hindered through a combination of the acid-induced degradation of the arabinan side chains of ManLAM and the partial decomplexation of ManLAM from interferents in whole serum. Treatment of serum samples with PK, a serine protease, proved more, but not fully, effective. Nevertheless, the increase in ManLAM recovery had a significant positive impact on the clinical accuracy

of an enzyme-linked immunosorbent assay (ELISA) for the diagnosis of TB-positive and TB-negative patient samples.

The continued optimization of these sample treatment methods is an ongoing investigation in our laboratory, along with determining how the extent of ManLAM degradation plays a role in its subsequent detection. We believe that these results document the unrecognized importance of sample treatment and shed light on the design rules for the development of a more effective test for TB and a number of other important infectious disease markers.

Having advanced methods by which PILAM and ManLAM can be rendered detectable, the subsequent chapters of this Dissertation assessed the utility of new detection strategies for ManLAM and the potential of handheld instrumentation for transitioning these and other diagnostic tests beyond the confines of the clinical laboratory. Chapter 3 described the development, characterization, and validation of a novel surface-enhanced resonance Raman scattering (SERRS) detection strategy for improved ManLAM detection. This approach utilized infrared external reflection spectroscopy and Raman spectroscopy to characterize the chemically modified substrates and to assess surface heterogeneity. This work also demonstrated an improved limit of detection (LOD) and analytical sensitivity of a SERRS immunoassay for ManLAM over that of our more traditional surface-enhanced Raman scattering (SERS) methodology. Finally, this study used scanning electron microscopy to begin to identify the origins of the improvement in detection.

While this study demonstrated an increased ManLAM detectability, measurement reproducibility and nonspecific adsorption hindered the ability to fully realize the expected level of improvement. We are currently working to more fully characterize the chemically

modified substrates with an aim at developing methods to improve the reproducibility and to establish approaches to reduce nonspecific adsorption. Nonetheless, this methodology shows real promise for realizing ultrasensitive analyte detection with relative ease. Moreover, preliminary data suggest that, in some cases, the use of alternate Raman reporter molecules (RRMs) on the gold nanoparticle surface used in typical SERS assays has a deleterious effect on colloidal stability, thereby reducing assay performance. Because the RRM modification is made to the underlying surface in the SERRS assay, as opposed to the nanoparticle label, this assay format may be less affected by the issues of particle aggregation and colloidal stability observed previously. Furthermore, because of the high signals per labeling event, this assay format may further enable the development of sensitive SERRS detection with small portable Raman spectrometers.

Finally, Chapter 4 described the validation of a handheld Raman spectrometer for the detection of PILAM spiked into human serum to begin the transition of SERS immunoassays towards PON applications. This work validated the instrument performance for PILAM spiked into buffer and human serum, demonstrating the ability to achieve low LODs for PILAM spiked into serum when detected using a handheld Raman spectrometer. This effort also studied the impact of excitation wavelength and the plasmonic interactions occurring between the extrinsic Raman labels (ERLs) and underlying planar gold substrate as a basis for improving diagnostic assays by choice in excitation wavelength or by adjusting, when tractable, the size of the gold nanoparticle used in the ERL fabrication.

Having demonstrated the potential utility of handheld Raman instrumentation to realize the sensitive detection of a TB marker simulant, much of the future work for this project revolves around improving performance for ManLAM detection and redesigning

the immunoassay into a more amenable PON platform. To improve the sensitivity of the readout, we are investigating the impact of particle size on detection. We have also begun to build on our past work in solid-phase extraction methodologies as a PON procedure for performing immunoassays .[19-20]

In closing, we believe that the work described in this Dissertation begins to meet some of the challenges faced with the current detection strategies for TB; and, from a fundamental standpoint, this work begins to demonstrate the potential applicability of sensitive SERS- and SERRS-based measurements outside the confines of the research laboratory. Advances in disease diagnostics can be a slow process; however, we feel that in building on existing work, the work described herein brings us one step closer to realizing methods to combat the burden of infectious diseases, like TB, as well as better prepare us for detecting emerging threats to human health.

5.2 References

1. Horton, J. B.; Hollier, L. H., The Current State of Health Care Reform: The Physicians' Burden. *Aesthetic Surg. J.* **2012,** *32* (2), 230-235.

2. Karwowski, M. P.; Nelson, J. M.; Staples, J. E.; Fischer, M.; Fleming-Dutra, K. E.; Villanueva, J.; Powers, A. M.; Mead, P.; Honein, M. A.; Moore, C. A., Zika Virus Disease: A CDC Update for Pediatric Health Care Providers. *Pediatrics* **2016,** *137* (5), e20160621.

3. World Health Organization, *Zika Situation Report (Zika Virus, Microcephaly and Guillain-Barré Syndrome)*; **2017**.

4. Lyon, G. M.; Mehta, A. K.; Varkey, J. B.; Brantly, K.; Plyler, L.; McElroy, A. K.; Kraft, C. S.; Towner, J. S.; Spiropoulou, C.; Ströher, U., Clinical care of two patients with Ebola virus disease in the United States. *N. Engl. J. Med.* **2014,** *371* (25), 2402-2409.

5. Worldk Health Organization, *Ebola Virus Disease (Fact Sheet)*; **2017**.

6. World Health Organization, *Global Tuberculosis Report 2015*; **2015**.

7. Pai, M.; O'brien, R., New Diagnostics for Latent and Active Tuberculosis: State of the Art and Future Prospects. *Semin. Respir.Crit. Care Med.* **2008,** *29* (05), 560-568.

8. Araj, G. F., Comparative Performance of PCR-based Assay Versus Microscopy and Culture for the Direct Detection of *Mycobacterium tuberculosis* in Clinical Respiratory Specimens in Lebanon. *Int. J. Tubercul. Lung Dis.* **2000,** *4* (9), 877-881.

9. Levy, H., A Reevaluation of Sputum Microscopy and Culture in the Diagnosis of Pulmonary Tuberculosis. *Chest* **1989,** *95* (6), 1193-1197.

10. Steingart, K. R.; Ng, V.; Henry, M.; Hopewell, P. C.; Ramsay, A.; Cunningham, J.; Urbanczik, R.; Perkins, M. D.; Aziz, M. A.; Pai, M., Sputum Processing Methods to Improve the Sensitivity of Smear Microscopy for Tuberculosis: A Systematic Review. *Lancet Infect. Dis.* **2006,** *6* (10), 664-674.

11. Honore-Bouakline, S.; Vincensini, J.; Giacuzzo, V.; Lagrange, P.; Herrmann, J., Rapid Diagnosis of Extrapulmonary Tuberculosis by PCR: Impact of Sample Preparation and DNA Extraction. *J. Clin. Microbiol.* **2003,** *41* (6), 2323-2329.

12. Pai, M.; Kalantri, S.; Dheda, K., New Tools and Emerging Technologies for the Diagnosis of Tuberculosis: Part II. Active Tuberculosis and Drug Resistance. *Expert Rev. Mol. Diagn.* **2006,** *6* (3), 423-432.

13. Pai, N. P.; Vadnais, C.; Denkinger, C.; Engel, N.; Pai, M., Point-of-Care Testing for Infectious Diseases: Diversity, Complexity, and Barriers in Low-and Middle-Income Countries. *PLoS Med.* **2012,** *9* (9), e1001306.

14. Pai, N. P.; Balram, B.; Shivkumar, S.; Martinez-Cajas, J. L.; Claessens, C.; Lambert, G.; Peeling, R. W.; Joseph, L., Head-to-Head Comparison of Accuracy of a Rapid Point-of-Care HIV Test with Oral Versus Whole-Blood Specimens: A Systematic Review and Meta-Analysis. *Lancet Infect. Dis.* **2012,** *12* (5), 373-380.

15. Mabey, D.; Peeling, R. W.; Ustianowski, A.; Perkins, M. D., Tropical Infectious Diseases: Diagnostics for the Developing World. *Nat. Rev. Microbiol.* **2004,** *2* (3), 231-240.

16. Peeling, R. W.; Holmes, K. K.; Mabey, D.; Ronald, A., Rapid Tests for Sexually Transmitted Infections (STIs): The Way Forward. *Sex Transm. Infect.* **2006,** *82* (suppl 5), v1-v6.

17. Crawford, A. C.; Laurentius, L. B.; Mulvihill, T. S.; Granger, J. H.; Spencer, J. S.; Chatterjee, D.; Hanson, K. E.; Porter, M. D., Detection of the Tuberculosis Antigenic Marker Mannose-Capped Lipoarabinomannan in Pretreated Serum by Surface-enhanced Raman Scattering. *Analyst* **2017,** *142*, 186-196.

18. Laurentius, L. B.; Crawford, A. C.; Mulvihill, T. S.; Granger, J. H.; Robinson, R.; Spencer, J. S.; Chatterjee, D.; Hanson, K. E.; Porter, M. D., Importance of Specimen Pretreatment for the Low-level Detection of Mycobacterial Lipoarabinomannan in Human Serum. *Analyst* **2017,** *142* (1), 177-185.

19. Gazda, D. B.; Fritz, J. S.; Porter, M. D., Multiplexed Colorimetric Solid-Phase Extraction: Determination of Silver (I), Nickel (II), and Sample pH. *Anal. Chem.* **2004,** *76* (16), 4881-4887.

20. Fritz, J. S.; Arena, M. P.; Steiner, S. A.; Porter, M. D., Rapid Determination of Ions by Combined Solid-Phase Extraction–Diffuse Reflectance Spectroscopy. *J. Chromatogr. A* **2003,** *997* (1), 41-50.